


Spring 3-8-2017

PRACTICAL CONSIDERATIONS IN DETERMINING TIMBER PILE DEPTH USING THE SONIC ECHO METHOD

Ali F. Jwary

Follow this and additional works at: https://digitalrepository.unm.edu/ce_etds

 Part of the [Civil Engineering Commons](#), [Geotechnical Engineering Commons](#), [Structural Engineering Commons](#), and the [Transportation Engineering Commons](#)

Recommended Citation

Jwary, Ali F. "PRACTICAL CONSIDERATIONS IN DETERMINING TIMBER PILE DEPTH USING THE SONIC ECHO METHOD." (2017). https://digitalrepository.unm.edu/ce_etds/165

This Thesis is brought to you for free and open access by the Engineering ETDs at UNM Digital Repository. It has been accepted for inclusion in Civil Engineering ETDs by an authorized administrator of UNM Digital Repository. For more information, please contact disc@unm.edu.

Ali F. Jwary

Candidate

Civil Engineering

Department

This thesis is approved, and it is acceptable in quality and form for publication:

Approved by the Thesis Committee:

Dr. Arup K. Maji

, Chairperson

Dr. Mahmoud Reda Taha

Dr. Rafiqul A. Tarefder

**PRACTICAL CONSIDERATIONS IN DETERMINING TIMBER
PILE DEPTH USING THE SONIC ECHO METHOD**

by

ALI F. JWARY

**BACHELOR OF SCIENCE, ENVIRONMENTAL
ENGINEERING, AL MUSTANSIRIYA UNIVERSITY, 2003**

**BACHELOR OF SCIENCE, CIVIL ENGINEERING,
UNIVERSITY OF NEW MEXICO, 2014**

THESIS

Submitted in Partial Fulfillment of the
Requirements for the Degree of

Master of Science

Civil Engineering

The University of New Mexico
Albuquerque, New Mexico

May, 2017

DEDICATION

I dedicate this thesis to my wife, Esraa, and children, Sarah, Mohammed and Ghada Jwary. Thank you for all of your support and the sacrifices that you have made for me. I love you, forever.

ACKNOWLEDGEMENT

I hereby extend special thanks to my advisor and committee chairperson, Dr. Arup Maji, for his support and guidance for my education during my graduate study at the University of New Mexico. His patience, insight, and guidance over the years has been invaluable, and will remain with me throughout my career. I also wish to extend thanks to my committee members, Dr. Mahmoud Reda Taha and Dr. Rafiqul A. Tarefder, for agreeing to serve on my committee. I would also like to thank my fellow graduate student, Saman Rashidyan, for his assistance with the conducting the field tests. Particular thanks must go to New Mexico Department of Transportation for their financial support of the project, which I am grateful to have been a part of. Also, I would like to thank all my friends for their love and support over the years. Lastly, I wish to acknowledge the cooperation, sacrifice and unconditional support from my wife Esraa Jwary throughout my graduate studies.

PRACTICAL CONSIDERATIONS IN DETERMINING TIMBER PILE DEPTH USING THE SONIC ECHO METHOD

by

Ali F. Jwary

B.S., Environmental Engineering, Al Mustansiriya University, 2003

B.S., Civil Engineering, University of New Mexico, 2014

M.S., Civil Engineering, University of New Mexico, 2017

ABSTRACT

The Federal Highway Administration indicates that about 85,000 bridges in the United States have no original contract documents with information about the type, depth, geometry and material of their foundations (FHWA, 2010). Furthermore, the National Bridge Inventory (NBI) provides information about 86,133 bridges nationwide that are rated as scour critical because of unknown foundation condition. In New Mexico, there are more than 281 bridges with unknown foundations, which are owned by the New Mexico Department of

Transportation; 71 of these are timber bridges. These data indicate a serious problem that needs decisive action to assess the unknown bridge foundation characteristics (types and depths of foundation) in order to evaluate the scour safety risk of timber bridges in New Mexico.

The objective of this study was to investigate the effectiveness of using the Sonic Echo (SE) method to determine unknown bridge foundation depths. The SE method was observed to be suitable for determining unknown pile depths for bridges that are supported by timber pile abutments or timber pile bents. The SE test method provides reliable and reasonable results for determining all tested piles with an accuracy of ± 15 percent. The SE tests were conducted on seventeen timber piles in different locations in New Mexico. The success rate of using the Sonic Echo method to determine the depth of unknown bridge piles is 94%. The range of the depths of tested timber piles was 16 feet to 38 feet.

TABLE OF CONTENTS

LIST OF FIGURES.....	x
LIST OF TABLES	xiv
Chapter 1 Introduction.....	1
1.1 Background	1
1.2 Problem Statement.....	1
1.3 Thesis Outline	2
Chapter 2 Literature Review.....	4
2.1 Introduction.....	4
2.2 Sonic Echo (SE) Definition	5
2.3 Impulse Response (IR) Definition.....	6
2.4 Limitation of Using SE/IR.....	6
2.5 Stress and Strain and Hooke’s Law	7
2.6 Stress Wave Within Solid Medium	8
2.7 Sound Wave Attenuation.....	9
2.8 Sound Wave Generation	11
2.9 Timber Bridges and Foundations	11
2.9.1 Beam Superstructures.....	12
2.9.2 Log Beams	13
2.9.3 Sawn Lumber Beams	13
2.9.4 Glued-Laminated Timber Beams	13
2.9.5 Laminated Veneer Lumber Beams.....	14
2.9.6 Bridge Substructures.....	14
2.9.7 Pile Abutments	14
2.9.8 Pile Bents	15
2.9.9 North American Timber Piles.....	15
2.10 Previous Work.....	16

Chapter 3 Experimental Methods	19
3.1 Introduction.....	19
3.2 Sonic Echo Test	19
3.2.1 SE Test Methodology	19
3.2.2 SE Test Procedure	21
3.2.3 Equipment and Materials.....	22
3.2.4 SE Data Processing, Display and Interpretation.....	26
3.3 Determination of Sound Wave Velocity Value Within the Timber Pile ...	27
3.4 Validation of SE Test Results	31
3.5 Site Selection and SE Test Field Application	34
3.5.1 Characteristics of Biology Annex Building Wooden Column	34
3.5.2 Characteristics of Bridge #1676	35
3.5.3 Characteristics of Bridge #6922	36
3.5.4 Characteristics of Bridge #1190	37
Chapter 4 Finite Elements Method	39
4.1 Introduction.....	39
4.2 Modeling and Simulation	39
4.3 Wooden Column Model.....	40
4.4 Influence of Impulse Shape on the Propagated Wave Travel Time	44
4.5 Influence of Boundary on the Propagated Wave Travel Time	47
4.6 Influence of Damping on the Propagated Wave Travel Time	49
4.7 Conclusion	52
Chapter 5 Results and Discussion	53
5.1 Introduction.....	53
5.2 Sonic Echo Field Test	53
5.2.1 Wooden Column of Biology Annex Building SE Field Test Results ...	53
5.2.2 Bridge #1676 SE Field Test Results	56
5.2.2.1 Determination of Wave Velocity Within Timber Pile	56
5.2.2.2 Pile C-1	58

5.2.2.3 Pile C-2.....	64
5.2.2.4 Pile B-4.....	67
5.2.3 Bridge #6922 SE Field Test Results	71
5.2.3.1 Determination of Wave Velocity Within Timber Pile	71
5.2.3.2 Pile 1	73
5.2.3.3 Pile 2	79
5.2.3.4 Pile 3	81
5.2.3.5 Pile 14	84
5.2.4 Bridge #1190 SE Field Test Results	86
5.2.4.1 Determination of Wave Velocity Within Timber Pile	86
5.2.4.2 Pile 8	87
5.2.4.3 Pile 21	89
5.3 Validation of SE Test Results	95

Chapter 6 Conclusion and Recommendations 98

6.1 Summary	98
6.2 Recommendation for Future Studies.....	99

References..... 101

LIST OF FIGURES

Figure 2-1: SE/IR Test Equipment and Test Reflection Theory	5
Figure 2-2: Sketch Shows Basic Components of a Timber Bridge	12
Figure 3-1: Mounting the Wooden Blocks and Attaching the Accelerometers	22
Figure 3-2: Types of Hammer Tips Used in SE Test.	23
Figure 3-3: Equipment and Hardware Components Used for SE Test.....	24
Figure 3-4: Aluminum Block Attaches to Side of Pile for Hammer Strike	25
Figure 3-5: Wooden Block Used to Attach Accelerometer	25
Figure 3-6: Wooden Block Attaches to Side of Pile for Hammer Strike	25
Figure 3-7: SE Test Setup and Typical Velocity Trace- Showing Clear Signal Bottom Echo	27
Figure 3-8: SE Test Setup to Determine the Wave Velocity Using Bridge Girder	28
Figure 3-9: Velocity Trace- Accelerometer 1- Bridge #1676 Girder	29
Figure 3-10: Velocity Trace-Accelerometer 2- Bridge #1676 Girder	29
Figure 3-11: The Joined Girder of Timber Bridge	30
Figure 3-12: Alternative Approaches Used for Estimation the Wave Velocity	31
Figure 3-13: IR Mobility Plot for Test b1 Showing Unclear Frequency Spacing-Bridge #1190	33
Figure 3-14: Typical IR Mobility Plot Showing Clear Frequency Spacing-Bridge #6922 ...	34
Figure 3-15: Biology Annex Building Wooden Column and SE Test Setup.....	35
Figure 3-16: Location and Street View of Bridge #1676	36
Figure 3-17: Piles Distributed Plan and Locations of Tested Piles of Bridge #1676.....	36
Figure 3-18: Location and Street View of Bridge #6922	37
Figure 3-19: Piles Distributed Plan and Locations of Tested Piles of Bridge #6922.....	37
Figure 3-20: Location and Street View of Bridge #1190	38
Figure 3-21: Piles Distributed Plan and Locations of Tested Piles of Bridge #1190.....	38
Figure 4-1: Timber Column Modeled Using Abaqus Software	40
Figure 4-2: Nodes #3901, #2620, and #1657 Locations on Timber Column Model.....	41
Figure 4-3: Stress Wave Propagation into Timber Column Model.....	42
Figure 4-4: Acceleration History Response for Nodes #3901, #2629, #1657	43
Figure 4-5: Velocity History Response for Nodes #3901, #2629, #1657	43
Figure 4-6: Velocity History Responses of Node #3901, #2629, #1657	44
Figure 4-7: Acceleration History Response of Node #3901- Sinusoidal Load Shape	45

Figure 4-8: Acceleration History Response of Node #3901- Rectangular Load Shape .	45
Figure 4-9: Acceleration History Response of Node #3901- Triangular Load Shape	45
Figure 4-10: Velocity History Response of Node #3901- Sinusoidal Load Shape	46
Figure 4-11: Velocity History Response of Node #3901- Rectangular Load Shape	46
Figure 4-12: Velocity History Response of Node # 3901- Triangular Load Shape.....	46
Figure 4-13: Acceleration History Responses of Node #3901 With Different Boundaries	47
Figure 4-14: Velocity History Responses of Node #3901 With Different Boundaries.....	48
Figure 4-15: Acceleration History Response of Node #3901, $\alpha=0.002$, $\beta=0.0002$	50
Figure 4-16: Velocity History Response of Node #3901, $\alpha=0.002$, $\beta=0.0002$	51
Figure 4-17: Acceleration History Response of Node #3901, $\alpha=0.05$, $\beta=0.0002$	51
Figure 4-18: Velocity History Response of Node #3901, $\alpha=0.05$, $\beta=0.0002$	51
Figure 5-1: Velocity Trace of SE Test Conducted on the Wooden Column- Ch7.....	55
Figure 5-2: SE Field Test Conducted on Bridge #1676 Girder to Measure Wave Velocity	57
Figure 5-3: Velocity Trace Using Hard Tip.....	57
Figure 5-4: Velocity Trace Using Medium Hard Tip	57
Figure 5-5: Velocity Trace Using Medium Soft Tip.....	58
Figure 5-6: Velocity Trace Using Soft Tip	58
Figure 5-7: The Image of Pile C-1 and SE Test Setup	59
Figure 5-8: Velocity Trace of SE Test No. b1 Using Hard Tip- A Downward.....	60
Figure 5-9: Velocity Trace of SE Test No. b2 Using Medium Hard Tip- A Downward ...	61
Figure 5-10: Velocity Trace of SE Test No. b3 Using Medium Soft Tip- A Downward ..	61
Figure 5-11: Velocity Trace of SE Test No. b4 Using Soft Tip- A Downward.....	61
Figure 5-12: Velocity Trace of SE Test No. b9 Using Hard Tip- B Upward	61
Figure 5-13: Velocity Trace of SE Test No. b14 Using Medium Hard Tip- B Upward....	62
Figure 5-14: Velocity Trace of SE Test No. b15 Using Medium Soft Tip- B Upward	62
Figure 5-15: Velocity Trace of SE Test No. b16 Using Soft Tip- B Upward	62
Figure 5-16: Velocity Trace of SE Test No. b20 Using Hard Tip- Wooden Block.....	62
Figure 5-17: Velocity Trace of SE Test No. b21 Using Medium Hard Tip- Wooden Block	63
Figure 5-18: Velocity Trace of SE Test No. b22 Using Medium Soft Tip- Wooden Block	63
Figure 5-19: Velocity Trace of SE Test No. B23 Using Soft Tip- Wooden Block.....	63

Figure 5-20: SE Test Setup of Pile C-2	65
Figure 5-21: Force Versus Time Graph Obtained from Hammer Sensor Using Softer Tip	66
Figure 5-22: SE Test Setup of Pile B-4.....	67
Figure 5-23: Velocity Trace of SE Test No. d1 Using Hard Tip- A Downward.....	69
Figure 5-24: Velocity Trace of SE Test No. d5 Using Hard Tip- C Upward.....	69
Figure 5-25: Velocity Trace of Test No. d9 Using Hard Tip- B Downward	69
Figure 5-26: Velocity Trace of Test No. d13 Using Hard Tip- D Downward on Pavement	69
Figure 5-27: Velocity Trace Shows Difficulty in Identifying the Initial Echo When the Strike is Conducted on Concrete Pavement	71
Figure 5-28: Velocity Trace Test No.m1 Using Peak Point Approach- CH5.....	72
Figure 5-29: Velocity Trace Test No. m1 Using Peak Point Approach- CH6.....	72
Figure 5-30: Velocity Trace Test No. m2 Using Peak Point Approach- Ch5	73
Figure 5-31: Velocity Trace Teat No. m2 Using Peak Point Approach- Ch6.....	73
Figure 5-32: The Image of Pile 1 and SE Test Setup	74
Figure 5-33: Velocity Trace of SE Test No.m1- Ch5- Using Hard Tip- A Downward.....	75
Figure 5-34: Velocity Trace of SE Test No. m1- Ch6- Using Hard Tip- A Downward....	75
Figure 5-35: Velocity Trace of SE Test No. m5- Ch5- Using Medium Hard Tip- A Downward	76
Figure 5-36: Velocity Trace of SE Test No. m5- Ch6- Using Medium Hard Tip- A Downward	76
Figure 5-37: Velocity Trace of SE Test No. m7- Ch5- Using Medium Soft Tip- A Downward	76
Figure 5-38: Velocity Trace of SE Test m7- Ch6- Using Medium Soft Tip- A Downward	76
Figure 5-39: Velocity Trace of SE Test m11- Ch5- Using Medium Hard Tip- Downward on Aluminum Block.....	78
Figure 5-40: Impulse Graph of the Hammer for Test m11 Shows Two Peaks	78
Figure 5-41: Typical Impulse Graph- Shows One Clear Peak	78
Figure 5-42: SE Test Setup for Pile 2 of Bridge #6922	80
Figure 5-43: Velocity Trace of SE Test No. m20 Using Medium Sot Tip Shows Unclear Initial Impulse	80
Figure 5-44: Test Setup for Pile 3 of Bridge #6922.....	81

Figure 5-45: Velocity Trace of SE Test No. m25 Using Hard Tip- Wooden Block.....	82
Figure 5-46: Velocity Trace of SE Test No. m26 Using Hard Tip- Wooden Block.....	83
Figure 5-47: Velocity Trace of SE Test No. m27 Using Hard Tip- Wooden Block.....	83
Figure 5-48: SE Test No. m32 Using Medium Hard Tip & Aluminum Block Shows Unclear Initial Impulse	84
Figure 5-49: SE Test Setup for Pile 14 of Bridge #6922	84
Figure 5-50: Longitudinal Crack Along Pile 14.....	85
Figure 5-51: SE Test Setup for Pile 8 of Bridge #1190	88
Figure 5-52: Velocity Trace of SE Test No. t14 Using Hard Tip- On Pile Top Edge.....	89
Figure 5-53: Velocity Trace of SE Test No. t17 Using Medium Hard Tip- On Pile Top Edge	89
Figure 5-54: Velocity Trace of SE Test No. t18 Using Medium Soft Tip- On Pile Top Edge	89
Figure 5-55: SE Test Setup for Pile 21 of Bridge #1190	90
Figure 5-56: Velocity Trace of SE Test No. c1 - Using Hard Tip- A Downward- Ch6	91
Figure 5-57: Velocity Trace of SE Test No. c5- Using Medium Hard Tip- A Downward- Ch6	92
Figure 5-58: Velocity Trace of SE Test No. c7- Using Medium Soft Tip- A Downward- Ch6	92
Figure 5-59: Velocity Trace of SE Test No. c10- Using Soft Tip- A Downward- Ch6	92
Figure 5-60: Velocity Trace of SE Test No. c14 - Using Hard Tip- B Upward- Ch6	93
Figure 5-61: Velocity Trace of SE Test No. c17- Using Medium Hard Tip- B Upward- Ch6	94
Figure 5-62: Velocity Trace of SE Test No. c20- Using Medium Soft Tip- B Upward- Ch6	94
Figure 5-63: Velocity Trace of SE Test No. c22 - Using Soft Tip- B Upward- Shows Unclear Echo	94
Figure 5-64: IR Mobility Plot for Test No. m1 Using Hard Tip- Pile 1- Bridge #6922	96
Figure 5-65: IR Mobility Plot for Test No. m5 Using Medium Hard Tip- Pile 1- Bridge #6922	96
Figure 5-66: IR Mobility Plot for Test No. m7 Using Medium Soft Tip- Pile 1- Bridge #6922	96

LIST OF TABLES

Table 3-1: Determined Sound Wave Velocity in Common Types of Timber Piles.....	28
Table 5-1: Characteristics and Results of SE Field Test for the Wooden Column	55
Table 5-2: Estimated Wave Velocities into Piles of Bridge #1676.....	58
Table 5-3: Strike Direction of Pile C-1	59
Table 5-4: Characteristics and Results of SE Field Test for Pile C-1	60
Table 5-5: Strike Directions on Pile C-2.....	65
Table 5-6: Characteristics and Results of SE Field Test for Pile C-2	66
Table 5-7: Strike Direction on Pile B-4.....	68
Table 5-8: Characteristics and Results of SE Field Test for Pile B-4	68
Table 5-9: Piles Depths Assessment for Bridge #1676.....	71
Table 5-10: Estimated Wave Velocity Using Peak Point Approach for Bridge #6922.	73
Table 5-11: Characteristics and Results of SE Field Test for Pile 1	75
Table 5-12: Characteristics and Results of SE Field Test for Pile 2.....	80
Table 5-13: Characteristics and Results of SE Field Test for Pile 3.....	82
Table 5-14: Characteristics and Results of SE Field Test for Pile 14	85
Table 5-15: Piles Depths Assessment for Bridge #6922	86
Table 5-16: Characteristics and Results of SE Field Test for Pile 8.....	88
Table 5-17: Characteristics and Results of SE Field Test for Pile 21	91
Table 5-18: Piles Depths Assessment for Bridge #1190	95
Table 5-19: Validation of the Pile 1 Depth Using Resonant Frequency Approach	97

Chapter 1

Introduction

1.1 Background

The Federal Highway Administration indicates that about 85,000 bridges in the United States have no original contract documents with information about the type, depth, geometry and material of their foundations (FHWA,2010). Furthermore, the National Bridge Inventory (NBI) provides information about 86,133 bridges nationwide that are rated as scour critical because of unknown foundation conditions. In New Mexico, there are more than 281 bridges with unknown foundations, which are owned by the New Mexico Department of Transportation; 71 of these are timber bridges. These data indicate a serious problem that needs decisive action to assess the unknown bridge foundation characteristics (type and depth of foundation) in order to evaluate the scour safety risk of timber bridges in New Mexico.

A wide range of possible Non Destructive Tests (NDT) could be used to determine the foundation depth. For purposes of this research, only timber bridges will be investigated, by using the Sonic Echo (SE) method to evaluate unknown foundation depths. The Impulse Response (IR) method is used to validate the data that is obtained from the SE test.

1.2 Problem Statement

Knowing the depth of bridge foundations is a very important factor for the New Mexico Department of Transportation (NMDOT) to evaluate bridge safety. At

present, many Non Destructive Tests (NDT) are used to evaluate bridge foundation types and depths. Some of these methods are costly because they require additional boring to perform the tests.

In this study, the Sonic Echo (SE) test was utilized to determine unknown foundation depths for three different timber bridges that are located in New Mexico. The advantages of using the SE method are that it uses low-cost equipment, the testing is inexpensive, and it does not need additional boring. In addition, it is effective for identifying the depth of exposed piles as a proven and potential NDT method for evaluating unknown bridge foundations (Olson et al. 1998).

The objectives of this research were to investigate the effectiveness of the SE method and to describe the technical procedure to evaluate unknown timber bridge pile depths and types. As part of this effort, the IR method was used to validate the results that were obtained from using the SE test. In addition, the SE test was conducted on a wooden column and three bridges located in New Mexico. The site numbers of these bridges, as listed in the NMDOT documents, are Bridge #1676, Bridge #6922, and Bridge #1190.

1.3 Thesis Outline

Chapter 2 of this thesis contains the literature review of the SE/IR tests and stress wave theory, including the definition, theoretical equations, and test limitations. Brief introductions are given about key terms; stress, strain, Hooke's law, pile impedance, sound wave generation, and about timber bridge and timber pile types. The chapter concludes with a literature review of previous SE applications and similar practices. Chapter 3 describes the SE test procedure and

setup, as well as the equipment and materials used, and SE data interpretation and analysis. Chapter 4 provides finite element analysis about wooden column models and investigates the impact of load shape, pile boundary condition, and damping on lapse times of stress wave (wave travel time) and on velocity trace shapes. Chapter 5 presents the SE test results and data interpretation with discussion. Finally, Chapter 6 summarizes and concludes the research project with recommendations for future work.

Chapter 2

Literature Review

2.1 Introduction

According to the Federal Highway Administration, about 85,000 bridges in the United States have no original contract documents with information about the type, depth, geometry and material of their foundations (FHWA,2010). Furthermore, the National Bridge Inventory (NBI) provides information about 86,133 bridges nationwide that are rated as scour critical because of unknown foundation conditions. In New Mexico, there are more than 281 bridges with unknown foundations, which are owned by the New Mexico Department of Transportation; 71 of these are timber bridges. These data indicate a serious problem that requires taking action soon to assess the unknown bridge foundation characteristics (type and depth of foundation) in order to evaluate the scour safety risk of timber bridges in New Mexico.

This chapter begins with brief definitions of Sonic Echo testing and Impulse Response testing, and then describes the limitations of using SE/IR tests. Then brief explanations follow about stress, strain, and Hooke's law, and longitudinal and shear waves equations within a solid medium. The chapter then provides an introduction about sound wave attenuation and pile impedance as well as sound wave generation. This will include brief introductions to timber bridge components and timber pile types. Finally, a literature review about the history of SE application is provided.

2.2 Sonic Echo (SE) Definition

The Sonic Echo Test (SE) is a low strain integrity test performed by striking the top of the pile with a light hammer and then measuring the response of the pile using a sensor attached to the top of pile or on the pile side in order to assess the pile condition and to determine unknown depths for existing bridge piles. The SE method could also be used to determine the depth of a shallow foundation. The SE method is based on issuing a hammer blow that generates a compressive stress wave, which is transmitted down to the pile tip, and then is partly reflected back towards the pile head by any change in the pile impedance within the pile. Among the kinds of examples of change in the pile impedance are cracks, necks, bulbs, soil intrusions, voids, etc. (Olson et al., 1998). The SE schematic diagram illustrating this process is presented in Figure 2-1.

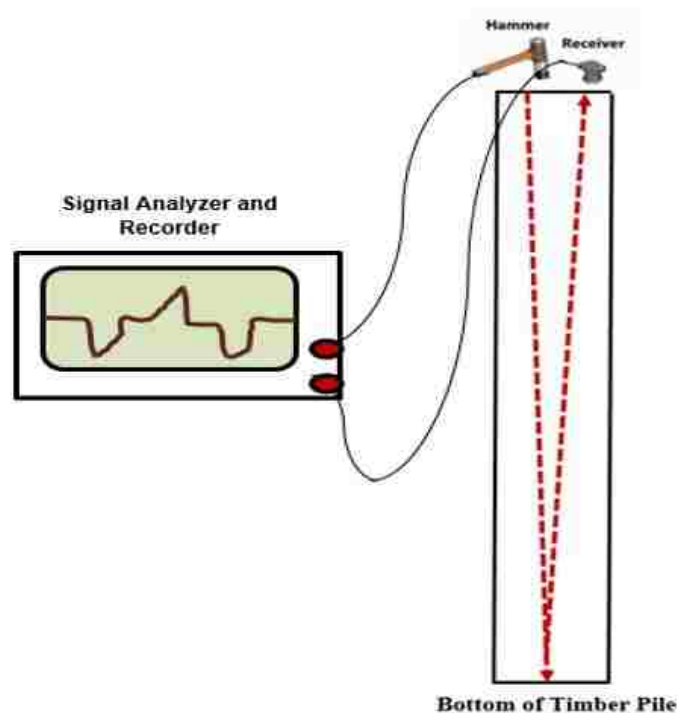


Figure 2-1: SE/IR Test Equipment and Test Reflection Theory

2.3 Impulse Response (IR) Definition

The IR test procedures are similar to those used with the SE test. IR is also a low strain integrity test performed by striking the top or upper side of the pile with a light hammer, and using the same test equipment as for the SE test. The data processing is different, however. The IR method utilizes frequency domain data processing. The vibration of the pile is measured by a geophone serving as a receiver, and then the results are processed with Fast Fourier transform (FFT) algorithms to generate transfer functions for analysis (Olson et al., 1998). The combination of the SE and IR tests are proven to be effective and potential Non Distractive Test methods for determination of the unknown characteristics of bridge foundations (Olson et al. 1998).

2.4 Limitation of Using SE/IR

It is necessary to understand the limitations of conducting SE/IR tests on timber piles in order to achieve an optimal test performance and to develop a reasonable interpretation. This section provides the limitations of the SE/IR tests as follows:

1. **Accessibility:** the basic requirement for performing a SE/IR test is to have an access area (3 inches X 5 inches) on the pile top. In cases where there is no such access to the pile top, alternative methods can be used to perform the test (see Chapters 3 and 5) (Olson et al. 1998).
2. **Impedance changes:** If there are gradual changes in the pile cross section, the reflection from the pile tip may not be detected. The reflection may be affected by any irregularities such as cracks, necks, bulbs, soil intrusions and

voids, etc. (Olson et al. 1998). Thus, testing more than 2 piles is recommended to avoid errors in depth assessments. The performance of SE/IR is better for timber piles that have constant cross-sections. The data may be neglected if there is any known defect in the pile integrity in order to avoid error in the assessment of pile depth.

3. **Length to diameter ratios:** SE/IR testing is effective for use with timber if the length to diameter ratios are more than 10 but do not exceed 50.
4. **Connection:** this refers to providing a smooth connection between the accelerometer and the pile top surface to ensure obtaining clean transmission of the stress wave to the pile tip. Providing a strong connection between the block that is used for the impact and the pile side surface reduces the possibility of having any sliding with the impact. Also, if the force versus time graph has two peaks, these results should be neglected as this is due to sliding.
5. **Test Repeating:** The SE test must be repeat at least three times to avoid erroneous readings.

2.5 Stress and Strain and Hooke's Law

Stress refers to the intensity of internal forces acting within a body, while strain indicates the deformation of the body that is caused by the stress (Hibbeler, R. C. 2005). First, consider the axial force applied to the top of the pile by a hammer; then the normal stress σ is the internal pressure within the pile, which equals the impacting force divided by the pile's cross sectional area:

$$\sigma = \frac{F}{A} \tag{2.1}$$

Where σ is the normal stress in psi, F is the impact force in lbs. and A is the pile's cross sectional area in square inches (in²). The strain ϵ is the displacement per unit length which is equal to:

$$\epsilon = \frac{\Delta l}{l} \quad 2.2$$

The relationship between stress and strain in a one-dimension case is a linear relationship within the elastic region. Consequently, an increase in stress causes a proportionate increase in strain. This fact was discovered by Robert Hooke in 1676 using springs and is known as Hooke's Law. It may be expressed mathematically as follows:

$$\sigma = E * \epsilon \quad 2.3$$

Where, E is Young's modulus

2.6 Stress Wave Within Solid Medium

A stress wave is a mechanical stress that is propagated into a solid medium in the form of a wave (Kolsky, 1963). The propagation of the stress wave within the solid medium causes an elastic movement of the particles of the medium. The stress waves move in the solid material as longitudinal waves and shear waves. Longitudinal waves are also called P-waves, compression waves, or primary waves, which direct the displacements of particles in the direction of wave propagation. Shear waves are also called S-waves, or transverse waves, which cause the particle displacements to occur perpendicular to the direction of the wave propagation. Rayleigh waves may also exist, occurring at the boundary of two medias that have different levels of stiffness or resistance such as with the timber pile and the soil. The velocity at which the oscillated particle travels is a

function of the elastic properties of the material and its density as shown in Eq. 2.4 and Eq. 2.5.

$$V_c = \sqrt{\frac{E}{\rho}} \quad 2.4$$

$$V_s = \sqrt{\frac{G}{\rho}} \quad 2.5$$

Here V_c is the phase velocity or longitudinal wave propagation velocity in the media. While V_s is the shear wave propagation velocity. Eq.2.4 is valid for longitudinal plane wave propagation in the solid medium where the wavelength is greater than the diameter or thickness of the propagation media. For instance, this occurs when the large wavelength propagation in the timber pile corresponds to a low frequency wave. Eq.2.4 does not work for propagating wavelengths that are smaller than the thickness of media such as a wave that is propagated within soil.

2.7 Sound Wave Attenuation

Many factors affect the attenuation of sound waves in solid material, such as material damping, homogeneity and inhomogeneity of the propagating media, and reflection from the change in stiffness (impedance). However, when load F is applied at the top of a pile, the pile will be vibrated and sound waves will be generated within the pile. The applied load and the particle velocity V_p at a specific point are related as follows:

$$F = Z * V_p \quad 2.6$$

Here Z is a constant called “pile impedance” which represents the measurement of the pile’s resistance to the sound velocity. Pile impedance is

proportional to Young's modulus E and the cross sectional area A of the pile. Since it is inversely proportional to the sound velocity V_c , the relationship can be expressed by applying Eq. 2.7:

$$Z = \frac{E * A}{V_c} \quad 2.7$$

Assume for example that the impedance changes from Z_1 to Z_2 at a certain depth down the pile. If the downward stress wave that is designated as W_i arrives at this depth, part of the wave is reflected upward (W_u) and part will transmit downwards (W_d), so that here both continuity and equilibrium will be satisfied (Hertlein & Davis, 2007). The simultaneous equations solution provides the following results:

$$W_d = W_i \left[2 * \frac{Z_2}{(Z_2 + Z_1)} \right] \quad 2.8$$

$$W_u = W_i \left[\frac{(Z_2 - Z_1)}{(Z_2 + Z_1)} \right] \quad 2.9$$

If the pile has a uniform cross sectional area, then $Z_1 = Z_2$, and neither W_d nor W_u are generated and W_i will never change. At the pile's tip, Z_2 is zero, the compressive downward stress wave will be completely reflected upwards and W_u will be in opposite sign (tensile upward stress wave). Producing a tensile wave occurs due to decreases in the stiffness of the pile (decreasing in either the cross sectional area A , or Young's modulus E). Simultaneously, the production of a compressive wave will occur due to increases in the stiffness of the pile. The concept of pile impedance could be depicted using a signal-response curve. The tensile reflected waves coming from the bottom of pile will arrive at the top of the

pile and produce a positive peak on the signal-response curve, while the compressive reflection waves with increasing pile stiffness (such as a pile on bedrock) will produce a negative peak on the response curve (Hertlein & Davis, 2007).

2.8 Sound Wave Generation

For Impact Echo, the frequency of the wave generated depends on the stiffness (Elastic modulus) of the impacting material (E_i) and the structure being inspected (E_s), as well as the radius of curvature r and density of the impactor ρ , and the velocity of the impact (v). The frequency of the sound wave generated is inversely proportional to the duration of the impact t and can be approximated by Eq. 2-10 (Maji et. al, 1990, based on Hertzian contact theory).

$$\frac{1}{f} \propto t \propto \rho \left(\frac{1}{E_i} + \frac{1}{E_s} \right)^{0.4} \frac{r}{v^{0.05}} \quad 2.10$$

Therefore, it is possible to adjust the amplitude (related to the energy content) and the frequency of the sound wave imparted to conduct the inspection using tips of different materials and by adjusting the impact velocity. Maji et al. (1990) used high-velocity impacts to conduct Impact Echo inspections of concrete slabs and to locate rebar close to the surface.

2.9 Timber Bridges and Foundations

The types and configurations of timber bridges vary greatly depending on the designs used and year of development. Some timber bridges in the United States were constructed many years ago and others were constructed using

modern technological advances in timber design. However, all timber bridges consist of two parts, the superstructure and the substructure, as shown in Figure 2-2. The components of the superstructure span include the deck, floor system, main supporting members, and railings. The types of superstructure are beam, deck, truss arch, and suspension superstructures. The timber substructure types consist of abutments and bents. Abutments support the bridge ends, while the bents are intermediate supports for multiple span bridge (Ritter, M. A. 1990). Timber bridges are classified based on the type of superstructure such as beam superstructures, longitudinal deck superstructures, trusses, trestles, glulam deck arches, and suspension bridges. More information is available in the National Design Specification (NDS). Here a brief introduction is being provided about beam superstructures.

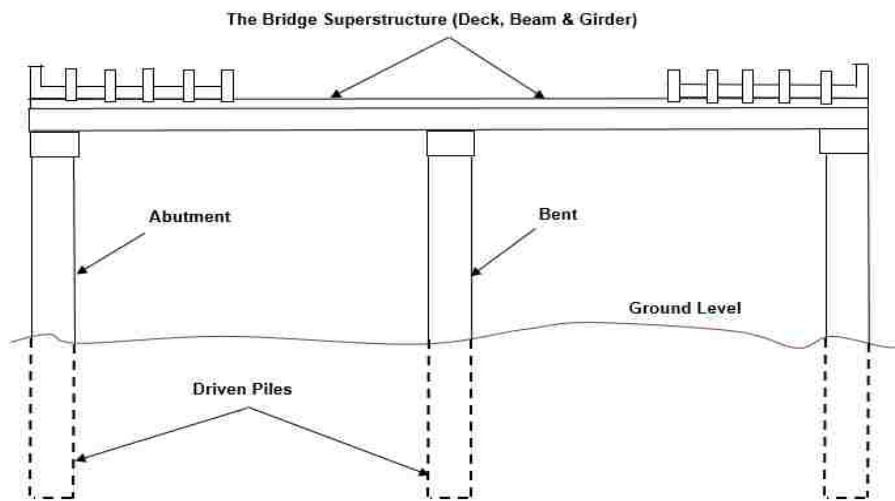


Figure 2-2: Sketch Shows Basic Components of a Timber Bridge

2.9.1 Beam Superstructures

Longitudinal beam superstructures are the most common timber bridge types in the United States. These consist of a deck system that is supported by a

series of timber beams between the supports. The main types of wood that are used in the beam bridges are logs, sawn lumber, glued-laminated timber, or laminated veneer lumber (Ritter, M. A. 1990).

2.9.2 Log Beams

Log beam is the simplest type of timber bridge. The round logs are bound together alternately tip to butt using steel cables. Transverse logs are attached under the bridge deck at the centers, and span to distribute the load. The deck is constructed using sawn lumber planks placed across the log tops or by placing soil on the logs. The most common clear spans range from 20 to 60 feet (Ritter, M. A. 1990).

2.9.3 Sawn Lumber Beams

Sawn lumber beam bridges are constructed using lumber beams 4 to 8 inches wide and 12 to 18 inches deep. The most common clear spans range from 15 to 25 feet. For longer bridges, a series of simple spans are used with intermediate supports. Many of this type of bridge were built in the 1930's and 1940's and they are still in service across the United States (Ritter, M. A. 1990).

2.9.4 Glued-Laminated Timber Beams

Glulam beams are constructed from bonding 1-1/2 inch- or 1-3/8 inch- thick lumber laminations together on their faces using waterproof structural adhesive. The beam widths in standard beams range from 3 to 14-1/4 inches. The clear spans are much longer than sawn lumber beam bridges, and the most common spans range from 20 to 80 feet. The first glulam beam bridges in the United states were built in the 1940's (Ritter, M. A. 1990).

2.9.5 Laminated Veneer Lumber Beams

Laminated veneer lumber comprises a subcategory of new products called structural composite lumber. It is made by gluing thin veneer sheets together, which is similar to how plywood products are produced. The thickness of veneer laminations is 1/10 inch to 1/2 inch (Ritter, M. A. 1990).

2.9.6 Bridge Substructures

The substructure is the portion of the bridge that support the superstructures and transfers loads to the soil. (Ritter, M. A. 1990). Discussion in this section will be limited to abutments and bents constructed of timber piles. Abutments consist of the bridge section that supports the ends of the bridge and contain roadway embankment material. There are three type of abutments: simplest timber abutments, post abutments, and pile abutments (Ritter, M. A. 1990). This section contains a brief introduction about pile abutments and bents as well as brief information about the common types of timber piles that exist and are used in North America.

2.9.7 Pile Abutments

Pile abutments are used when a sufficient support footing type is required. These types of abutments are installed using a pile driven method. The timber piles are driven to a specific depth that is needed to provide a required load capacity at the bridge ends. The superstructure is connected to the pile surface by a continuous or joined cap (beam) at the bearing point (Ritter, M. A. 1990).

2.9.8 Pile Bents

Bents are intermediate supports located between abutments and used for multiple span bridges. These are also constructed from timber piles or sawn lumber frames. For pile bents and pile abutments, bracing between members is required to provide stability and lateral load resistance.

2.9.9 North American Timber Piles

This section provides information about the most common types of timber that used as piles for timber bridges in North America. The piles mentioned are identified by their common timber names in the United States:

1. **Douglas Fir** is found in many varieties in the western part of the United States. The timber is very strong and thus is excellent for use as piles. It is available in long lengths and is commonly used in constructing highway bridges (American Wood Preservers Institute, 2002).
2. **Southern Pine** is found nationwide with many varieties such as longleaf and shortleaf. It is widely used as foundations for highway timber bridges (American Wood Preservers Institute, 2002).
3. **Cypress (southern)** is found in the swamp areas of the Gulf and Atlantic coasts and the Mississippi River Valley. There are many varieties such Tidewater red, Yellow, and White. Cypress has medium strength (American Wood Preservers Institute, 2002).
4. **Oak** is used for various types of short piles. It is an expensive material for piles as compared to other types. There are many types of Oak, all of which are strong and durable (American Wood Preservers Institute, 2002).

2.10 Previous work.

Sonic Echo tests first surfaced in the literature in 1968 as “la méthode d’écho” or the “echo method.” Jean Paquet is the first person who in 1968 published a paper on nondestructive testing of piles in the French National Building and Civil Engineering Annuals, which was translated by Xiang Yee in 1991 (Yee, 1991). Paquet proposed the fundamental theories of stress wave transmission into piles (Hertlein & Davis, 2006). Recently, Li et al. (2012) investigated wave propagation in timber poles, obtaining numerical and experimental results, using Continuous Wavelet Transform (CWT) analysis; Ni et al. (2007) performed the same work for concrete. Li et al. (2012) showed that CWT is an effective method, even when the impact was at middle level of specimens tested or were found to have defects. Chakraborty and Brown (1997) used SE/IR methods to ascertain the lengths of unknown piles for the Alabama River Bridge that has concrete abutments. The results were indicative of pile depth. In addition, Gassman et al. (2000) used impulse response tests to overcome complications related to inaccessibility of pile heads due to the presence of a pile cap or other structure. They showed that the method is limited by the ratio of the tributary area of the intervening structure above the shaft to the area of the drilled shaft, and the ratio of the thickness of the pile cap to the shaft diameter. Moreover, Miranda et al. (2012) studied the propagation of sonic waves through stone masonry walls. They showed that a smooth contact surface with using the accelerometer enhances signal reception. Earlier Sansalone et al. (1991) conducted numerical and experimental studies of solid concrete shafts, as well as shafts containing cracks

and voids and shafts in soil. For solid shafts, they observed characteristic peaks of amplitude spectrum at the depth frequency and its multiples, and determined shaft depth by recognizing the characteristic frequency patterns produced by a solid shaft that consists of the depth frequency and multiples of this fundamental frequency. They showed also that the impact duration should be about equal to or slightly greater than that given theoretically, and that record length should be at least three times the period of multiple wave reflections. They showed that the finite element method can accurately detect the defect size. This was followed by Rausche et al. (1992), who confirmed that time or frequency domain analysis can be utilized to find defects and the pile depth of concrete. Finno et al. (1999) showed that the length of the shafts can be accurately determined with 5% errors based in propagation wave velocities. Regarding timber piles, Anthony and Pandey (1996) demonstrated that the stress wave technique was reliable to with $\pm 15\%$ error for estimating pile lengths of 20-60 feet. Finally, Lo et al. (2010) showed that an analysis of the test results in both the time and frequency domains maximizes the reliability of the readings.

Finno et al. (1999) also demonstrated that the shaft slenderness ratio limits the integrity of the evaluation. Ni et al. (2010) showed that the detectable shaft slenderness ratio is from 10 to 32, depending on the shaft stiffness ratio. Ambrosini and Ezeberry (2005) showed that the impact-echo technique is valid up to the slenderness ratio of 40 for relatively long piles. Meanwhile, Romanescu and Ionescu (2009) tried to organize and document standardized tests to accurately identify the defects and the pile depth of bridges. Moreover, Huang et al. (2010)

investigated the effects of defect size, the ratio of defect depth-to-shaft diameter, and the ratio of shaft-to-soil stiffness on the response of the Sonic Echo test using 3D axisymmetric finite element models. They developed a formula to determine the defect size, correlating these factors simultaneously. This formula is similar to that developed subsequently by Ni et al. (2011) who used flaw depth ratio and stiffness ratio. In the other hand, Soo and Woo (2004) evaluated with numerical and experimental studies the base condition of drilled shafts using the impact-echo method, specifically focused on base conditions such as free, fixed, rock-socketed, and soft-bottom. They applied polarity discrimination techniques to distinguish between the free end and fixed condition in the waveform to identify those base conditions, similar to Baxter et al. (2004). It is important to mention that Gassman et al. (1999) used four geophones to record particle motion that was induced by a hammer impact. This process was used successfully on five inaccessible drilled shafts to reduce the effect of surface waves and reflections caused by pile cap boundaries.

The objective of this study was to investigate the effectiveness of using the Sonic Echo (SE) method to determine unknown bridge foundation depths. SE tests were conducted on 18 piles belong to 3 New Mexico bridges in different locations that were constructed with timber piles. The percentage of success rate of using the Sonic Echo method to determine the depth of unknown bridge piles is 94%. The range of the depths of tested timber piles was 16 to 38 feet, while the Sonic Echo method provided reliable and reasonable results in determining the depths of all tested piles with an accuracy rate of $\pm 15\%$.

Chapter 3

Experimental Methods

3.1 Introduction

This chapter presents the Sonic Echo (SE) test methodology, SE test procedures, SE data processing and interpretation, equipment, materials, and approaches used to determine stress wave velocity propagation magnitudes within timber piles. The chapter begins with describing the methodology of SE testing and the theoretical equations that are used to determine the pile depths of timber bridges. This is followed by explanations of SE test procedures, and defining the equipment and materials that are used for conducting the SE tests in the field. This chapter introduces interpretation of velocity trace obtained from SE tests, and explains the theoretical and experimental approaches to determine the propagated wave velocity magnitude into the timber piles. Finally, the chapter explains how to use the Impulse Response (IR) approach to validate SE test results.

3.2 Sonic Echo Test

3.2.1 SE Test Methodology

The Sonic Echo Test (SE) is a low strain integrity test which is conducted by striking the top of the pile with a light hammer, and measuring the response of the pile with a sensor attached to pile top or mounted to the pile side. The SE test is used to assess the pile condition and to determine the depth of the unknown foundation. The test equipment consists of three devices: a 3-pound hammer (source of energy), a receiver (accelerometer or geophone), and the data

acquisition platform. The hammer blow generates a compressive stress wave that is transmitted down to the pile tip, and then it is partly reflected back towards the pile head by any change in the pile impedance (Hertlein & Davis, 2007).

The stress wave is transmitted into the pile with phase velocity V and time lapse t which are necessary for the stress wave to reach the pile tip and reflect back to the pile head. The receiver measures the vibration response of the pile for each impact. The data acquisition platform collects, processes, and displays the receiver outputs in a velocity versus time graph. The time lapse is identified and analyzed, then it used to assess the echo depth. The equation determines the echo depth (D) by multiplying the reflection time (t) by the stress wave velocity (V) and dividing this quantity by 2:

$$D = \frac{V t}{2} \quad 3.1$$

If the accelerometer is attached on the pile side using a wooden block, then the total depth and buried depth of the pile is determined by using these equations:

$$L_t = \frac{V \Delta t}{2} + d \quad 3.2$$

$$L_b = L_t - h \quad 3.3$$

Where:

L_t represents the total pile depth (ft.), V is the propagated wave velocity (ft./s), Δt is the reflection time, d is the distance from the top of the pile to the accelerometer, L_b is the buried pile depth, and h is the measured distance from the bottom of the pile cap to the ground level.

3.2.2 SE Test Procedure

The general procedure to conducting the SE test is to begin with a level test surface on the top of the pile. The pile top must also be relatively smooth and clean (absence of micro cracking) to ensure clear transmission of the stress wave to the pile tip. In most cases, the pile top is not accessible in the field, so that alternative methods were used to transmit the impact. A rubber tipped hammer is used to generate a low strain compressive wave. In cases of no accessibility, one of three alternative approaches are used to create the impacts:

1. Striking a wooden or aluminum block that is coupled to the pile side.
2. Downward striking on the pile edge or directly on the pile cap.
3. Upward striking on the pile cap close to the top of the pile.

In using the first method, a square wooden block with 4 inches X 4 inches dimensions is used to create the impact. It must be coupled to the pile side with an adhesive material (epoxy) or anchor bolts (anchor bolts are recommended). Another wooden block with 2 inches X 2 inches dimensions is used to attach the accelerometer on top of it. It is recommended to attach the accelerometer as near to the top edge of the pile as possible, using an adhesive material (epoxy) as shown in Figure 3-1.

The American Society for Testing and Material (ASTM) standardized the SE testing procedure in ASTM D5882, "Standard Test Method for Low Strain Integrity Testing of Piles."



Figure 3-1: Mounting the Wooden Blocks and Attaching the Accelerometers

3.2.3 Equipment and Materials

The SE test is conducted using three devices: the hammer (with or without a force sensor) as the source of energy, the accelerometer (sensor) as the signal receiver, and the Olson Freedom Data PC as the processor. The hammer mass is between 0.6 and 11 lbs., depending on the size of the pile to be tested. For testing timber piles, smaller hammers are recommended for use because sharp and narrow input pulses are better suited for this task than wider ones; in addition, smaller hammers have shorter rise time and higher frequency content (Hoyle, J. R & Rutherford, S. P. 1987). Shown below in Figure 3-2 are four types of hammer tips that used to conduct the impact which differ in their hardness. Each color represents a different level of hardness: the hard tip is black, the medium hard tip is red, the medium soft tip is dark-brown, and the soft tip is gray.

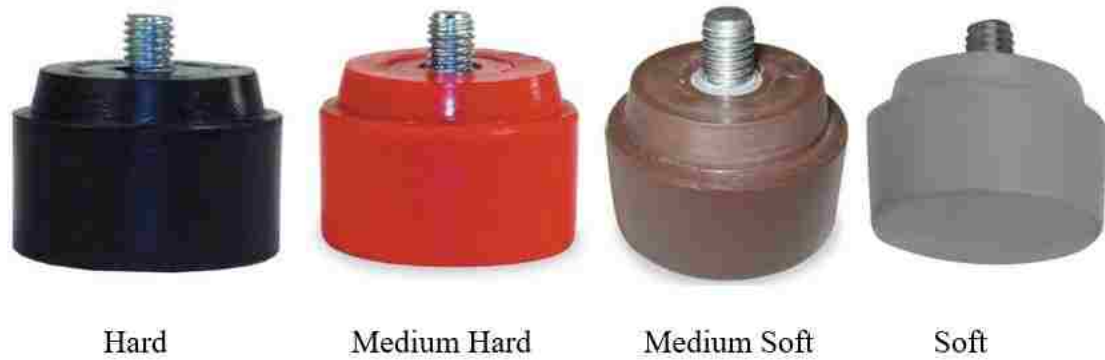


Figure 3-2: Types of Hammer Tips Used in SE Test

Two types of motion sensors that are used in the SE test are accelerometers or geophones. They exhibit different properties in their high and low frequency ranges. The accelerometer represents more truthful results in the high frequencies, while geophones have low frequency range and there is no need for calculating an integration constant. Empirically, all bridges were tested using accelerometers instead of geophones, because geophones weigh more than accelerometers, which makes the attachment process more difficult (Rausche et al., 1992). The Olson Freedom Data PC system consists of basic components, including a platform for data acquisition, analysis and display. A processor depicts the sonic pulse in both a time domain and a frequency domain on an analog oscilloscope. This acceleration is digitally integrated to the velocity traces, which are then easier to interpret (Hertlein & Davis, 2007). Figure 3-3 provides a list of all the equipment, hardware components, and software used in conducting a SE test.



Figure 3-3: Equipment and Hardware Components Used for SE Test

1. One Olson Freedom Data PC
2. One Input Module Containing: one Channel Wideband for Hammer, one Channel Wideband for Accelerometer and one Channel Wideband for Input Geophone
3. One Impulse Hammer
4. One 5.5 Hz Geophone
5. One Accelerometer
6. Two BNC Cables
7. Two BNC 4 Pin Adapter Cables
8. One Female-Female BNC Adapter
9. One Microdot to BNC Cable
10. One Phone Plug to 4 Pin Adapter Cable

11. Coupling Grease

12. Electric Tape

Other equipment, software and hardware components, and material for testing that are not included in Figure 3-3 are:

1. WinTFS Software
2. Filed Notebook and Pen
3. Carpenter Hammer
4. Different Sizes of Wrenches
5. Measuring Tape
6. Portable Electric Drill
7. Different Sizes of Drill Tips
8. Different Sizes of Nails
9. Different Sizes of Bolts and Nuts
10. Occupational Safety and Health Supplies
11. Super Glue
12. 4"X 4" Aluminum Block (Figure 3-4)
13. 2"X 2" Wooden Block (Figure 3-5)
14. 4"X 4" Wooden Block (Figure 3-6)
15. Electric Saw
16. Ladder
17. Portable Plastic Table



Figure 3-4: Aluminum Block Attaches to Side of Pile for Hammer Strike



Figure 3-5: Wooden Block Used to Attach Accelerometer



Figure 3-6: Wooden Block Attaches to Side of Pile for Hammer Strike

3.2.4 SE Data Processing, Display and Interpretation

The signal obtained from accelerometers is integrated to obtain the velocity as mentioned previously. These recorded values of velocity are then plotted versus time as shown in Figure 3-7. Sometime, a reflection may not come from the bottom of the timber pile in cases where there are defects in the pile cross section. The SE test is very sensitive to defects in the cross section of piles. It is also sensitive to soil intrusions when soil gradients surround the pile. Therefore, the propagated wave may reflect from these irregularities thereby making it difficult to accurately determine the depth of piles. For this reason, it is recommended that more than three piles for each bridge be tested in order to be able to compare the test results for piles depths and to avoid having an inaccurate result from testing only one pile.

In general, there are two ways to measure the wave velocity, either by determining this from the material properties of the timber piles, or by measuring it in the field. However, the wave velocity magnitudes for the most common timber piles in North America range from 11000 ft./s to 17000 ft./s, depending on the material properties of the timber pile. Figure 3-7 shows an example of an SE test setup and the velocity trace of a tested timber pile at Bridge #1676. The blue lines in the velocity trace presents the initial wave and the first reflection, respectively. This involves using an estimated wave velocity equal to 14845 ft./s that is propagated into Bridge #1676 piles. For this test, the time difference between the initial response and the initial echo is 3660 μ s. Using Eq. 3.2, as shown below, the total estimated pile depth equals 28 feet:

$$D = \frac{\left(14845 \frac{\text{ft}}{\text{s}} \times 3660 \times 10^{-6} \text{ s}\right)}{2} + 1 \text{ ft.}$$

$$D = 27 \text{ ft.} + 1 \text{ ft.} = 28 \text{ ft.}$$

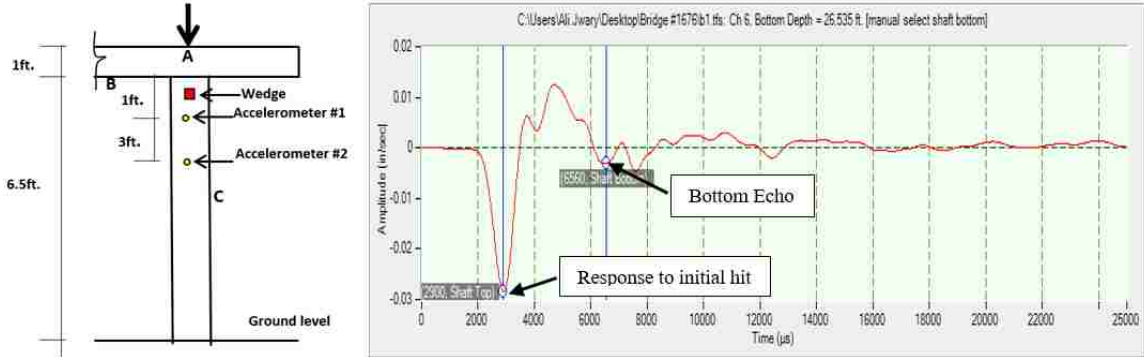


Figure 3-7: SE Test Setup and Typical Velocity Trace- Showing Clear Signal Bottom Echo

3.3 Determination of Sound Wave Velocity Value within the Timber Pile

The sound velocity at which the oscillated particle travels is a function of the elastic properties of the material and its density. Accordingly, the velocity (V), elasticity (E), and density (ρ) relationship is expressed as:

$$V = \sqrt{\frac{E}{\rho}} \tag{3.4}$$

Where:

E is the Elastic modulus of the timber in psf, and ρ is the density in slugs/in³

Table 3-1 shows the sound wave velocity that evaluated using Eq. 3.4 which depends on the mechanical properties of each type of wood for the most common types of timber piles in North America (American Wood Preservers Institute, 2002). Green et al. (1999) disclosed the information about the mechanical properties of

woods that were used in determining the sound wave velocity as shown in Table 3-1.

Table 3-1: Determined Sound Wave Velocity into Common Types of Timber Piles (Green et. al, 1999).

Group No.	Timber Piles		E (psf X10 ⁶)		Specific Gravity	Density slugs/ft ³	Wave velocity ft./s	Type of wood
1	Oak, white	Bur	127	148	0.58	1.1	10612	Hardwood
		White	180	256	0.6	1.2	12435	Hardwood
2	Oak, red	Northern red	194	262	0.56	1.1	13377	Hardwood
		Southern red	164	215	0.52	1	12756	Hardwood
3	Cypress	Southern	132	147	0,93	1.8	12568	Hardwood
4	Southern Pine	Loblolly	216	258	0.47	0.9	15391	Softwood
		Lodgepole	156	193	0.38	0.7	14524	Softwood
		longleaf	216	285	0.554	1.1	14177	Softwood
		Red	184	234	0.41	0.8	15223	Softwood
		Shortleaf	216	252	0.47	0.9	15391	Softwood
5	Douglas Fir	Coast	216	281	0.45	0.9	15730	Softwood

An empirical method that is used in the field for directly determining the propagated wave velocity involves measuring the wave travel time into a known (measured) distance for timber pile or bridge girder. Here accelerometers are used for sensing the propagated wave as it starts at a point near to strike and arrives at another point at the end of the girder. Figure 3-8 shows the SE test setup ready to determine the propagated wave velocity upon entry into the girder of Bridge #1676.

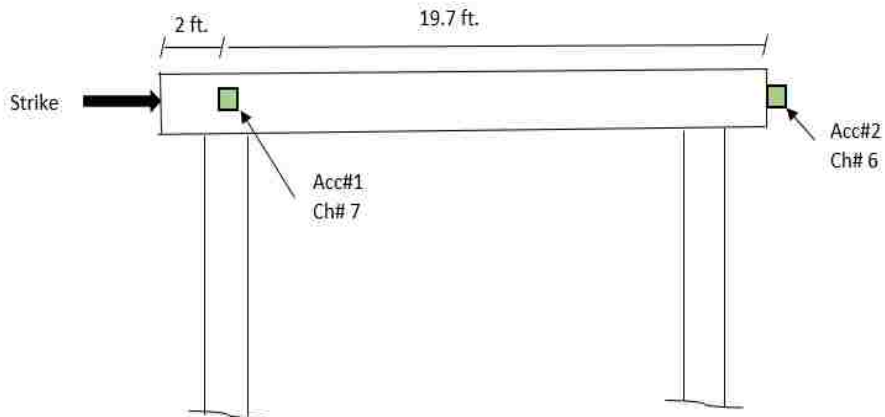


Figure 3-8: SE Test Setup to Determine the Wave Velocity Using Bridge Girder

The Olson Freedom Data PC depicts a collected data for each accelerometer and displays it using a velocity versus time graph. Figures 3-9 to 3-10 show typical velocity versus time graphs that are obtained from conducting the SE test on a girder of Bridge #1676 for both accelerometers respectively:

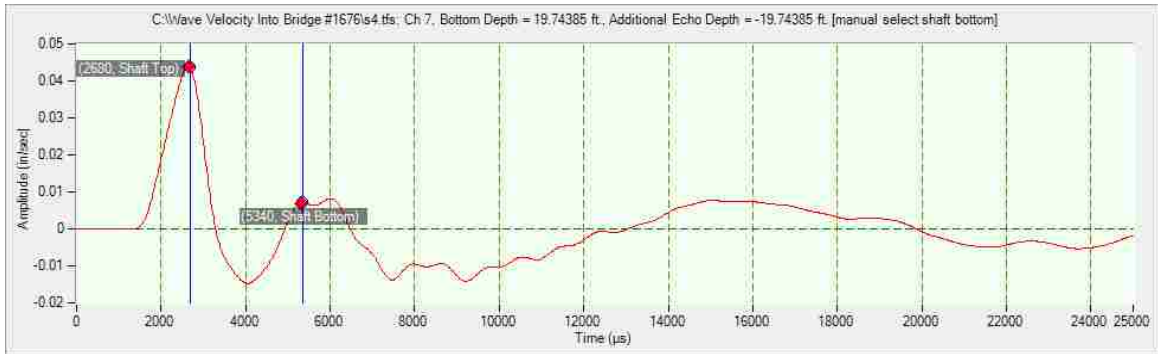


Figure 3-9: Velocity Trace- Accelerometer 1- Bridge #1676 Girder

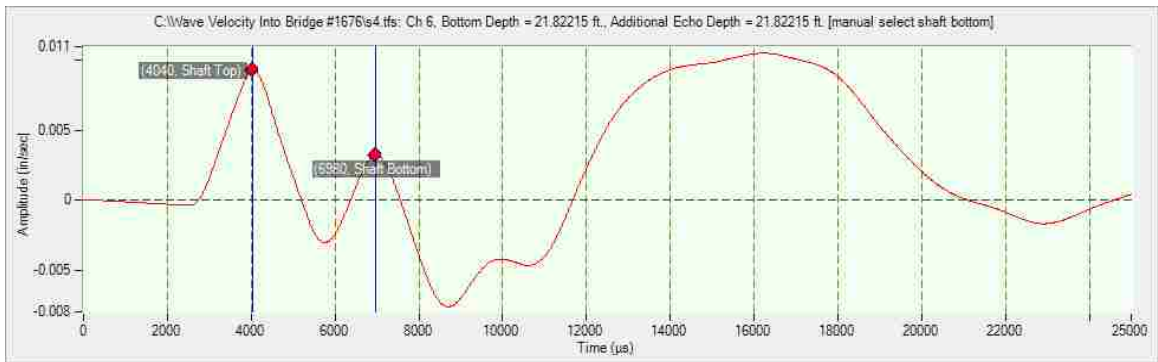


Figure 3-10: Velocity Trace- Accelerometer 2- Bridge #1676 Girder

The velocity trace displays the time in microseconds. The propagated wave velocity is then calculated from Eq. 3.1.

In Figure 3-9, the compression wave that was generated from the impact subsequently arrived at accelerometer 1 where it was sensed and measured. The velocity trace identified this disturbance as an initial impulse at time lapse 2680 μ s. Then the propagated wave passed through 19.7 feet to be reflected back at the opposite free end of the girder as a tensile wave passing the same distance (19.7

feet) and it was sensed again at accelerometer 1 and presented as an initial echo at time lapse 5340 μs . The time difference between the impulse and initial echo Δt represents the time needed for the propagated wave to arrive at the free end and to be reflected back to accelerometer 1 where it was identified as follows:

$$\Delta t = 5340 \mu\text{s} - 2680 \mu\text{s} = 2660 \mu\text{s}$$

The propagated stress wave velocity is equal to:

$$V = \frac{2 \times 19.7 \text{ ft}}{2660 \times 10^{-6}} = 14812 \text{ ft./s}$$

The average estimated propagated wave velocity will be used to determine depths of piles for the following SE tests of Bridge #1676.

Alternative approaches were used to estimate the sound wave velocity for timber bridge that has joints in the girder, as shown in Figure 3-11.



Figure 3-11: The Joined Girder of Timber Bridge

Two accelerometers are attached on the pile side. The preferred distance between the accelerometers should be more than 3 feet to obtain a reasonable result. The propagated wave will pass a certain distance to arrive at accelerometer

1, then another known distance to arrive at accelerometer 2. The accelerometer senses the signal at a specific time, which is called the start point, as shown in Figure 3-12. Each velocity trace that is obtained from each accelerometer has different start points. The differences between the start points of each graph represents the time need for the propagated wave to travel the distance between the accelerometers. The times are tabulated for every 60 μ s into velocity traces, which allows human error if the start point is selected inaccurately. Instead, the peak point of impulse may be selected as another alternative approach to estimate the wave velocity as shown in Figure 3-12. However, the average of propagated wave velocity into Bridge #1676 piles that are estimated using the start point approach equals 15672 ft./sec, while it equals 14927 ft./sec when the peak points approach is used.

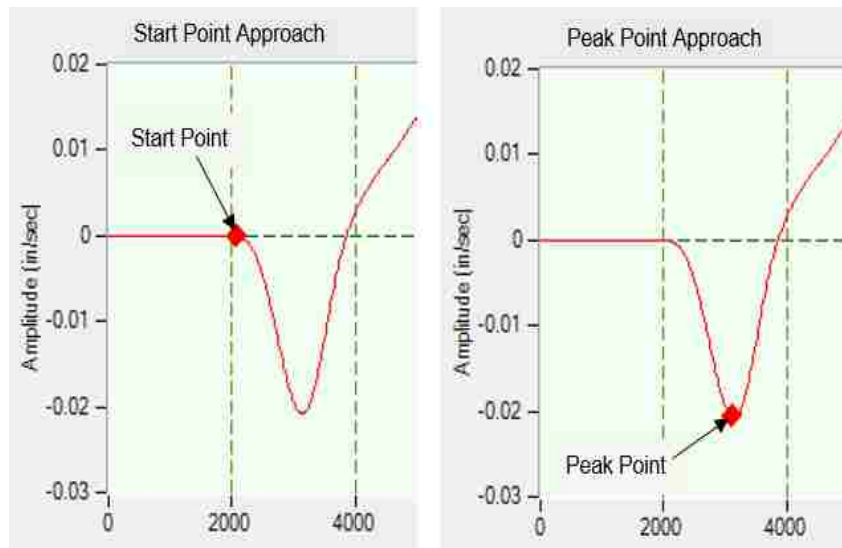


Figure 3-12: Alternative Approaches Used for Estimating the Wave Velocity

3.4 Validation of SE Test Results

The technique of determining the timber pile depth is based on the stress wave propagation within the pile. The stress wave is produced by the hammer

impact and then travels along the pile and consistently reflects back at boundaries until the energy decays. Two approaches are used to determine the depth of the pile: first, by measuring the travel time of the stress wave that is required to pass the full depth of the pile and then to return back, which involves time domain data processing. The second method involves measuring the resonant frequency of the pile, which is the inverse of the travel time of the stress wave (the inverse of SE reflection time Δt). Hence, the reflections are indicated by equally spaced resonant peaks (the change in frequency Δf) that present in the Impulse Response (IR) mobility plot. This second method involves frequency domain data processing. Thus, measurement of resonant frequency and stress wave velocity will be used to evaluate the timber piles depths (Olson et al., 1998). The theory for determining the reflector depth (D) could be expressed as:

$$D = \frac{V}{2 * \Delta f} \quad 3.5$$

If the accelerometer is attached on the pile side by using wooden block, then the total depth and buried depth of the pile determinations are represented by using the following equations:

$$L_t = \frac{V}{2 * \Delta f} + d \quad 3.6$$

$$L_b = L_t - h \quad 3.7$$

Where:

L_t is the total pile depth in feet, V is the propagated wave velocity in (ft./s), Δf is the change in frequency between resonant peaks in (Hz), d is the distance from the

top of the pile to the accelerometer, L_b is the buried pile depth, and h is the measured distance from the bottom of the pile cap to the ground level.

In general, the first approach (the time domain analysis) is considered to be more accurate for estimating the depth of timber pile than the resonant frequency analysis method. Practically, some tests do not provide a good frequency record (due to unclear frequency spacing in the IR mobility plot) for purposes of estimating pile depth. For example, Figure 3-13 indicates frequency data that was obtained from testing Pile C-1 of Bridge #1190. This IR mobility plot shows unclear frequency spacing (the plot has only one domain peak), which makes the estimation of Δf difficult. Figure 3-14 represents the typical IR mobility plot that could be used for validating the results, where the resonant frequency spacing could be obviously identified. Accordingly, the IR method can be used to validate the SE test results when the frequency data obtained from the field tests shows clear resonant frequency spacing in the IR mobility plot.

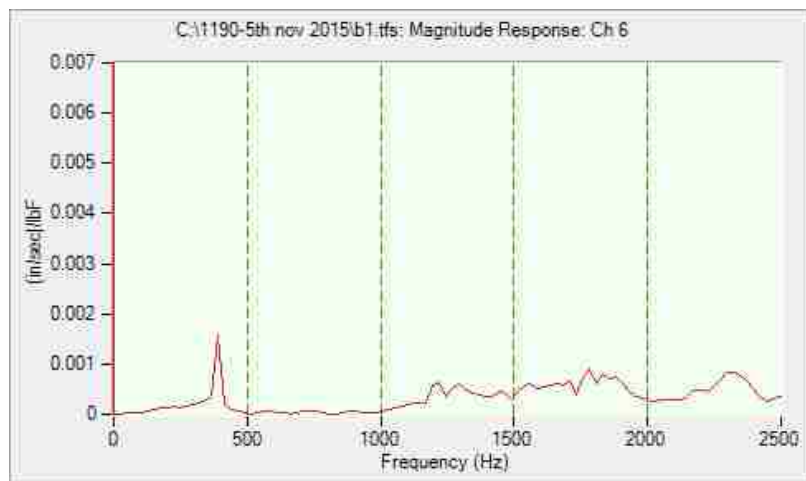


Figure 3-13: IR Mobility Plot for Test b1 Showing Unclear Frequency Spacing for Bridge #1190

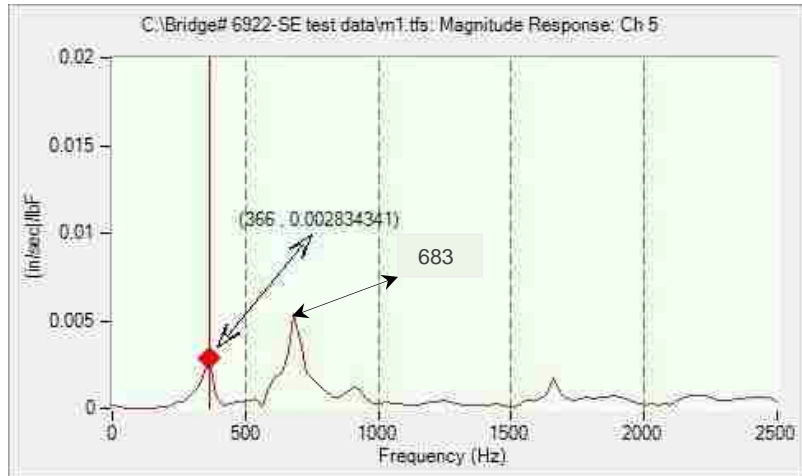


Figure 3-14: Typical IR Mobility Plot Showing Clear Frequency Spacing for Bridge #6922

3.5 Site Selection and SE Test Field Application

This section presents the SE test applications at field sites and the characteristics of each site. During this study three timber bridges, with a pile as the foundation type for each of them, were selected to investigate the unknown foundation depth. The bridges are owned by New Mexico Department of Transportation (NMDOT). The site numbers of these bridges are Bridge #1676, Bridge #6922, and Bridge #1190 as mentioned in the NMDOT documents. The SE test was conducted on a wooden column at the University of New Mexico campus.

3.5.1 Characteristics of Biology Annex Building Wooden Column

The decorative wooden column that was SE tested is located on the Biology Annex Building at the University of New Mexico campus in Albuquerque, New Mexico. The observed length of this column is known, and equals 19.75 feet, while the total length is predicted to be 11.75 feet. Two accelerometers were attached to the column's side. The SE tests that were conducted at the field site used hard, medium hard, medium soft, and soft hammer tips, in order to study the obtained signals. Figure 3-15 shows the wooden column image and the SE test setup.

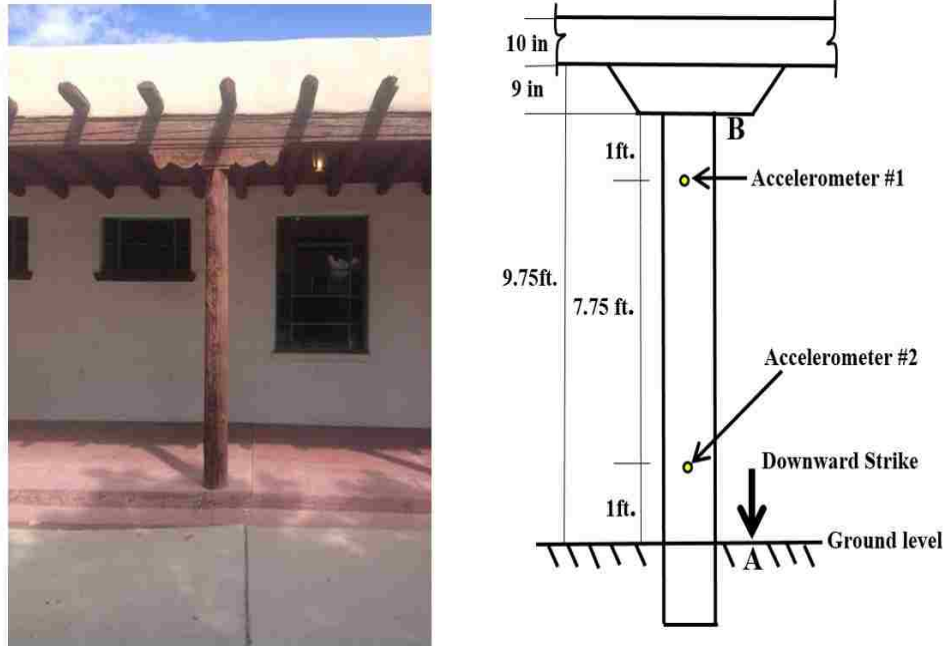


Figure 3-15: Biology Annex Building Wooden Column and SE Test Setup

3.5.2 Characteristics of Bridge #1676

Bridge #1676 is located 67 miles south of Albuquerque, New Mexico, in District 1, on a frontage road to Interstate highway 25. The bridge's coordinates are (34.211303, -106.921087). Figure 3-16 shows the location and the street view of the bridge. The bridge is a sawn lumber beam bridge with 4 spans supported by two pile abutments at each end and three intermediate pile bents. There are 25 piles with a square cross section supporting the superstructure. SE tests were conducted on Pile C-1, Pile C-2, Pile B-4, and Pile D-4. Figure 3-17 illustrates the bridge piles distributed plan and the locations of each tested pile as identified by a red circle.



Figure 3-16: Location and Street View of Bridge #1676

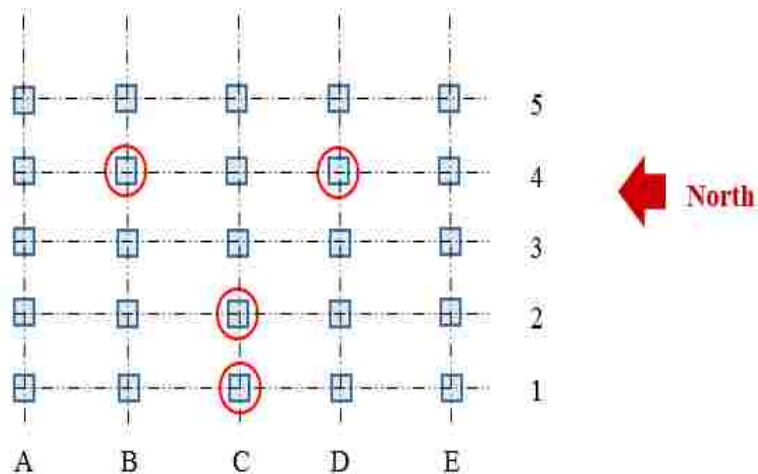


Figure 3-17: Piles Distributed Plan and Locations of Tested Piles of Bridge #1676

3.5.3 Characteristics of Bridge #6922

Bridge #6922 is located 40 miles east of Las Vegas, New Mexico, in District 4, on New Mexico highway 104. The bridge's coordinates are (35.477197, -104.613580). Figure 3-18 shows the location and the street view of the bridge. The bridge is a sawn lumber beam bridge built in 1966. It has one span that is supported by two pile abutments. Fifteen piles support the superstructure, seven piles at the east abutment and eight piles at the west abutment. The piles have a circular cross section. SE tests were conducted on Piles 1, 2, 3, 14, 15 and A.

Figure 3-19 illustrates the bridge piles distributed plan and the location of each tested pile, as highlighted in red.



Figure 3-18: Location and Street View of Bridge #6922

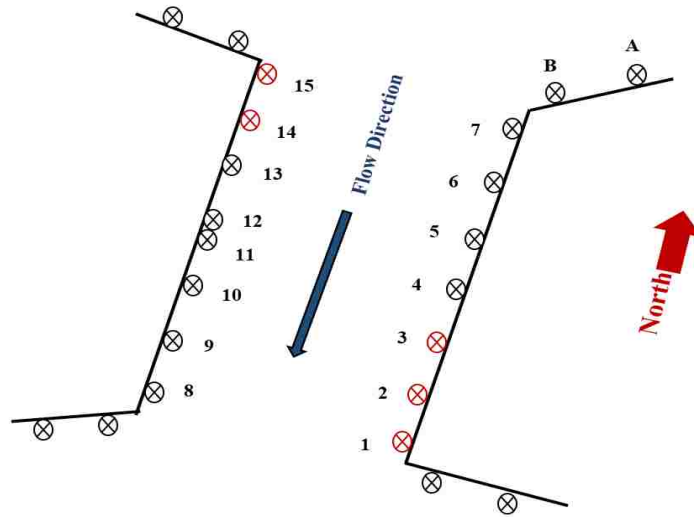


Figure 3-19: Piles Distributed Plan and Locations of Tested Piles of Bridge #6922

3.5.4 Characteristics of Bridge #1190

Bridge #1190 is located 23 miles west of Springer, New Mexico, in District 4, over Rayado Creek Stream. The bridge's coordinates are (36.368383, -104.929533). Figure 3-20 shows the location and the street view of the bridge. The bridge is a sawn lumber beam bridge built in 1965. It has two spans that are

supported by two pile abutments and one intermediate bent. Twenty-one piles support the superstructure, seven piles at the east abutment, seven piles at the intermediate bent, and seven piles at the west abutment. The piles have a circular cross section. SE tests were conducted on Piles 1, 8, 10, 15, 19, 21, A and B. Figure 3-21 illustrates the bridge piles distributed plan and the location of each tested pile, as highlighted in red.

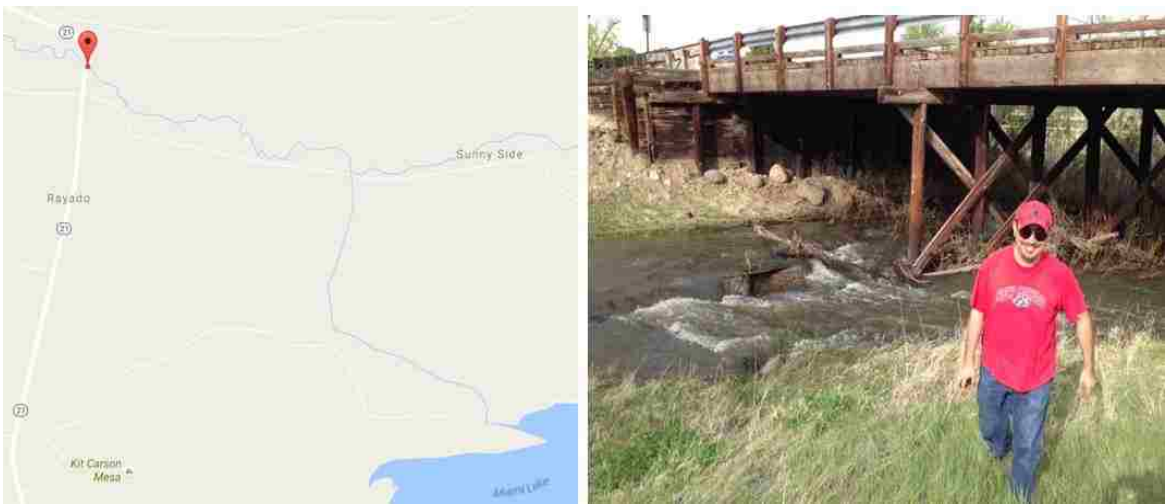


Figure 3-19: Location and Street View of Bridge #1190

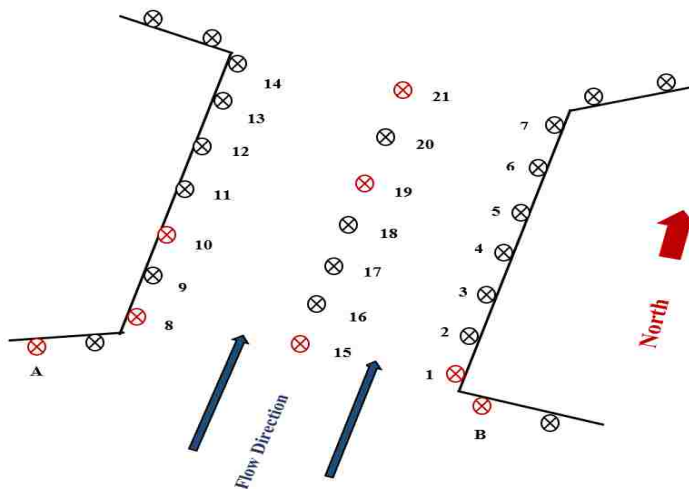


Figure 3-20: Piles Distributed Plan and Locations of Tested Piles of Bridge #1190

Chapter 4

Finite Element Method

4.1 Introduction

This chapter describes modeling with the example of a wooden column using finite element software to study the effects of the boundary condition of the pile, the hammer impulse shape, and the damping (attenuation) of sound waves on the travel time of the wave propagated with the impact into the timber pile.

4.2 Modeling and Simulation

Modeling is a method of problem solving using a simple object to study the behavior of a real system. Simulation is used when conducting experiments on a real system, that are otherwise impossible or impractical to conduct. The primary reason for modeling the timber pile is to study and then compare these results with SE field test results. In this chapter, a finite element model will be developed for a timber column in order to study and investigate the effects of changing impulse shapes, boundary conditions, and material damping on the wave travel time as well as acceleration and velocity traces. The length of the column will be estimated based on the acceleration and velocity responses at specific nodes. In the beginning, the damping into the column is neglected in the analysis. Abaqus, a suite of finite element analysis software, is used to model the timber piles. Abaqus/Explicit is a complementary and integrated analysis tool that is used to solve issues in dynamic finite element modules.

4.3 Wooden Column Model

A wooden column that has a total length of 5.5 m (18 ft.) is modeled using Abaqus software version 6.14. Figure 4-1 shows the boundary condition and the load that is applied on the timber pile model. Three nodes located in different spots on the column are investigated, as shown in Figure 4-2. The geometry and material properties of the timber pile are as follows: total length is 5.5 m (18 ft.), and diameter is 0.24 m (0.79 ft.). Modulus of elasticity (E) is 9.5 Gpa (198,411,625 psf.), the density is 700 kg/m³ (1.36 slug/ft³), and Poisson's ratio is 0.08. The wave velocity (V in m/s) obtained by using Eq. 3.4 consists of the following:

$$v = \sqrt{\frac{E}{\rho}} = \sqrt{\frac{9.5 \times 10^9}{700}} = 3684 \text{ m/s which is equal } 12083 \text{ ft./s}$$

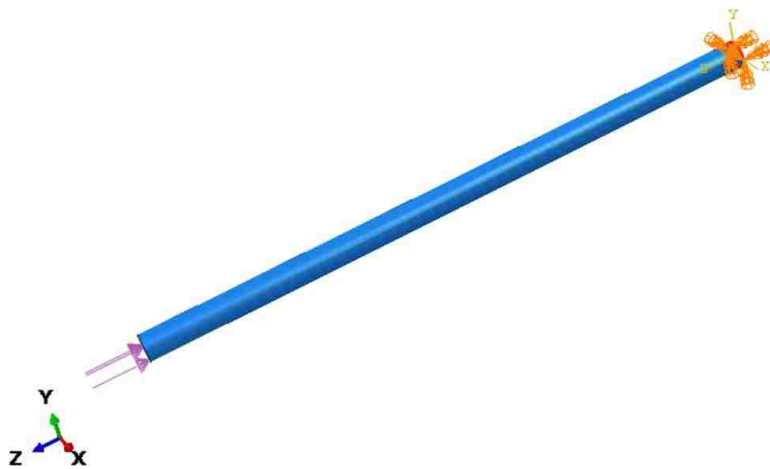


Figure 4-1: Timber Column Modeled Using Abaqus Software

The model is fixed at one end and free at the other. A $1 \times 10^6 \text{ N/m}^2$ uniform load is applied at the top of the pile, as shown Figure 4-1. The waveform shape and duration of impulse used in this model is the same as those observed in the SE field test. The impulse has a sinusoidal shape with a duration equal to 2000 μs .

The location of node #3901 is 0.2 m (0.656 ft.) from the free end, while node #1657 is located at 3.2 m (10.5 ft.) from the free end and 2.3 m (7.5 ft.) from the fixed end. The third node, node #2629, is located at 1.8 m (6 ft.) from the free end (at 1/3 of length of the column), as shown in Figure 4-2. The stress wave travels through the timber column and reflects at any change in impedances such as the fixed or free ends. Figure 4-3 shows a snapshot of stress wave propagation along the timber column.

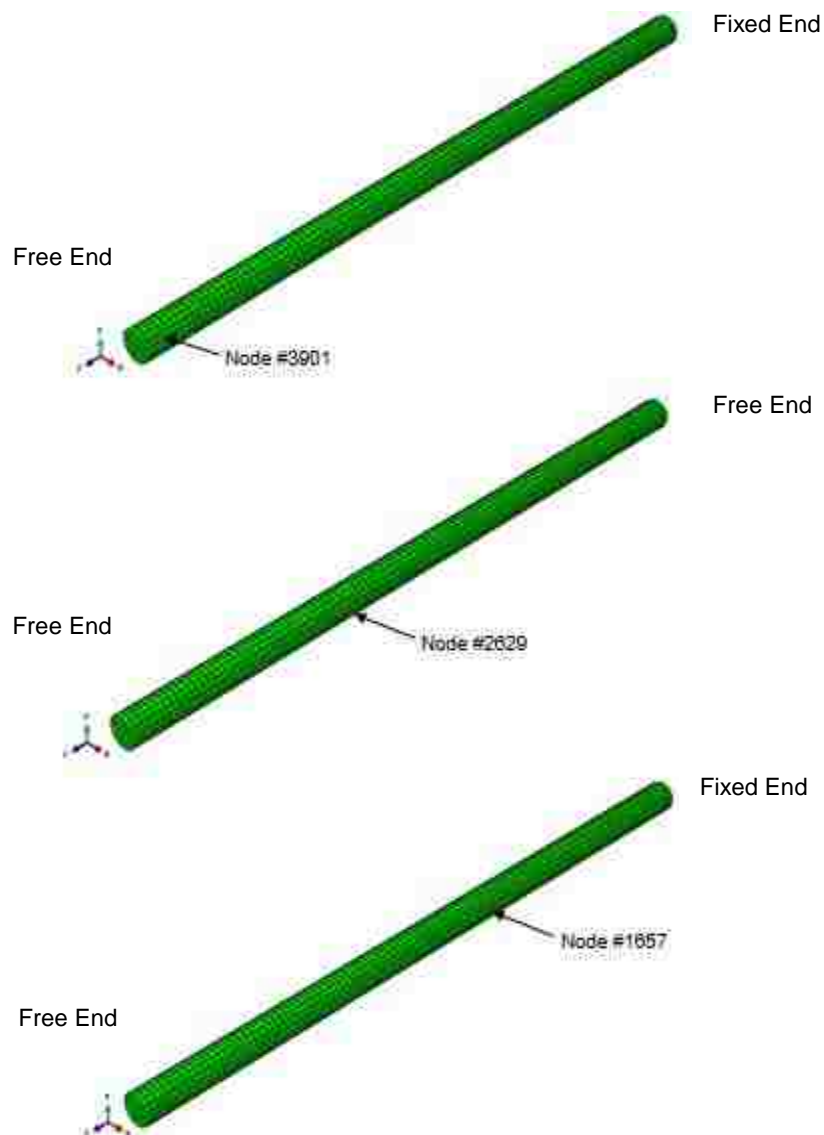


Figure 4-2: Nodes #3901, #2629, and #1657 Locations on Timber Column Model

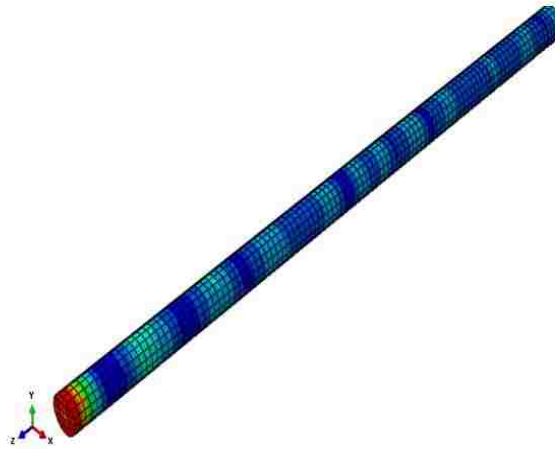


Figure 4-3: Stress Wave Propagation into Timber Column Model

The wave requires a specific time to arrive at each node. The wave speed is 3684 m/s (12083 ft./s), therefore, the time required for the wave to reach node #3901 is 2.7×10^{-5} second, while it required 5×10^{-4} second to arrive at node #2629 and 8.7×10^{-4} second to arrive at node #1657. Figures 4-4 and 4-5 show the required travel time for the wave to arrive at each node in terms of results obtained from the finite element model in both acceleration and velocity history responses. Whereas, both figures show reliable outcomes for node #2629 and node #1657, but erroneous reading of arrival time for node #3901. That is because node #3901 is very close to the top surface, and thus the required travel time for the wave to arrive at the node is very short nearly approaching zero value, while the other nodes are further away. In addition, the time difference between the initial response and the initial echo in both the acceleration and velocity graphs for all nodes is $0.003 \mu\text{s}$, which is double the time required for a wave to pass the total length of the timber column model, as shown in Figure 4-6.

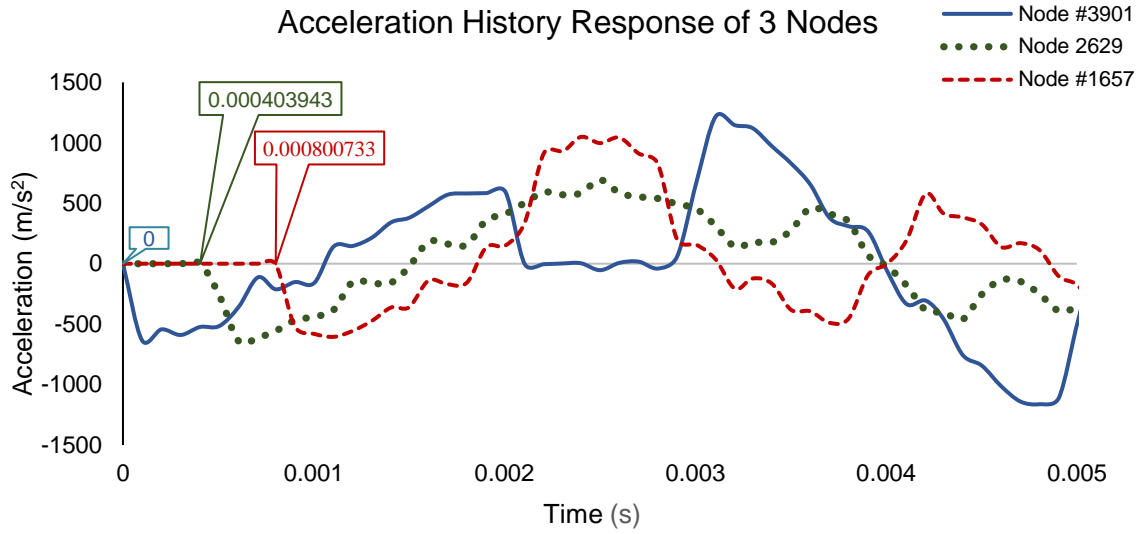


Figure 4-4: Acceleration History Response for Nodes #3901, #2629, #1657

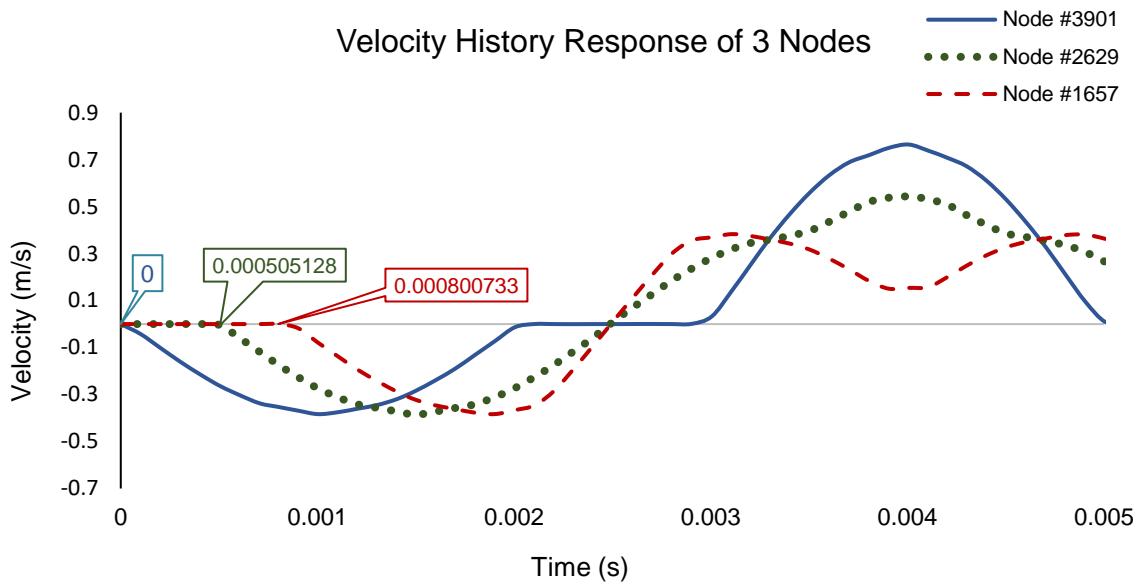


Figure 4-5: Velocity History Response for Nodes #3901, #2629, #1657

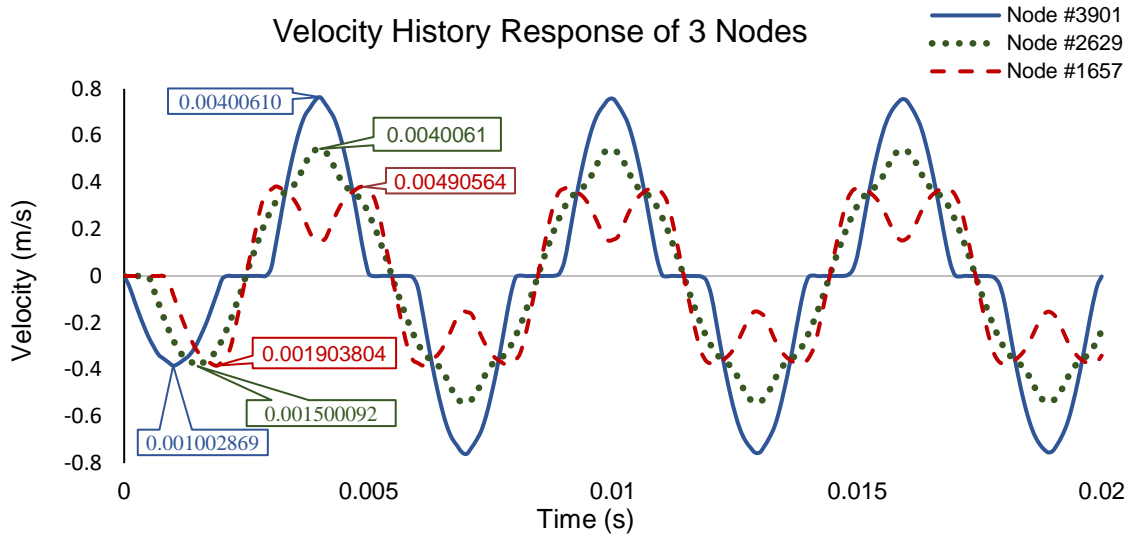


Figure 4-6: Velocity History Responses for Nodes #3901, #2629, #1657

4.4 Influence of Impulse Shape on the Propagated Wave Travel Time

Different load shapes were applied on the finite element model in order to investigate the impact of the load shapes on time lapse of the stress wave within the column as well as the acceleration and velocity traces. The time history responses of acceleration and velocity at node #3901 were studied and investigated. The stress wave moves through the timber pile and reflects at the fixed end, and then reflects again from free end. The compressive downward stress wave will be reflected upwards from the fixed end, and then will be reflected again from the free end in opposite sign as the tensile stress wave. Hence, the time difference between two consecutive positive peaks is the same as the difference between the negative peaks, which is four times the length of the column. The wave consequently takes 1.5×10^{-3} second to travel the 5.5 m (18 ft.) length of the column. The effectiveness of three selected shapes of impulse were

studied; these were sinusoidal, rectangular, and triangular impulses. Figures 4-7 to 4-12 show the acceleration and velocity responses of sinusoidal, rectangular, and triangular impulses, respectively:

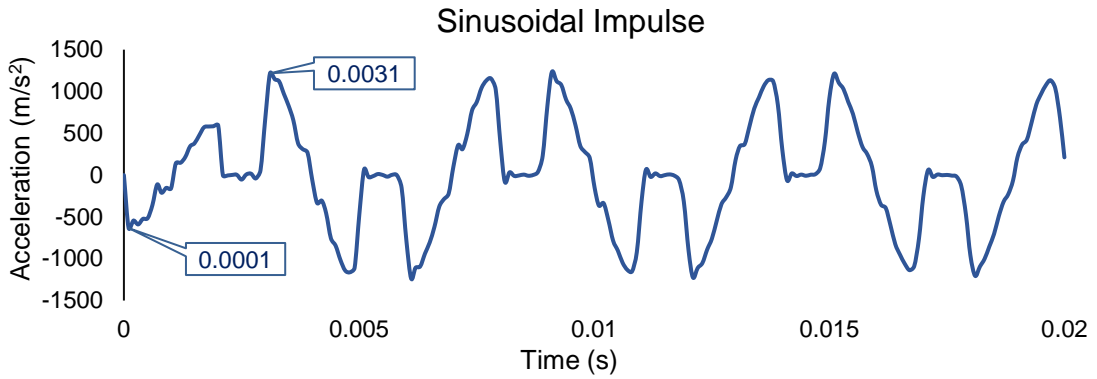


Figure 4-7: Acceleration History Response of Node #3901-Sinusoidal Load Shape

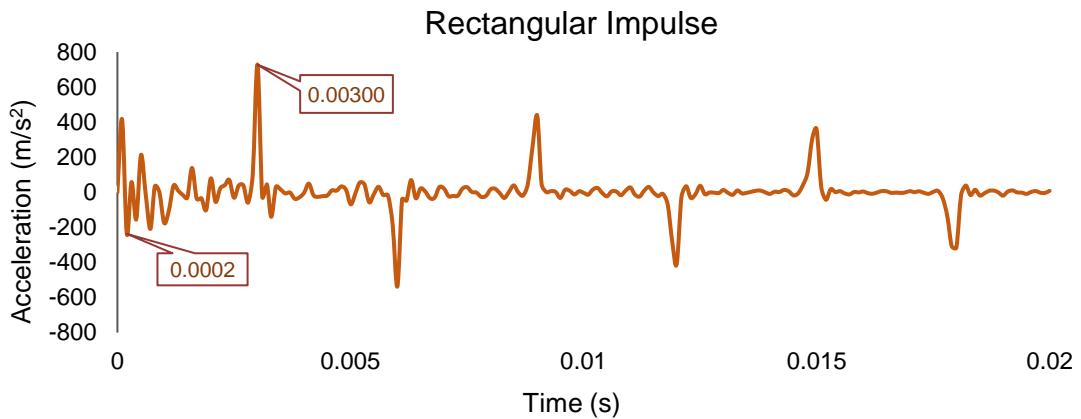


Figure 4-8: Acceleration History Response of Node #3901- Rectangular Load Shape

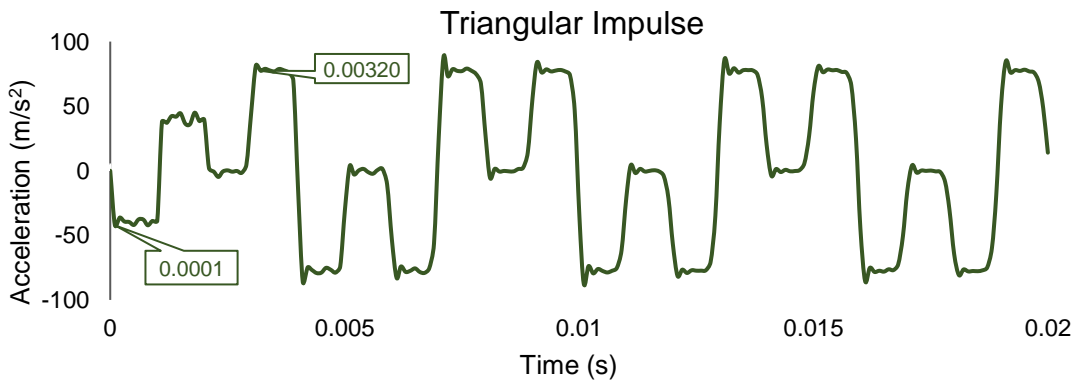


Figure 4-9: Acceleration History Response of Node #3901- Triangular Load Shape

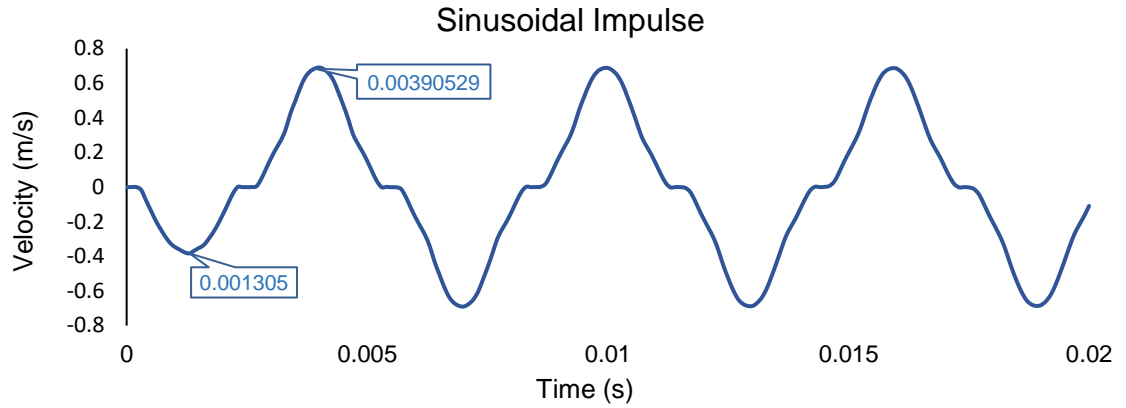


Figure 4-10: Velocity History Response of Node #3901- Sinusoidal Load Shape

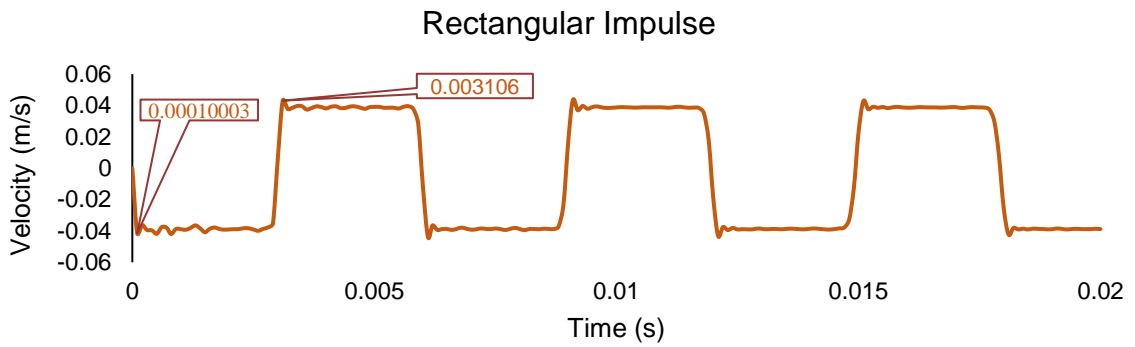


Figure 4-11: Velocity History Response of Node #3901- Rectangular Load Shape

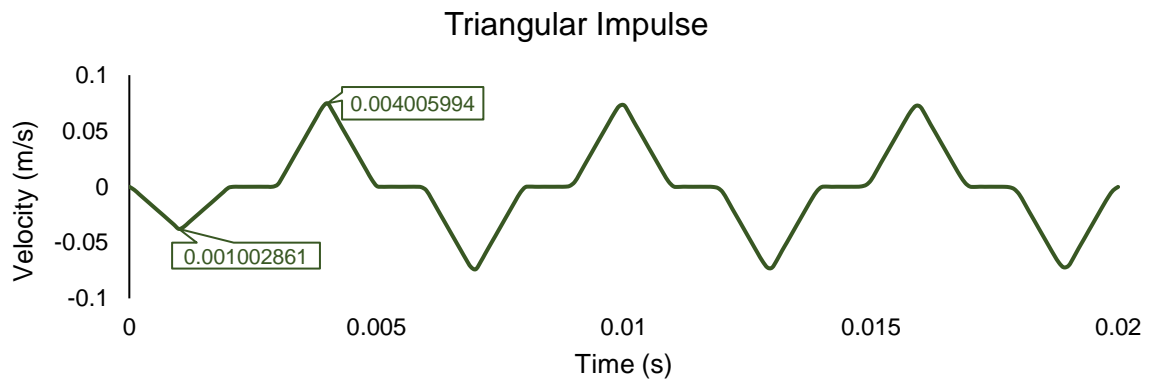


Figure 4-12: Velocity History Response of Node #3901- Triangular Load Shape

In these figures, the reflections can be clearly identified; this proved that impulse shape does not influence travel time Δt of the stress wave.

4.5 Influence of Boundary on the Propagated Wave Travel Time

Different boundaries were tested for the column pile model to investigate the influences of boundary conditions on the time lapse of the stress wave as well as the acceleration and velocity traces. Three types of boundary conditions were studied. The first case involved fixed-free ends. In the second case free-free ends were used while node #2629 was fixed to ensure stability of the pile. And the third case used hinged-free ends. Figures 4-13 and 4-14 show the acceleration and velocity responses, respectively, of node #3901:

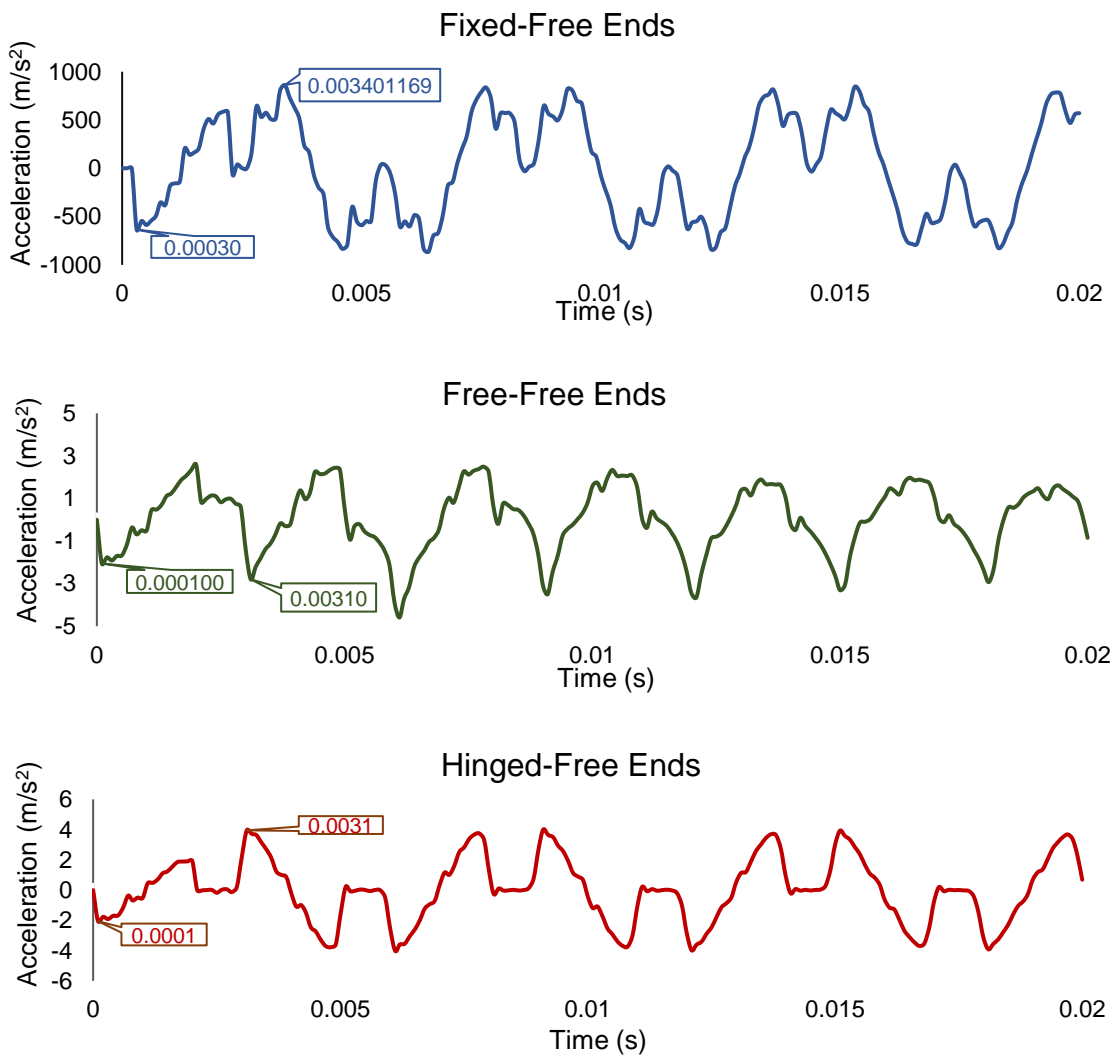


Figure 4-13: Acceleration History Responses of Node #3901 With Different Boundaries

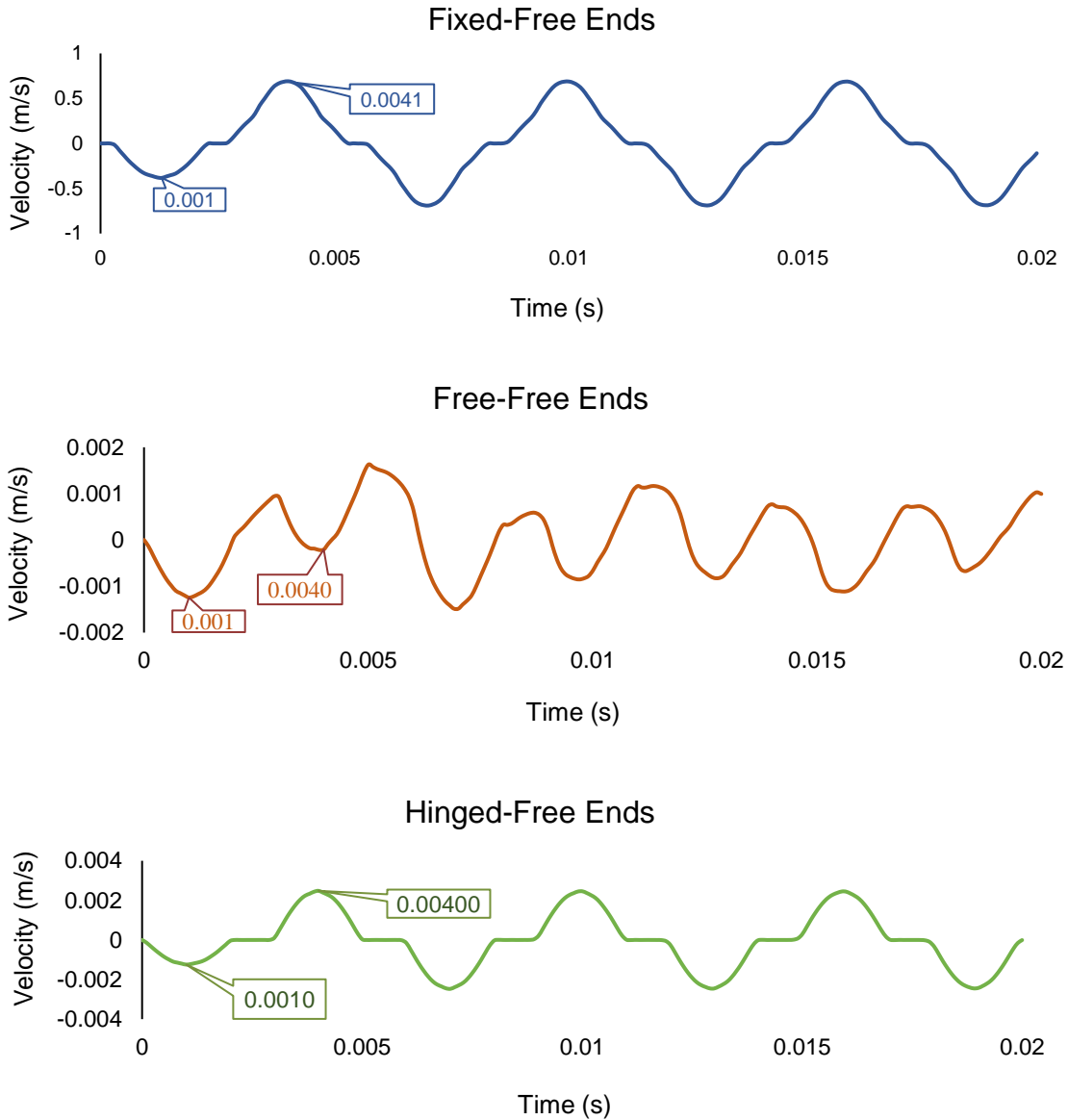


Figure 4-14: Velocity History Responses of Node #3901 With Different Boundaries

It is obvious from these figures that change in the waveform depends on the boundary conditions of the pile. For instance, in the first and third cases, the waveform is inverted each time it travels the full depth of the column. This can be an attribute of the pile where the far end is fixed or hinged (such as a pile on bedrock). Obviously, the compressive wave is reflected as a compression wave at a fixed boundary when the impedance is increased, while by contrast, it converted

and refracted as a tensile wave at the free end when the impedance is decreased. Similarly, a tensile wave is converted into a compressional wave at the free end. This process continues in succession. Therefore, for each back and forth of the wave traveling, the acceleration sign is changed since the tensile and compressive waves are interchanged each time they are reflected from the free end of the pile. Again, by contrast, in the second case when both ends of the pile are free, the incoming compressive wave reflects as a tensile wave from the free end, and then the wave is reflected as a compressive wave again. Therefore, the waveform remains the same at the end of each complete back and forth travel route. However, in the second case the two negative peaks in the waveform represents the complete travel time for reflection from the bottom of the pile, which is similar to the waveforms obtained from the SE field tests. However, the boundary condition of the pile has an effect on the shape of the acceleration and velocity graphs, but it does not influence the determination of travel time Δt as is obvious in the previous figures.

4.6 Influence of Damping on the Propagated Wave Travel Time

In reality, the sound energy that is injected into the pile from the impact dissipates because of two factors: first, because of the effect of damping that is inherent in the pile material (wood); and second, because of material that surrounded the pile, such as soil and rocks. Therefore, damping is introduced in to the wooden column model in order to study the influence of damping on the wave travel time. Here, to treat damping within a modal analysis framework, an

assumption takes place that the damping value is equivalent to Rayleigh damping.

Therefore, the Rayleigh damping equation is used, as shown:

$$[C] = \alpha [M] + \beta [K] \quad 4.1$$

Where:

C is the damping matrix of the physical system, M is the mass matrix of the physical system, K is the stiffness matrix of the system, α is the Rayleigh damping factor for mass proportional damping, and β is the Rayleigh damping factor for stiffness proportional damping. The damping coefficients are values that are assumed to be as follows: First; $\alpha=0.001$ and $\beta=0.0002$. Then; $\alpha=0.05$ and $\beta=0.0002$.

Figures 4-15 to 4-18 show the acceleration and velocity traces, respectively, at node #3901:

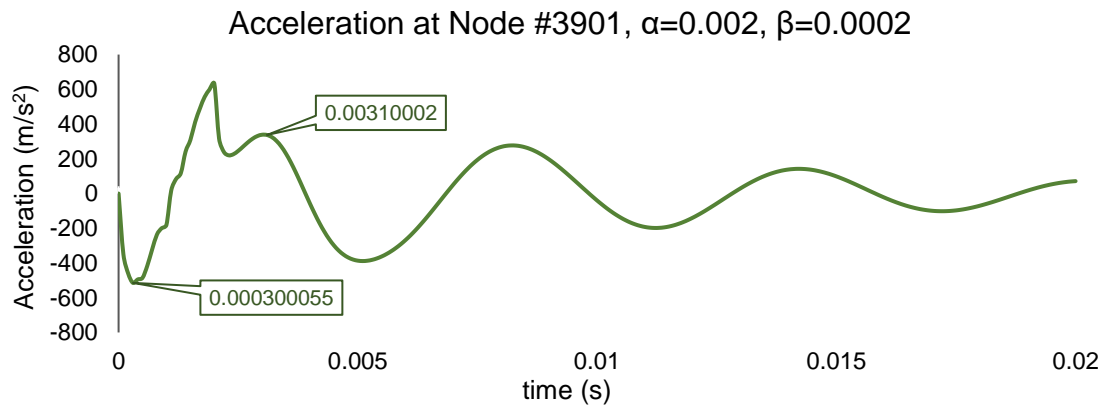


Figure 4-15: Acceleration History Response of Node #3901, $\alpha=0.002$, $\beta=0.0002$

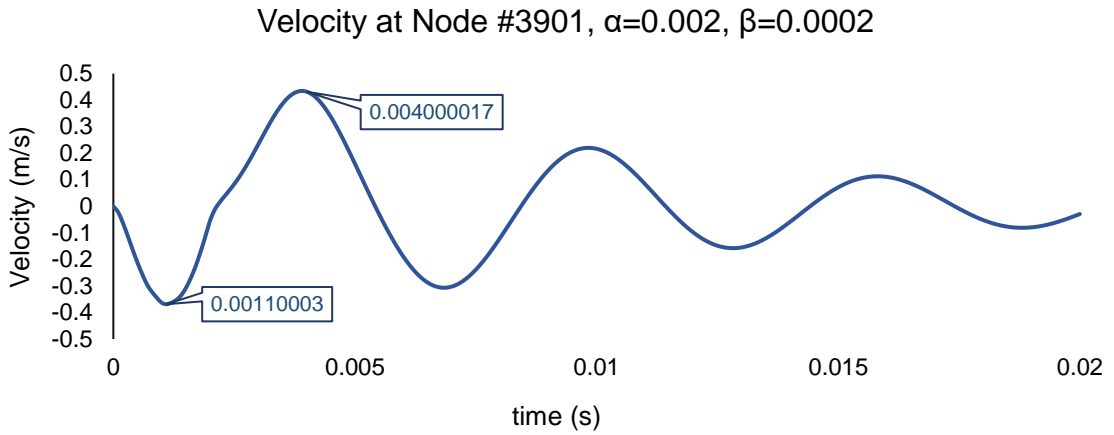


Figure 4-16: Velocity History Response of Node #3901 $\alpha=0.002$, $\beta=0.0002$

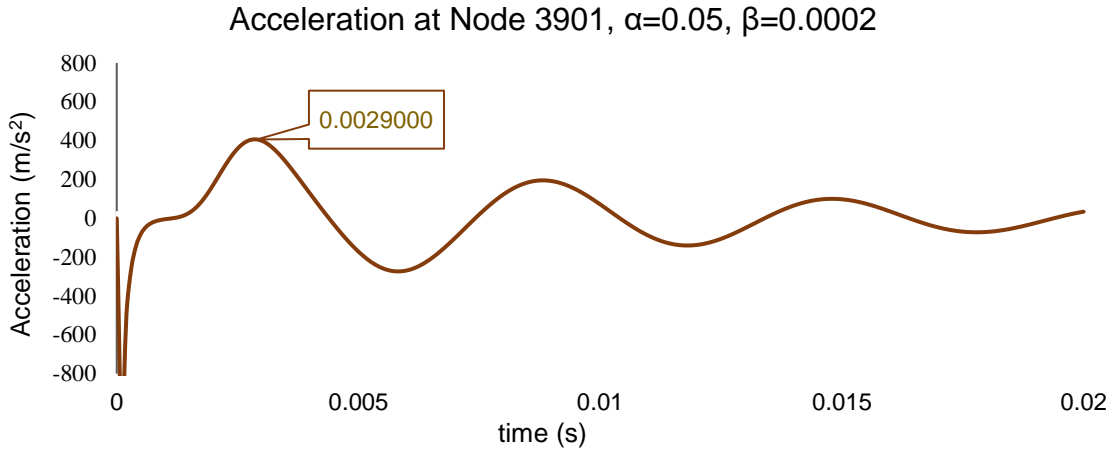


Figure 4-17: Acceleration History Response of Node #3901, $\alpha=0.05$, $\beta=0.0002$

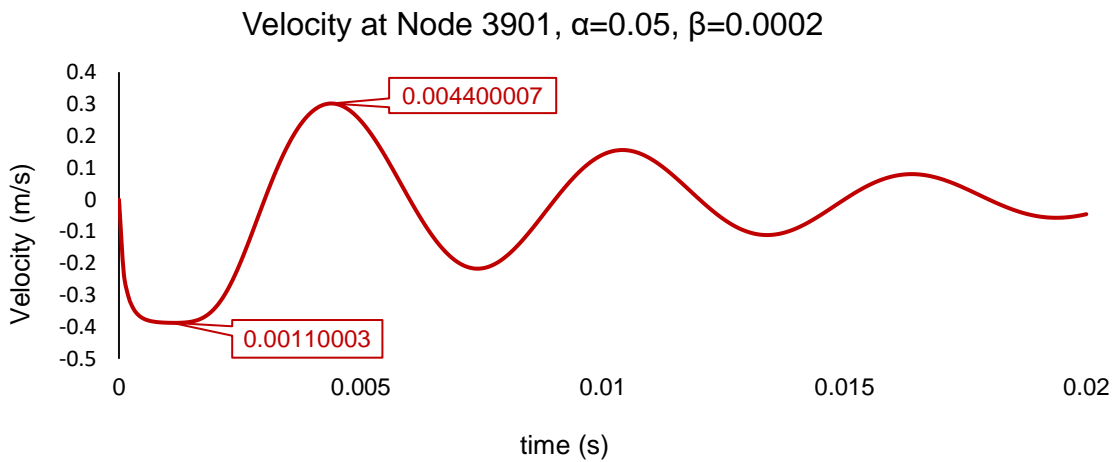


Figure 4-18: Velocity History Response of Node #3901, $\alpha=0.05$, $\beta=0.0002$

In these figures, it is obvious that varying the alpha values only changes the amplitude and does not affect the time interval. The influence of damping is only represented by smoothing out and dissipating the high frequency content of the acceleration over time. The effect of beta was not studied as part of this effort, even though it can have an effect on the shape of the pulse and hence the time interval between subsequent peaks. The shape of the velocity trace obtained from finite element analysis, when damping is taken into account, is like the velocity trace that are observed in the SE field test when the softer hammer tips are used.

4.7 Conclusion

It was obvious from the previous study and investigation about finite element models that wave travel time was not affected by impulse shapes, nor by boundary conditions of piles, and also not by the damping due to pile material or surrounding soil. However, impulse shapes effect the shape of acceleration and velocity curves. Thus, the shapes of velocity curves of vibrated particles (nodes) take the same shape of impulse, as shown in Figures 4-10 to 4-12. Also, the boundary conditions of piles define the shape of velocity curves which will be strongly influenced for determining the wave time lapse, while damping only affects the rate of dissipation of the wave.

Chapter 5

Results and Discussion

5.1 Introduction

This chapter presents the results of Sonic Echo field tests that were conducted on the timber piles of three bridges located in different locations in New Mexico. The depths of these timber piles are unknown. In addition, SE tests were conducted on a wooden column located at the Biology Annex Building at the University of New Mexico. The length of this wooden column is known, it was tested to validate the equipment performance. Finally, using the Impulse Response (IR) method for validation the results of SE field tests. In this chapter, all SE field tests results are reviewed, analyzed and discussed to provide a technical approach that will be recommended for use to determine the unknown timber piles depths of bridges in New Mexico.

5.2 Sonic Echo Field Test

A Sonic Echo test was applied on the decorative wooden column located on the Biology Annex Building at the University of New Mexico. Furthermore, three timber bridges were also field tested in several locations in New Mexico; these were Bridge #1676, Bridge #6922, and Bridge #1190. The results of these Sonic Echo tests will be discussed.

5.2.1 Wooden Column of Biology Annex Building SE Field Test Results

The column tested is a decorative wooden column, as shown in Figure 3-15. Sixteen SE tests were conducted using hard, medium hard, medium soft, and

soft tips. The goal in testing the wooden column with its length known is to study how the signals are obtained with Olson Freedom Data PC equipment. Eight tests were conducted by striking the concrete pavement at point A next to the column. To receive signals, two accelerometers were mounted vertically to the top surface of the wooden block, using super glue to attach the wooden blocks to the wooden column, as shown in Figure 3-16. Although the striking was not directly applied to the column, the wave traveled to the column top end and then reflected back. Furthermore, the other SE tests were conducted by vertically striking the capital of the column at point B (striking in an upward direction). Table 5-1 summarized the characteristics and results of the SE field test of the Biology Annex Building wooden column.

The propagated wave velocity within the wooden column was estimated using the known length of the wooden column and the time difference between the initial response and the initial echo of the velocity trace that were obtained from accelerometer 1 and accelerometer 2. The time difference (Δt) between the initial response and initial echo of velocity trace that was obtained from accelerometer 2 is 1380 μs . The distance from the accelerometer 2 to the pavement (D) is 1 foot. and the total clear length of wooden column is 9.7 feet. Hence, the determined average velocity that was propagated into the wooden column is 12600 ft./s by using Eq. 3.1 as shown below:

$$V = \frac{2D}{\Delta t} = \frac{2 \times 9.7}{0.00138} = 12600 \text{ ft./s}$$

This magnitude of the propagated wave velocity V was used to compute the observed length of the column (L_{obs}) using data that was obtained from acceleration 2 and Eq. 3.1. While the total length (L_t) was directly determined using the data that was obtained from accelerometer 1 and using Eq. 3.2. Figure 5-1 shows the velocity trace obtained from accelerometer 2 (channel 7).

Table 5-1: Characteristics and Results of SE Field Test for the Wooden Column

Test No	Hammer Tip's Type	Direction of Strike	Accelerometer 1			Accelerometer 2		
			Δt (μs)	L_t (ft.)	D (ft.)	Δt (μs)	L_{obs} (ft.)	D (ft.)
1	Hard	A -Downward	1900	11.97	1	1380	9.7	1
2	Hard	A -Downward	1880	11.8	1	1360	9.6	1
3	Med-hard	A -Downward	1940	12.2	1	1440	10.1	1
4	Med-hard	A -Downward	1960	12.35	1	1460	10.2	1
5	Med-soft	A -Downward	2040	12.85	1	1460	10.2	1
6	Med-soft	A -Downward	2020	12.7	1	1460	10.2	1
7	Soft	A -Downward	2060	12.98	1	1420	9.95	1
8	Soft	A -Downward	2040	12.85	1	1420	9.95	1
9	Hard	B -Upward	1680	11.584	1	1980	12.5	1
10	Hard	B -Upward	1760	12.1	1	1520	9.6	1
11	Med-hard	B -Upward	1660	11.5	1	2600	16.4	1
12	Med-hard	B -Upward	1680	11.6	1	2320	14.6	1
13	Med-soft	B -Upward	1980	13.5	1	2620	16.5	1
14	Med-soft	B -Upward	NS	NS	1	NS	NS	1
15	Soft	B -Upward	2020	13.7	1	NS	NS	1
16	Soft	B -Upward	2300	15.5	1	NS	NS	1

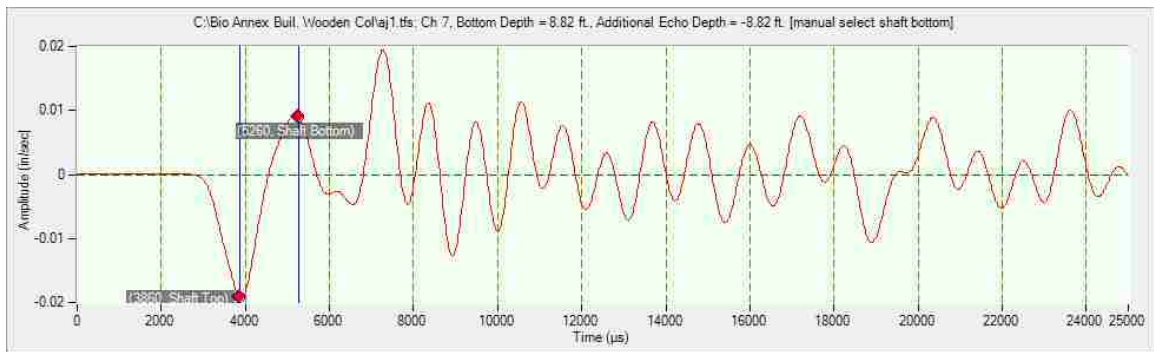


Figure 5-1: Velocity Trace of SE Test Conducted on the Wooden Column- Ch7

The results obtained from accelerometer 2, when the striking was vertical on the concrete pavement, are reasonable, very close to the actual length of the

column for all types of hammer tips used. Figure 5-1 is similar to Figure 4-14, which was obtained from the finite element model under the boundary condition of fixed-free ends. Conversely, the results obtained from accelerometer 2 were inappropriate when the strikes that were applied were vertically upward strikes the capital. The reason for the inappropriate results was that accelerometer 2 was too far from the source of energy. However, the assessed total length of the wooden column using the data obtained from accelerometer 1 was close enough to the predicted length of 11.7 feet. The buried length of the column was unknown, but it was predicted to be 2 feet. The results obtained from the accelerometers are reliable for all types of hammer tips, as shown in Table 5-1, except when a soft tip is used. Hence, the upward strike on the capital or girder could be used as an alternative in cases where the top of the pile or column is not accessible.

5.2.2 Bridge #1676 SE Field Test Results

5.2.2.1 Determination of Wave Velocity Within Timber Pile

Twelve SE tests were conducted on the bridge girder to measure the wave velocity propagated within the timber pile that will be used further to determine the total and buried depths of piles for Bridge #1676. The girder is struck horizontally, as shown in Figure 5-2, using different hammer tips. For each test, the time differences were measured between the initial impulse and initial echo that were obtained from both accelerometers. Accelerometer 1 was connected to channel 7 and accelerometer 2 was connected to channel 6. The distance difference between the accelerometers was 19.7 feet. The average wave velocity that was propagated within the girder was computed and equaled 14845 ft./s, as shown in

Table 5-2. Figures 5-3 to 5-6 show examples of velocity traces that were obtained from SE tests using different types of hammer tips.

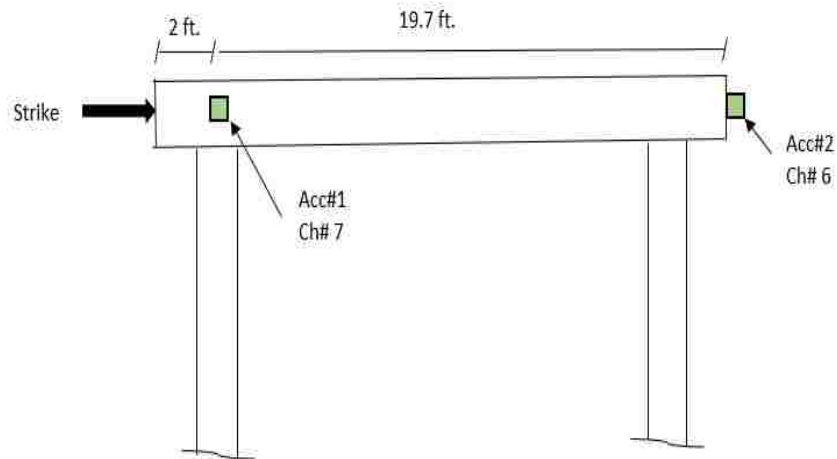


Figure 5-2: SE Field Test Conducted on Bridge #1676 Girder to Measure Wave Velocity

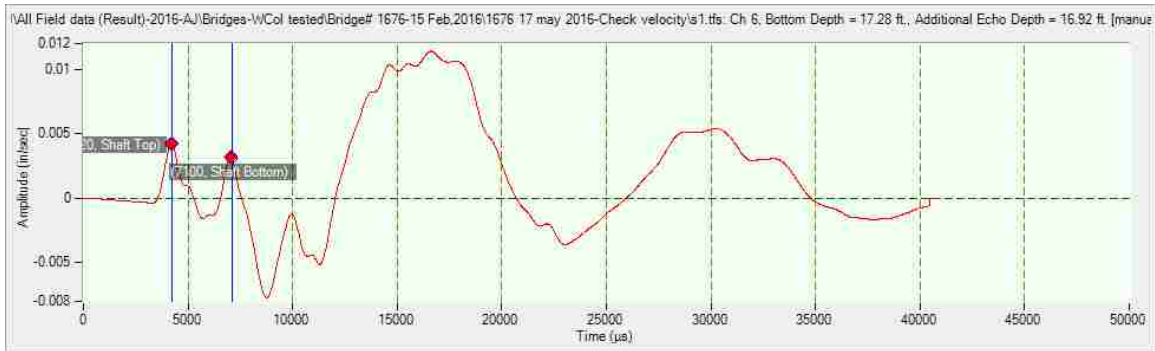


Figure 5-3: Velocity Trace Using Hard Tip

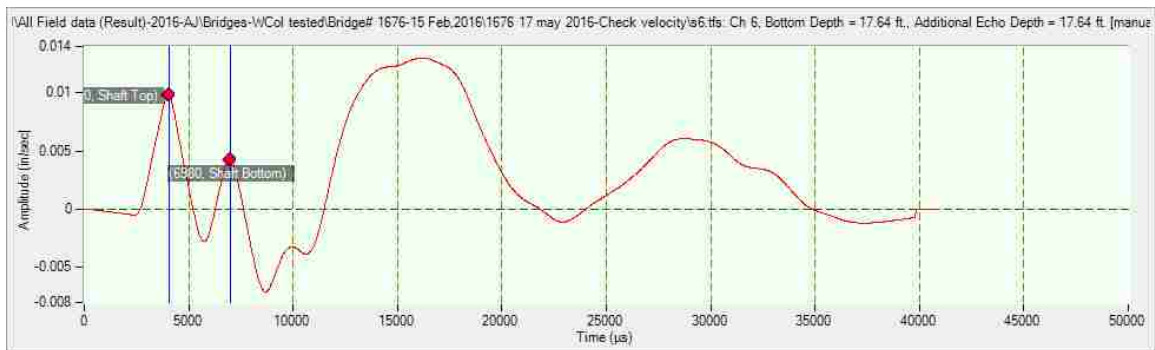


Figure 5-4: Velocity Trace Using Medium Hard Tip

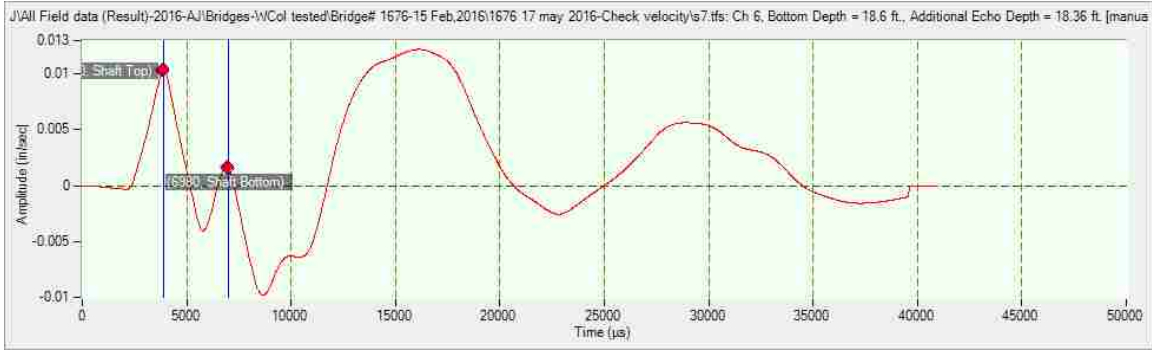


Figure 5-5: Velocity Trace Using Medium Soft Tip

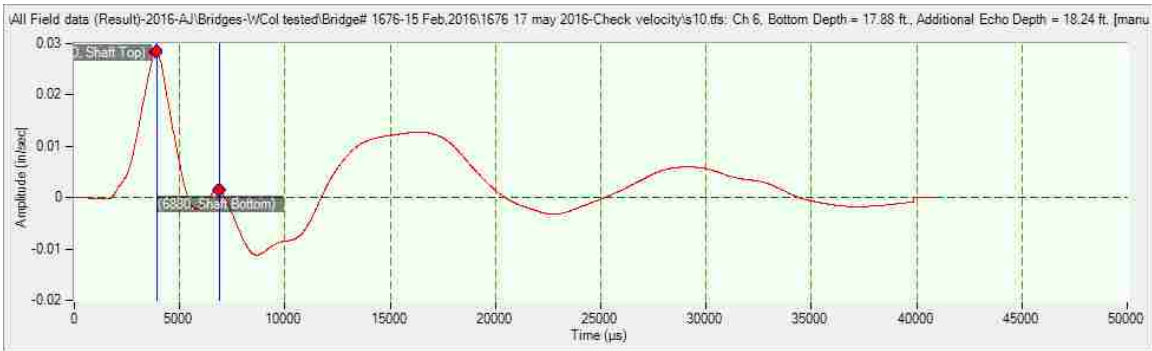


Figure 5-6: Velocity Trace Using Soft Tip

Table 5-2: Estimated Wave Velocities into Piles of Bridge #1676

Test No.	Hammer tip	Δt (μs)	Girder length	V (ft./s)
1	Hard	2820	22.7	15390
2	Medium-Hard	2960	22.7	14662
3	Medium-Soft	3000	22.7	14466
4	Soft	2920	22.7	14863

5.2.2.2 Pile C-1

Pile C-1 is located at the west side of the bridge, as shown in Figure 3-17. Here, twenty-three SE tests were conducted on Pile C-1 in order to study the results obtained from the acquisition equipment. Different hammer tips were used to strike the pile. The striking directions were vertical on three points, downward either at point A on the pile cap or the wedge (block), and upward at point B on the pile cap. Two accelerometers were attached vertically to the top surface of wooden

block to receive the signal, then the wooden blocks were mounted onto the tested pile side using super glue. Accelerometer 1 was connected to channel 6 and accelerometer 2 was connected to channel 7, and the distance between the accelerometers was 3 feet. The image of Pile C-1 and the SE test setup details are shown in Figure 5-7. Table 5-3 shows the directions and locations of strikes on Pile C-1.

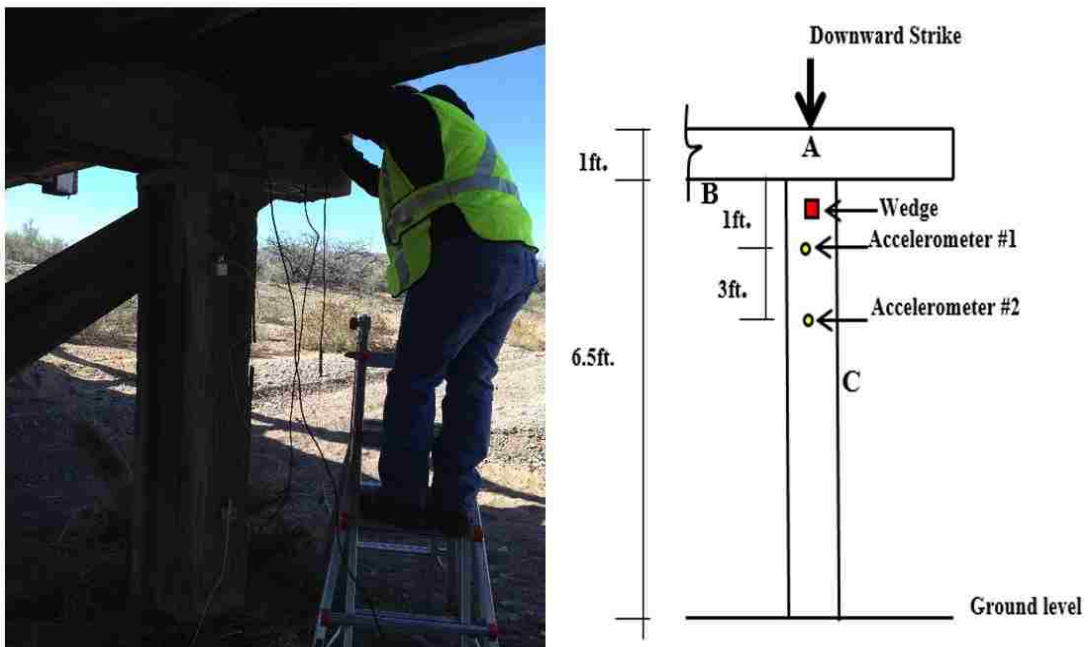


Figure 5-7: The Image of Pile C-1 and SE Test Setup

Table 5-3: Strike Direction of Pile C-1

Point	Strike Direction
A	Downward
B	Upward
C	Horizontally
Wedge	Downward

Table 5-4 shows the characteristics and results of SE field tests for Pile C-1. The estimated wave velocity V equals 14845 ft./s. Hence, Eq. 3.2 and Eq. 3.3 were

used to compute the total depth L_t and buried depth L_b of Pile C-1. Examples of data that were obtained from accelerometer 1 are indicated in Figures 5-8 to 5-19, respectively.

Table 5-4: Characteristics and Results of SE Field Test for Pile C-1

Test No	Hammer Tip's Type	Direction of Strike	Accelerometer 1			Accelerometer 2		
			Δt (μs)	L_t (ft.)	L_b (ft.)	Δt (μs)	L_t (ft.)	L_b (ft.)
b1	Hard	A -Downward	3600	27.7	21.2	2980	26.1	19.6
b2	Med-hard	A -Downward	3960	30.4	24	4320	36.1	29.6
b3	Med-soft	A -Downward	4120	31.6	25	4060	34.1	27.6
b4	Soft	A -Downward	4480	34.3	27.8	4340	36.2	29.7
b9	Hard	B -Upward	3220	24.9	18.4	3160	27.5	21
b10	Hard	B -Upward	3320	25.6	19.1	2880	25.4	19
b11	Hard	B -Upward	3140	24.3	17.8	3180	27.6	21.1
b12	Hard	B -Upward	3200	24.75	18.25	2980	26.1	19.6
b13	Hard	B -Upward	3220	25	18.4	3020	26.4	20
b14	Med-hard	B -Upward	4840	37	30.4	3800	32.2	25.7
b15	Med-soft	B -Upward	4880	37.2	30.7	3400	29.2	22.7
b16	Soft	B -Upward	5260	40	33.5	3620	30.87	24.4
b20	Hard	Wood Block-Downward	3580	27.6	21.1	3540	30.3	23.76
b21	Med-hard	Wood Block-Downward	3560	27.4	21	4080	34.3	27.8
b22	Med-soft	Wood Block-Downward	3580	27.6	21.1	5140	42.2	35.6
b23	Soft	Wood Block-Downward	3560	27.4	21	4800	39.6	33.1

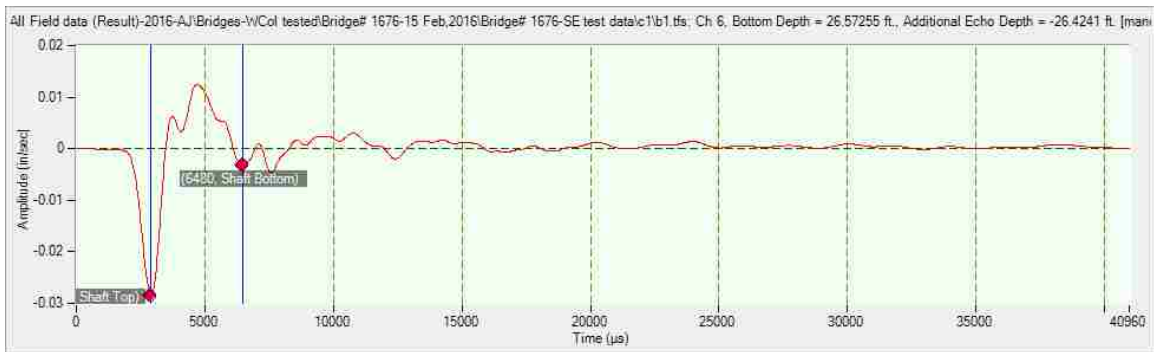


Figure 5-8: Velocity Trace of SE Test No. b1 Using Hard Tip- A Downward

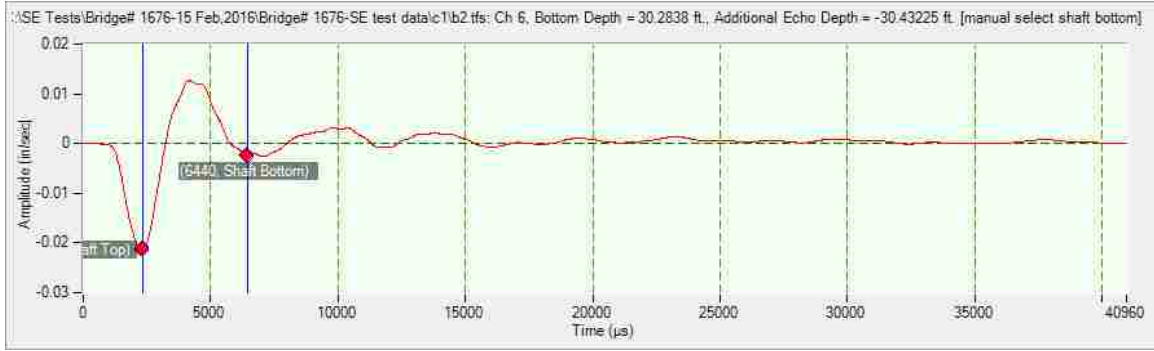


Figure 5-9 Velocity Trace of SE Test No. b2 Using Medium Hard Tip- A Downward

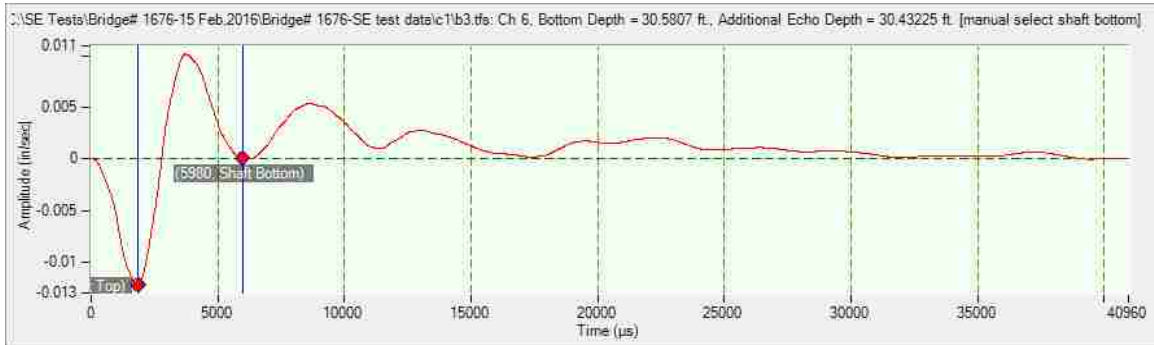


Figure 5-10: Velocity Trace of SE Test No. b3 Using Medium Soft Tip- A Downward

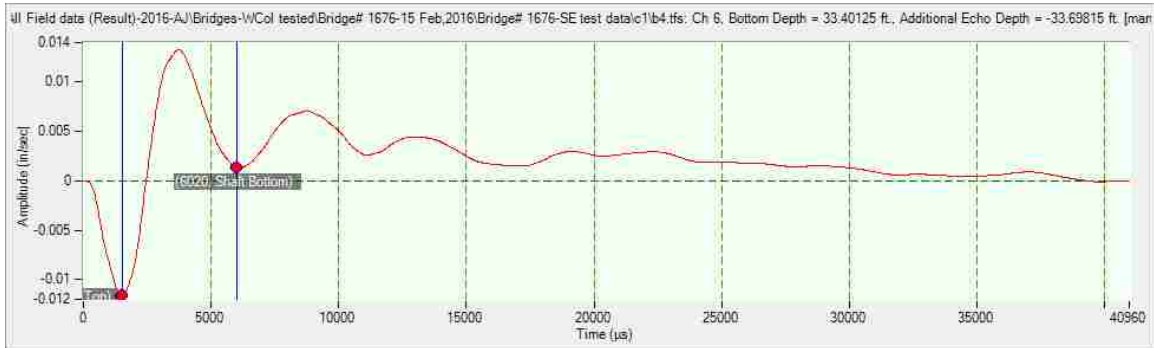


Figure 5-11: Velocity Trace of SE Test No. b4 Using Soft Tip- A Downward

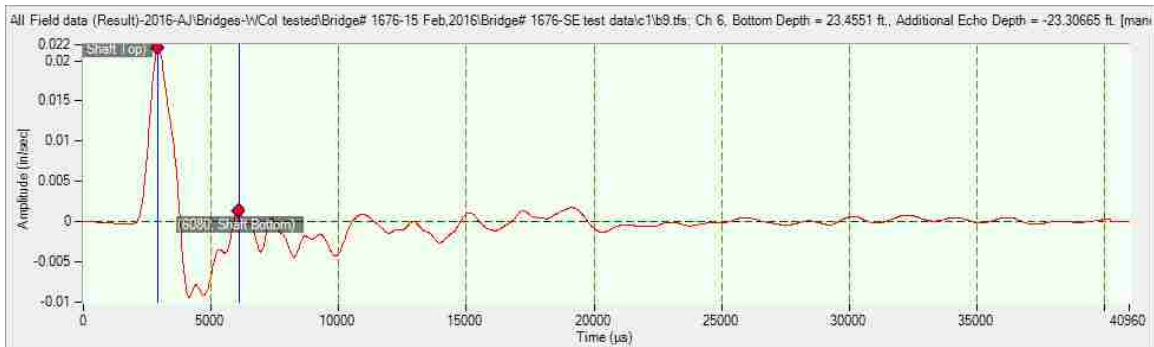


Figure 5-12: Velocity Trace of SE Test No. b9 Using Hard Tip- B Upward

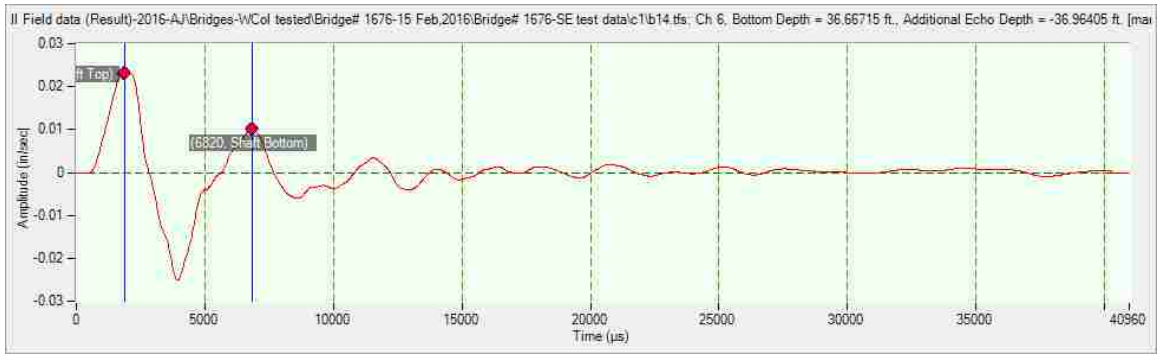


Figure 5-13: Velocity Trace of SE Test No. b14 Using Medium Hard Tip- B Upward

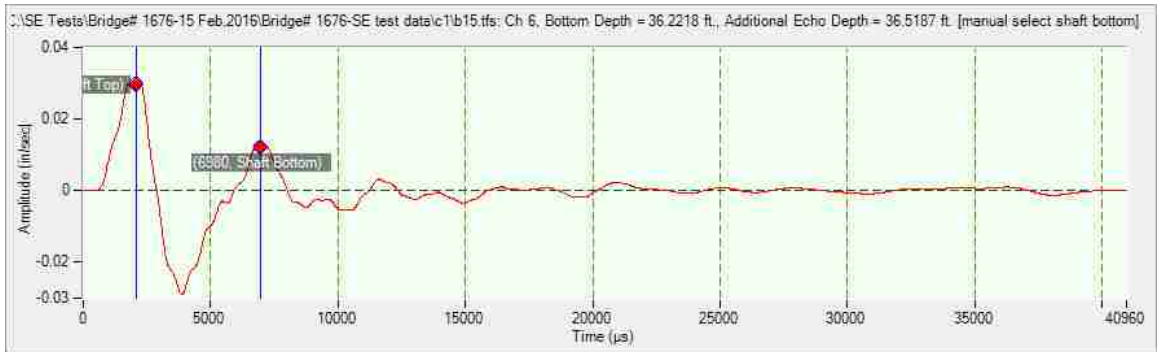


Figure 5-14: Velocity Trace of SE Test No. b15 Using Medium Soft Tip- B Upward

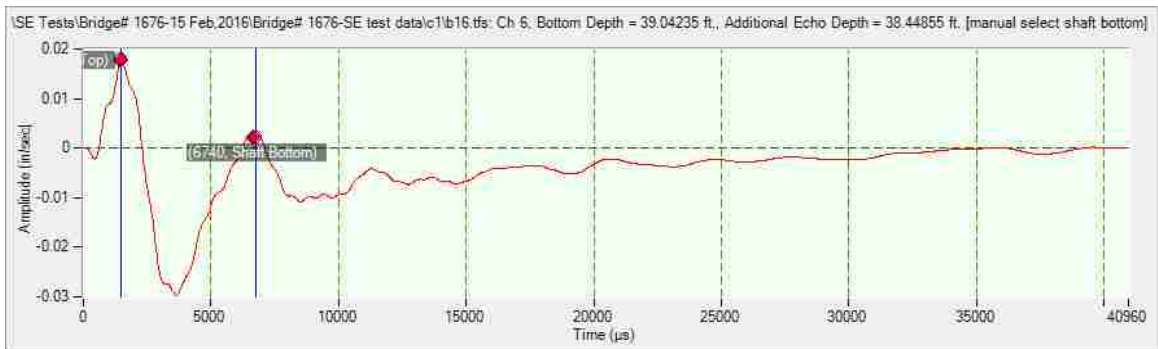


Figure 5-15: Velocity Trace of SE Test No. b16 Using Soft Tip- B Upward

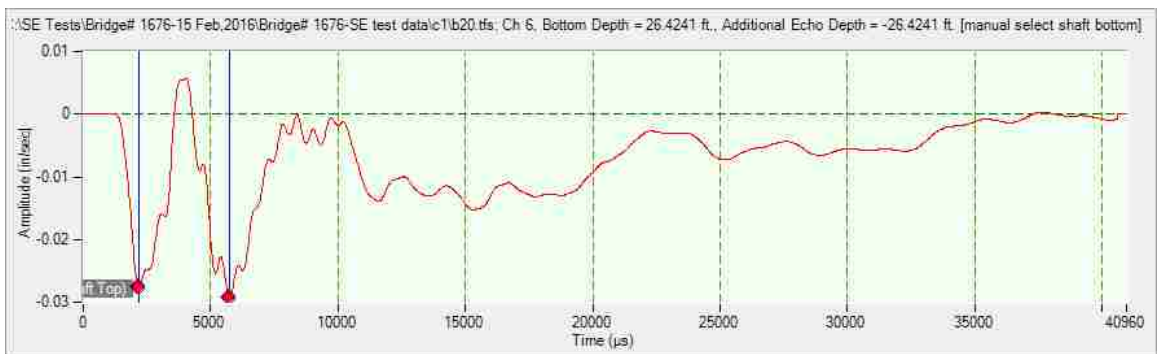


Figure 5-16: Velocity Trace of SE Test No. b20 Using Hard Tip- Wooden Block



Figure 5-17: Velocity Trace of SE Test No. b21 Using Medium Hard Tip- Wooden Block

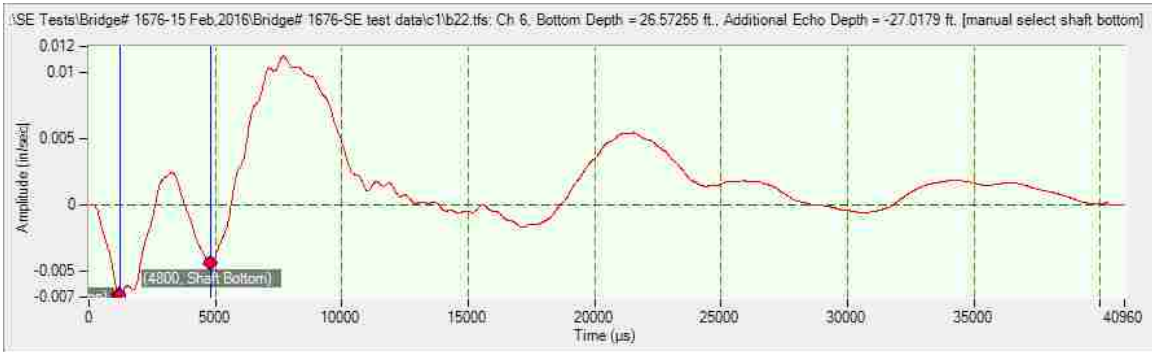


Figure 5-18: Velocity Trace of SE Test No. b22 Using Medium Soft Tip- Wooden Block



Figure 5-19: Velocity Trace of SE Test No. B23 Using Soft Tip- Wooden Block

The blue lines in the velocity trace present the initial wave and the first reflection respectively. The time difference between the initial response and the first echo Δt is used to calculate the wave travel depth, as shown in Table 5-4. The velocity traces obtained from accelerometer 1 (mounted close to the pile top) present good data for tests from b1 to b3. Hence, hard, medium hard, and medium soft hammer tips can result in having tests with good data when the strikes were

conducted at point A. Although, the data obtained from using the softer hammer tips gives a clear impulse and echo (test b4), the assessed pile length is longer than the lengths obtained from other hammer tips. Comparatively, the data obtained from upward strikes at point B indicate reliable and clear data when the hard hammer tip was used. The data obtained when the medium hard, medium soft, and soft hammer tips were used show a wide range of variation in the assessment pile depths, so the results are neglected. While tests b20 to b23 show that reliable and consistent results were obtained when the strikes were conducted on wood block for all types of hammer tips. The average total depth of Pile C-1 calculated from the data obtained from accelerometer 1 is 27.6 feet, and the average buried depth is 21 feet. Meanwhile, the data obtained from channel 7, which is connected to accelerometer 2 and mounted far from the source of energy, shows a range variation in the assessment pile depths for all types of hammer tips. However, the average total depth of Pile C-1 from accelerometer 2 is 28.2 feet, and the average buried depth is 21.7 ft. which is very close to the average depths that obtained from accelerometer 1.

5.2.2.3 Pile C-2

Pile C-2 is located at the west side of the bridge and beside pile C-1, as shown in Figure 3-17. The direction of striking was vertical on three points, downward either at point A or B on the pile cap, and upward at point C on the pile cap close to the pile. The test setup is similar to Pile C-1; two accelerometers were attached vertically to the top surface of the wooden block. Accelerometer 1 was connected to channel 6 and accelerometer 2 was connected to channel 7 and the

distance between the accelerometers was 4 feet. Figure 5-20 shows the SE test setup details of Pile C-2. Table 5-5 shows the directions and locations of strikes on Pile C-2.

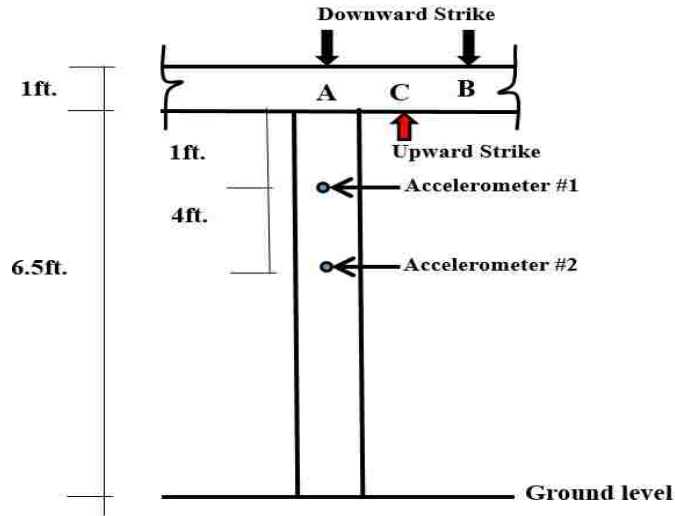


Figure 5-20: SE Test Setup of Pile C-2

Table 5-5: Strike Directions on Pile C-2

Point	Strike Direction
A	Downward
B	Downward
C	Upward

Table 5-6 shows the characteristics and results of SE field test for Pile C-2. The same procedure was used to estimate the depth of Pile C-1.

The velocity traces obtained from both accelerometers indicated good data where the strikes were conducted at the top of the pile cap directly at point A using hard and medium hard hammer tips. However, the velocity trace has unclear initial impulse and echo results when the medium soft and soft hammer tips were used. The cause of the unreliable data is due to the longer impact duration and lower

energy as shown in the hammer force versus time graph in Figure 5-21. Furthermore, the results from both accelerometers show longer depths for all types of hammer tips when the strike is conducted downward at point B or upward at point C. Hence, the average total depth of Pile C-2 that was calculated from the data obtained from accelerometer 1 is 32.7 feet, and the average buried length is 27 feet.

Table 5-6: Characteristics and Results of SE Field Test for Pile C-2

Test No	Hammer Tip's Type	Direction of Strike	Accelerometer 1			Accelerometer 2		
			Δt (μs)	L_t (ft.)	L_b (ft.)	Δt (μs)	L_t (ft.)	L_b (ft.)
c1	Hard	A -Downward	3760	28.9	22.4	3080	27.9	21.4
c2	Med-hard	A -Downward	4140	31.7	25.2	3720	32.6	26.1
c3	Med-soft	A -Downward	NS	NS	NS	NS	NS	NS
c4	Soft	A -Downward	NS	NS	NS	NS	NS	NS
c5	Hard	B -Downward	4700	35.9	29.4	3720	32.6	26.1
c6	Med-hard	B -Downward	4500	34.4	27.9	3640	32	25.5
c7	Med-soft	B -Downward	4820	36.8	30.3	3780	33.1	26.6
c8	Soft	B -Downward	4700	35.9	29.4	3800	33.2	26.7
c9	Hard	C -Upward	4660	35.6	29.1	3720	32.6	26.1
c10	Med-hard	C -Upward	4600	35.1	28.6	3660	32.2	25.7
c11	Med-soft	C -Upward	5100	38.9	32.4	4240	36.5	30
c12	Soft	C -Upward	4900	37.4	30.9	4020	34.8	28.3

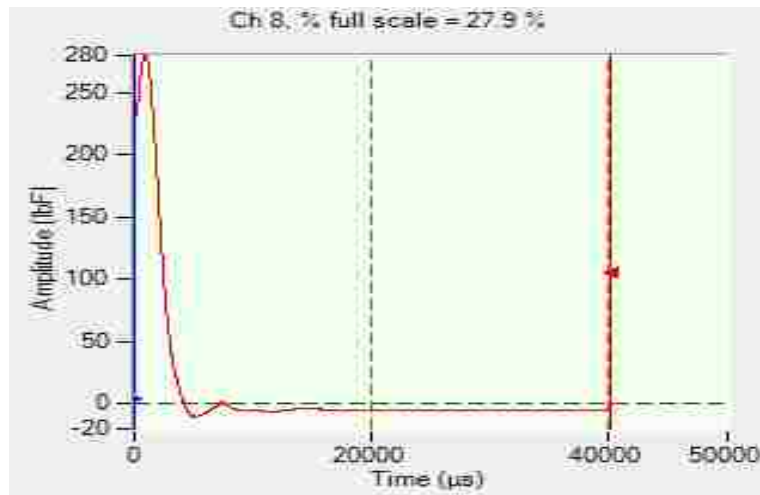


Figure 5-21: Force Versus Time Graph Obtained from Hammer Sensor Using Softer Tip

5.2.2.4 Pile B-4

Pile B-4 is located at the east side of the bridge, as shown in Figure 3-17. Here sixteen SE tests were conducted on Pile B-4 to obtain results and compare these estimated pile depths to the depths of Pile C-1 and Pile C-2. Different hammer tips were used in striking the pile. The direction of striking was vertical on four points, downward either at point A or B on the pile cap, or at point D on the bridge pavement, and upward at point C on the pile cap. The test setup is similar to Pile C-1 and Pile C-2; two accelerometers were attached vertically to the top surface of a wooden block; Accelerometer 1 was connected to channel 6 and accelerometer 2 was connected to channel 7, and the distance between the accelerometers was 2 feet. Figure 5-22 shows the SE test setup details on Pile B-4. Table 5-7 shows the directions and locations of strikes on Pile B-4.

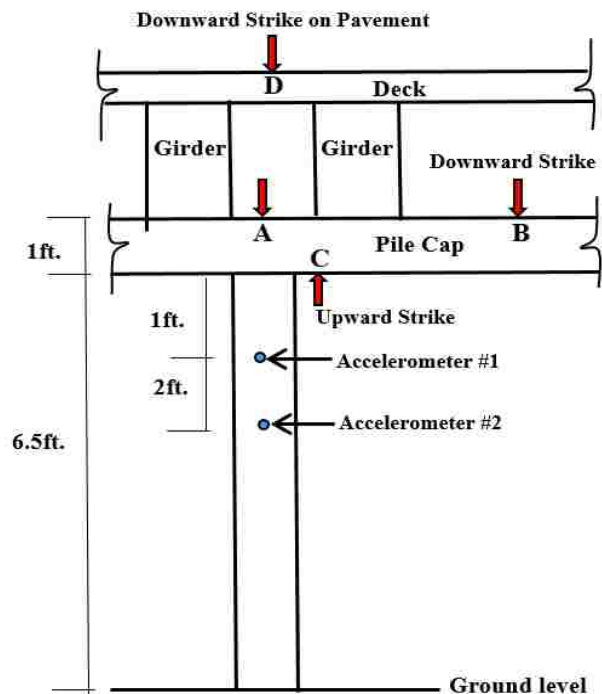


Figure 5-22: SE Test Setup of Pile B-4

Table 5-7: Strike Direction on Pile B-4

Point	Strike Direction
A	Downward
B	Downward
C	Upward
D	Downward on Pavement

Table 5-8 shows the characteristics and results of SE field tests for Pile C-2. The same procedure was used to estimate the depths of Pile C-1 and Pile C-2. Examples of data that was obtained from accelerometer 1 when the hard hammer tip was used (tests d1, d5, d9 and d13) are presented in Figures 5-23 to 5-26, respectively.

Table 5-8: Characteristics and Results of SE Field Test for Pile B-4

Test No	Hammer Tip's Type	Direction of Strike	Accelerometer 1			Accelerometer 2		
			Δt (μs)	L_t (ft.)	L_b (ft.)	Δt (μs)	L_t (ft.)	L_b (ft.)
d1	Hard	A -Downward	5380	40	33.5	5320	42.5	36
d2	Med-hard	A -Downward	NS	NS	NS	4880	39.2	32.7
d3	Med-soft	A -Downward	5020	38.3	31.8	4740	38.2	31.7
d4	Soft	A -Downward	5180	39.4	32.9	4500	36.4	29.9
d5	Hard	C -Upward	4780	36.5	30	4520	36.5	30
d6	Med-hard	C -Upward	4780	36.5	30	4560	36.8	30.3
d7	Med-soft	C -Upward	5140	39.2	32.7	4200	34.2	27.7
d8	Soft	C -Upward	5000	38.1	31.6	NS	NS	NS
d9	Hard	B -Downward	2780	21.6	15.1	2820	23.9	17.4
d10	Med-hard	B -Downward	3000	23.3	16.8	2980	25.1	18.6
d11	Med-soft	B -Downward	3360	25.9	19.4	3300	27.5	21
d12	Soft	B -Downward	NS	NS	NS	NS	NS	NS
d13	Hard	D -Downward-Pavement	NS	NS	NS	NS	NS	NS
d14	Med-hard	D -Downward-Pavement	NS	NS	NS	NS	NS	NS
d15	Med-soft	D -Downward-Pavement	NS	NS	NS	NS	NS	NS
d16	Soft	D -Downward-Pavement	NS	NS	NS	NS	NS	NS

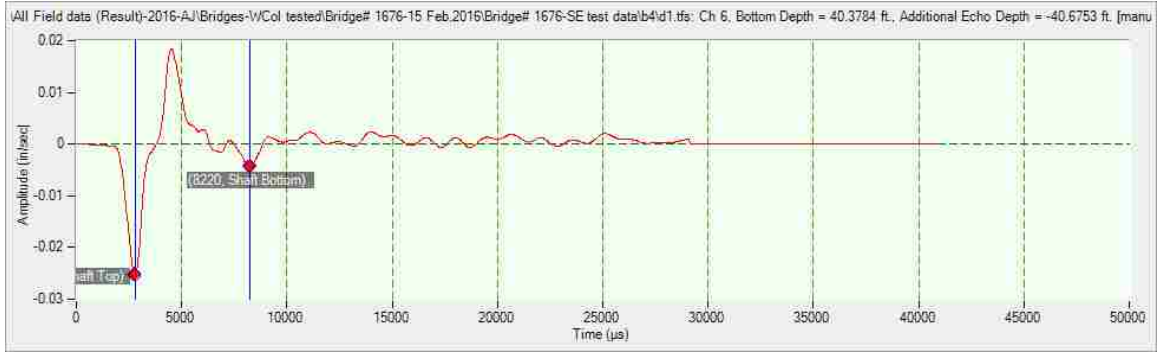


Figure 5-23: Velocity Trace of SE Test No. d1 Using Hard Tip- A Downward

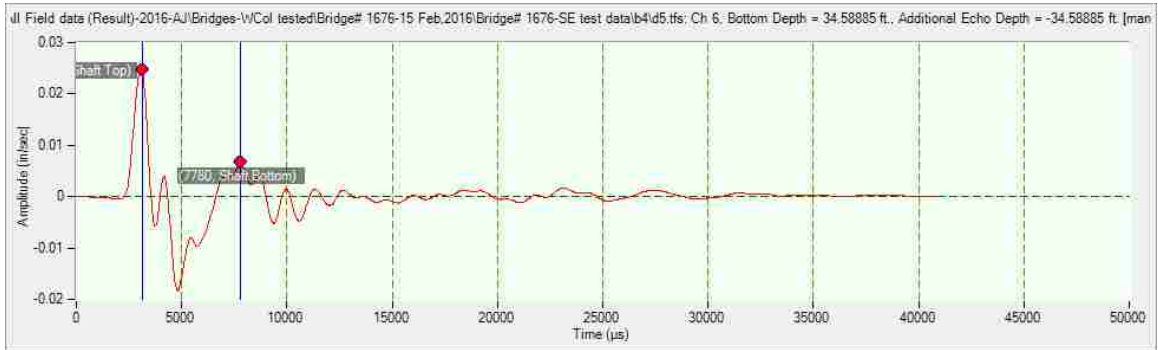


Figure 5-24: Velocity Trace of SE Test No. d5 Using Hard Tip- C Upward

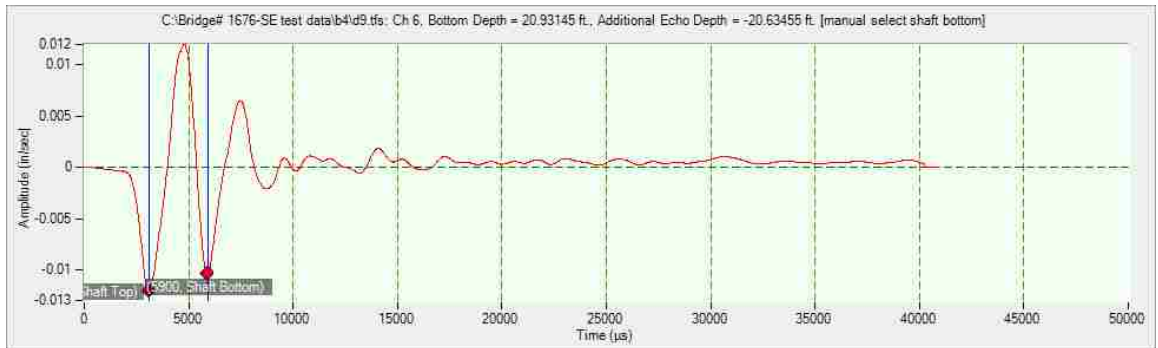


Figure 5-25: Velocity Trace of Test No. d9 Using Hard Tip- B Downward

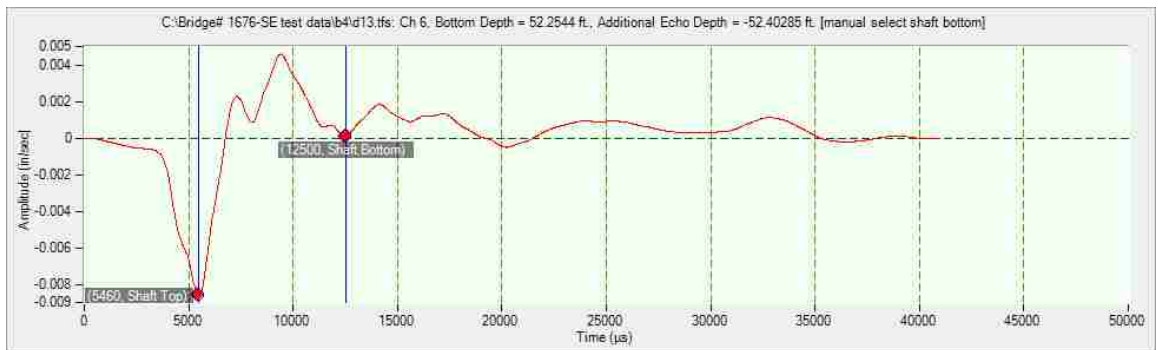


Figure 5-26: Velocity Trace of Test No. d13 Using Hard Tip- D Downward on Pavement

The velocity traces that were obtained from accelerometer 1 are used in this discussion. The data obtained when the strikes were directly downward at point A presented good results for all tests d1 to d4 with all types of hammer tips. The assessment total depth was reasonable but it longer comparing to assessment total lengths of Pile C-1 and Pile C-2. However, upward strikes at point C provided reasonable results this time for all types of tips. While SE tests did not present good data when the strikes were conducted at point B whereby a variation of pile depth assessment was indicated. Regarding the striking at point D (on the pavement), the results failed to indicate a clear echo in the velocity traces for all tests. Figure 5-27 shows a difficulty in identifying the initial echo when the strikes were conducted at the pavement. For example, if point 1 was selected as the initial echo, then the determined pile depth equals 14 feet, but it equals 19 feet if point 2 was selected. However, if points 3 and 4 were considered as initial echo peaks, then the assessment of pile depth equaled 29.4 feet and 52.5 feet, respectively. Comparing these depths with test d1 to d9, the data should be neglected due to resulting doubtful depths assessment. In conclusion, conducting the strike on pavement is not a viable alternative striking method in the absence of accessibility to pile cap. The data obtained from accelerometer 2 show reliable and reasonable assessment pile depths for all types of hammer tips when the strikes are conducted downward at point A and upward at point C. However, the data obtained from tests d9 to d16 are neglected due to a doubtful depths assessment. Thus, the total depth of Pile B-4 as determined from accelerometer 1 equals 33 feet, and the buried depth is 26 feet, while the data from accelerometer 2 indicates that L_t equals 37.7

feet and L_b is 31.2 feet. Table 5-9 summarizes the average total and buried depths of the tested piles for Bridge #1676:

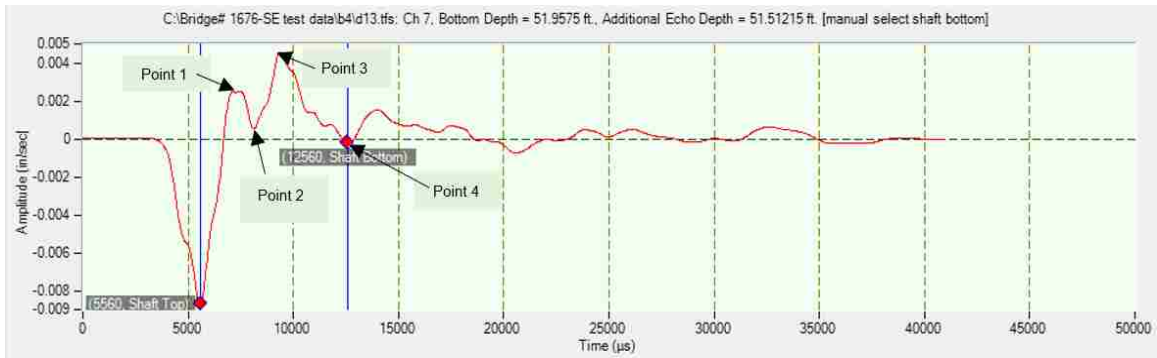


Figure 5-27: Velocity Trace Shows Difficulty in Identifying the Initial Echo When the Strike is Conducted on Concrete Pavement

Table 5-9: Piles Depths Assessment for Bridge #1676

Pile No.	Assessed Total Pile Depth (ft.)	Assessed Buried Pile Depth (ft.)
C-1	28	21
C-2	33	26
B-4	38	32
D-4	35	29

5.2.3 Bridge #6922 SE Field Test Results

5.2.3.1 Determination of Wave Velocity Within Timber Pile

Bridge #6922 has joints in the girder, so the data obtained from the SE tests of the piles was used to determine the propagated stress wave velocity (see section 3-3 in Chapter 3). Two accelerometers were attached on the pile side. The distance between the accelerometers was 1.5 feet. Striking on the pile cap directly downward at point A generated a wave within the pile. A hard hammer tip was used in these SE tests, and the wave reached accelerometer 1, and then accelerometer 2 in specific travel times. The wave travel time between these two

accelerometers was measured and used to determine the wave velocity by using the peak points approach, as mentioned in section 3-3 in Chapter 3. However, the average propagated wave velocity that was determined from the difference of initial impulses of velocity traces that were obtained from both accelerometers is 15000 ft./sec. This average wave velocity in timber pile was used to compute the buried and total depths of Bridge #6822 piles. Figures 5-28 to 5-31 present examples of the velocity traces that were obtained from accelerometers 1 and 2. Table 5-10 shows the estimated wave velocity using the peak point approach.

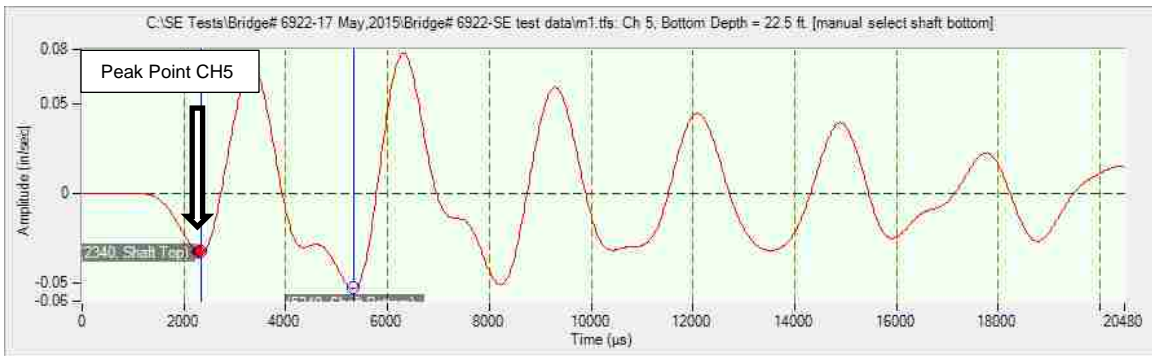


Figure 5-28: Velocity Trace Test No.m1 Using Peak Point Approach- CH5

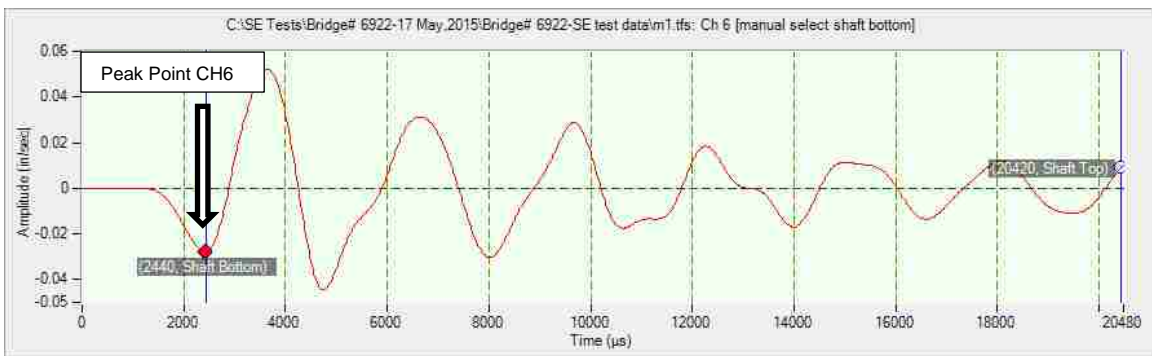


Figure 5-29: Velocity Trace Test No. m1 Using Peak Point Approach- CH6

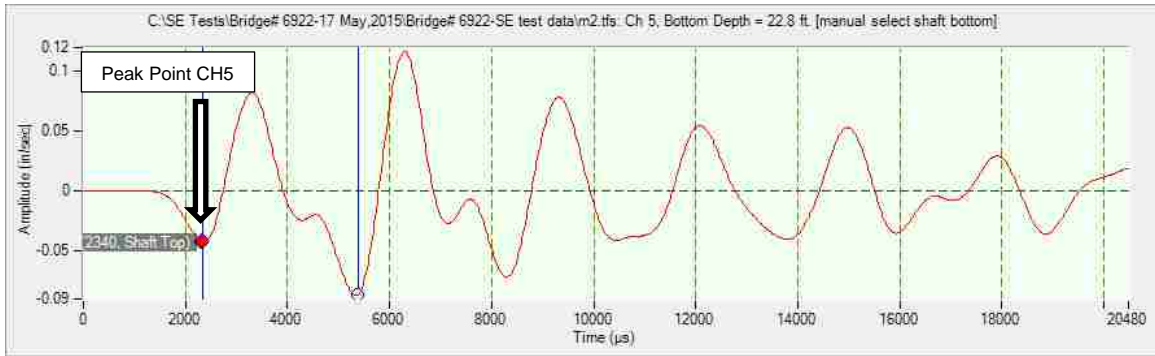


Figure 5-30: Velocity Trace Test No. m2 Using Peak Point Approach- Ch5

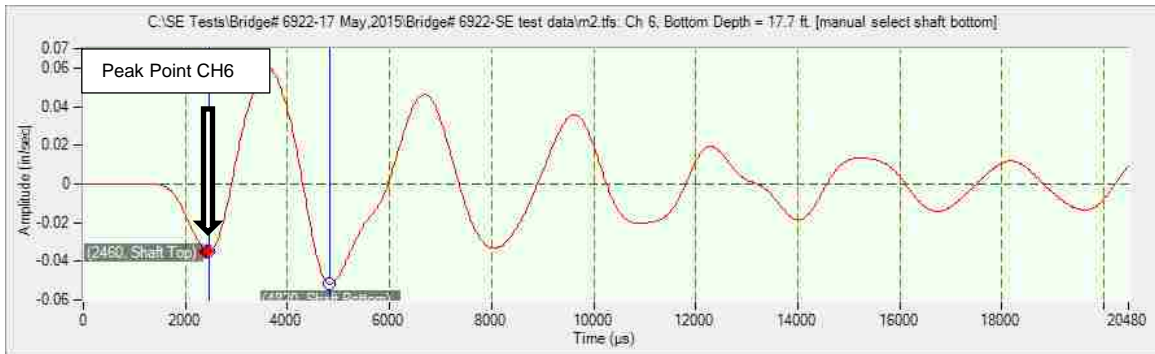


Figure 5-31: Velocity Trace Test No. m2 Using Peak Point Approach- Ch6

Table 5-10: Estimated Wave Velocity Using Peak Point Approach for Bridge #6922

Pile No.	Hammer Tip Type	Test No.	t1 (μs.) [Ch5]	t2 (μs.) [CH6]	Δt (μs.)	Δd Between Accels. (ft.)	Measured Velocity (ft./s)
Pile #1	Hard	m1	2340	2440	100	1.5	15000
	Hard	m2	2360	2460	100	1.5	15000
Pile #2	Hard	m13	2780	2880	100	1.5	15000
	Hard	m14	2780	2880	100	1.5	15000
	Hard	m15	2280	2380	100	1.5	15000
Pile #14	Hard	m37	2800	2900	100	1.5	15000
	Hard	m38	3360	3460	100	1.5	15000
	Hard	m39	3300	3400	100	1.5	15000

5.2.3.2 Pile 1

Pile 1 is located at the east side of the bridge, as shown in Figure 3-19. Here, twelve SE tests were conducted on Pile 1 in order to study the obtained signals from the data acquisition equipment. Three types of hammer tips were

used in striking the pile: hard, medium hard, and medium soft. The soft hammer tip was not used in testing Pile 1. The direction of the strikes was vertical on two points, downward either at point A or at the wedge (block). Upward strikes at point B did not apply for Bridge #6922. SE tests were conducted using two accelerometers that were attached vertically to the top surface of a wooden block. Accelerometer 1 was connected to channel 5 and accelerometer 2 to channel 6. The distance between the accelerometers was 1.5 feet. The image of Pile 1 and the SE test setup details are shown in Figure 5-32. Table 5-11 shows the characteristics and results of SE field tests for Pile 1. The estimated wave velocity V equals 15000 ft./s. Eq. 3.2 and Eq. 3.3 were used to compute the total depth L_t and buried depth L_b of Pile 1. Examples of data that obtained from the accelerometers for tests m1, m5, and m7 are indicated in Figures 5-33 to 5-38, respectively.

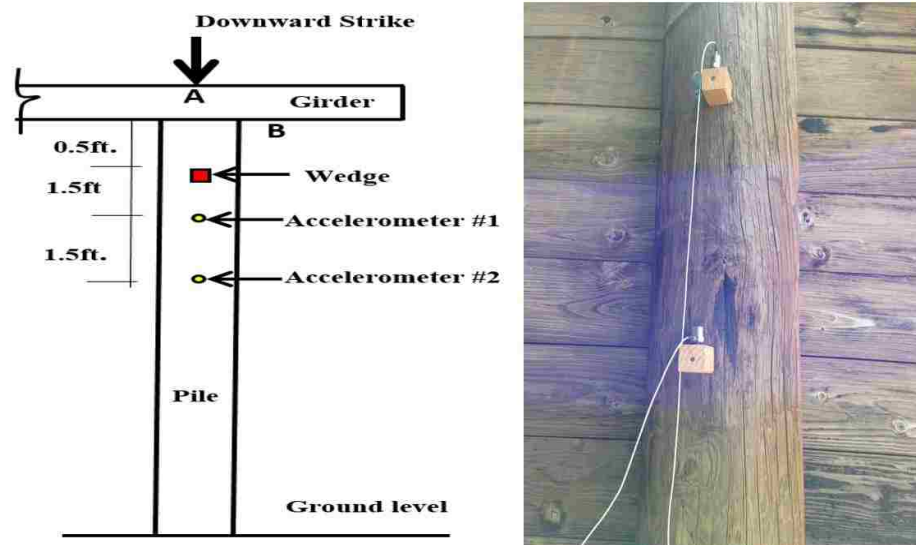


Figure 5-32: The Image of Pile 1 and SE Test Setup

Table 5-11: Characteristics and Results of SE Field Test for Pile 1

Test No	Hammer Tip's Type	Direction of Strike	Accelerometer 1			Accelerometer 2		
			Δt (μs)	L_t (ft.)	L_b (ft.)	Δt (μs)	L_t (ft.)	L_b (ft.)
m1	Hard	A -Downward	3000	24.5	15.25	2400	21.5	12.25
m2	Hard	A -Downward	3000	24.5	15.25	2400	21.5	12.25
m3	Hard	A -Downward	2860	23.45	14.2	2420	21.65	12.4
m4	Med-hard	A -Downward	3500	28.25	19	3620	30.65	21.4
m5	Med-hard	A -Downward	2840	23.3	14.05	3060	26.45	17.2
m6	Med-hard	A -Downward	2960	24.2	14.95	3060	26.45	17.2
m7	Med-soft	A -Downward	3100	25.25	16	3540	30.05	20.8
m8	Med-soft	A -Downward	3000	24.5	15.25	3500	29.75	20.5
m9	Med-soft	A -Downward	3000	24.5	15.25	3240	27.8	18.55
m10	Hard	AI- Block-Downward	3040	24.8	15.55	2300	20.75	11.5
m11	Med-hard	AI- Block-Downward	3180	25.85	16.6	NS	NS	NS
m12	Med-soft	AI- Block-Downward	3040	24.8	15.55	NS	NS	NS

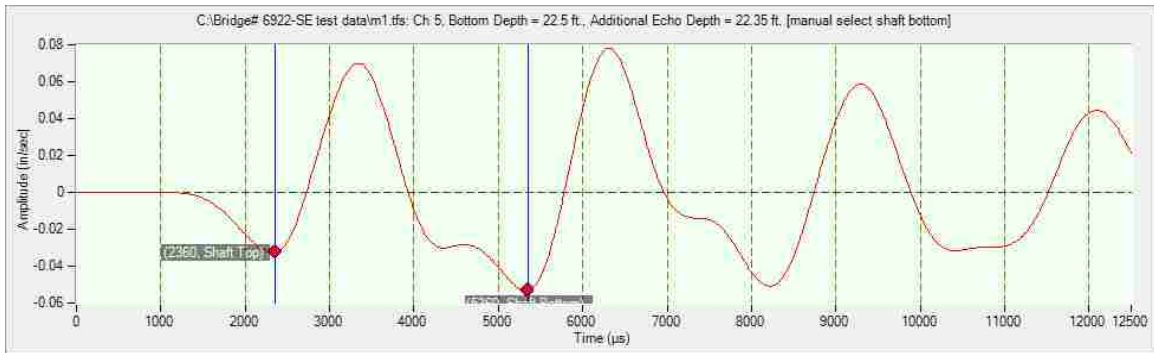


Figure 5-33: Velocity Trace of SE Test No.m1- Ch5- Using Hard Tip- A Downward

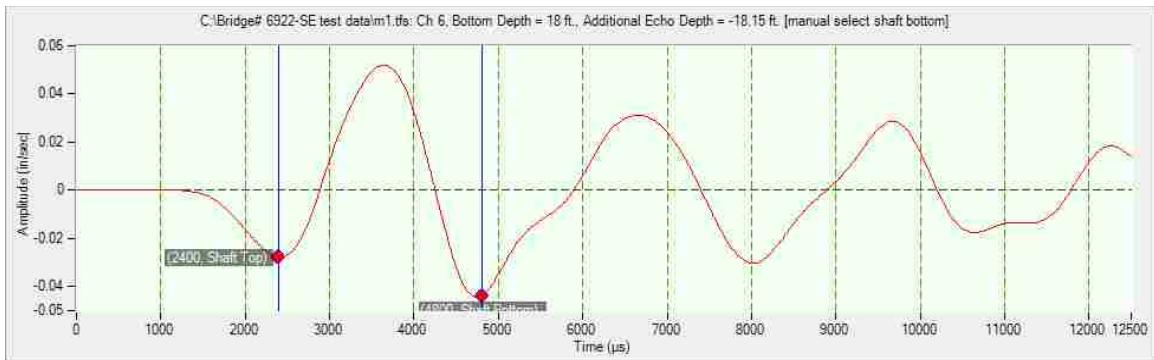


Figure 5-34: Velocity Trace of SE Test No. m1- Ch6- Using Hard Tip- A Downward

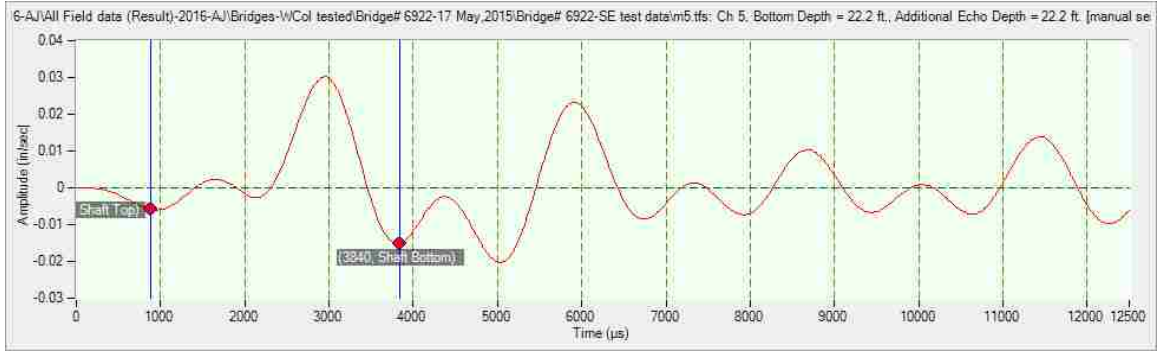


Figure 5-35: Velocity Trace of SE Test No. m5- Ch5- Using Medium Hard Tip- A Downward

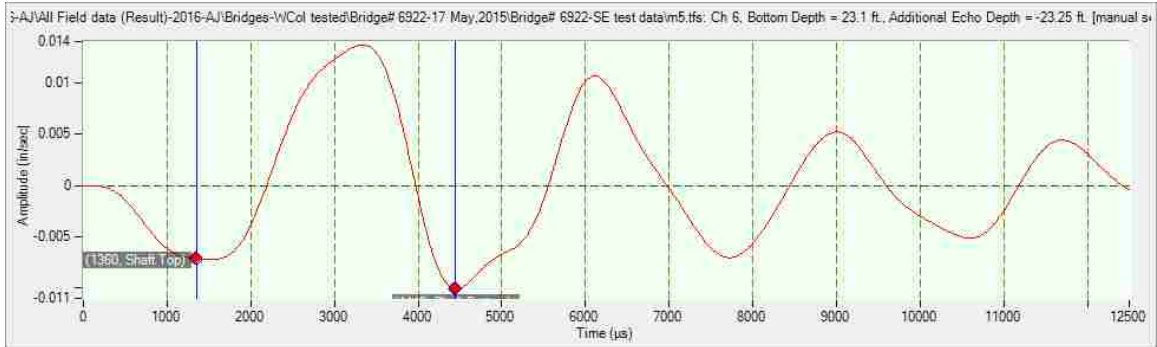


Figure 5-36: Velocity Trace of SE Test No. m5- Ch6- Using Medium Hard Tip- A Downward

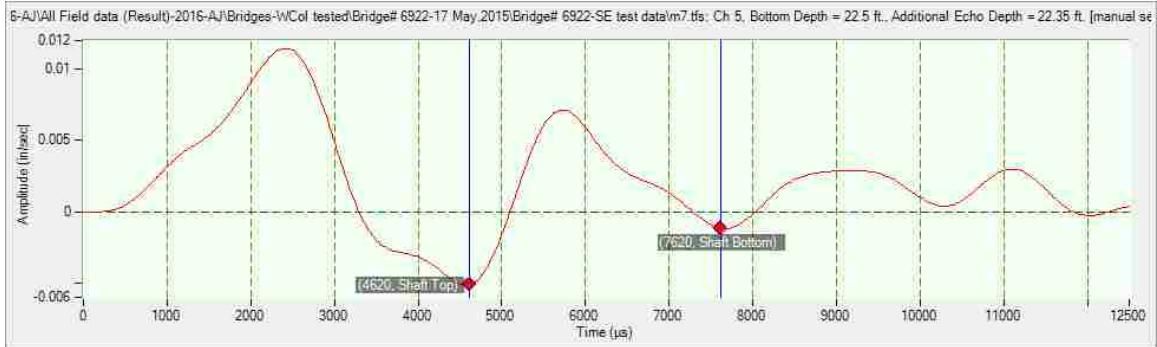


Figure 5-37: Velocity Trace of SE Test No. m7- Ch5- Using Medium Soft Tip- A Downward

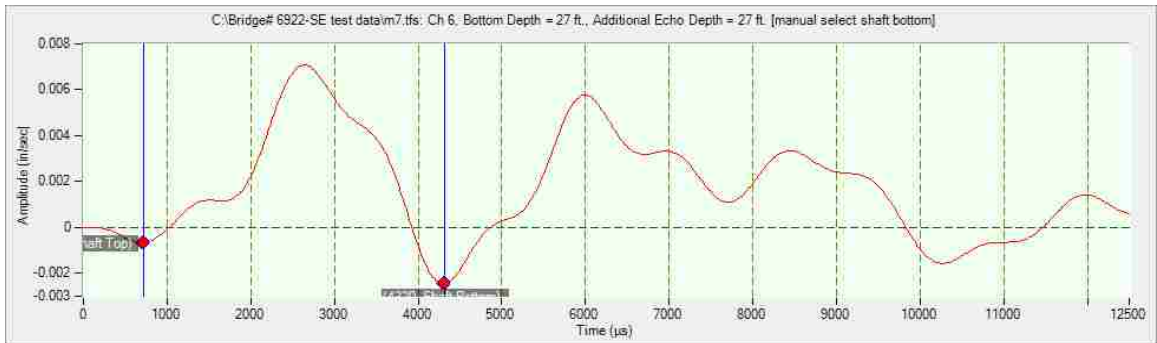


Figure 5-38: Velocity Trace of SE Test m7 - Using Medium Soft Tip- A Downward

The velocity traces that were obtained from accelerometer 1, which was mounted close to the top of the pile, present a good set of data for all tests, m1, m6 and m7. Hence, the use of hammer tips, hard, medium hard, and medium soft, could achieve the tests providing good data when the pile top is struck at point A. Conversely, the data that was obtained from accelerometer 2, which was mounted far from the source of energy, shows a range variation in the assessment of pile depths for all types of hammer tips. The average total depth of Pile 1 that was determined from data obtained from accelerometer 1 is 24.5 feet. and the average buried depth is 16 feet. Likewise, SE tests m10, m11 and m12 were conducted by vertically striking an aluminum block and using hard, medium hard, and medium soft hammer tips, respectively. Figure 5-39 shows the velocity traces that were obtained from accelerometer 1 for test m11.

The presence of the unfavorable oscillation at the initial part of the velocity traces may be caused by a tiny bit of sliding that may have occurred between the aluminum wedge (block) and the pile surface during the impact. This sliding clearly appears in the impulse graph for test m11, as shown in Figure 5-40. However, this oscillation part could be neglected and instead the next deeper valley be selected as the initial impulse and thus can be compared in the assessment Δt with time difference that obtained from striking at point A in validating the results. The assessment time difference between the initial impulse and first echo for test m11 is 3180 μs and the average total depth of Pile 1 is 25 feet, which is a reliable value.

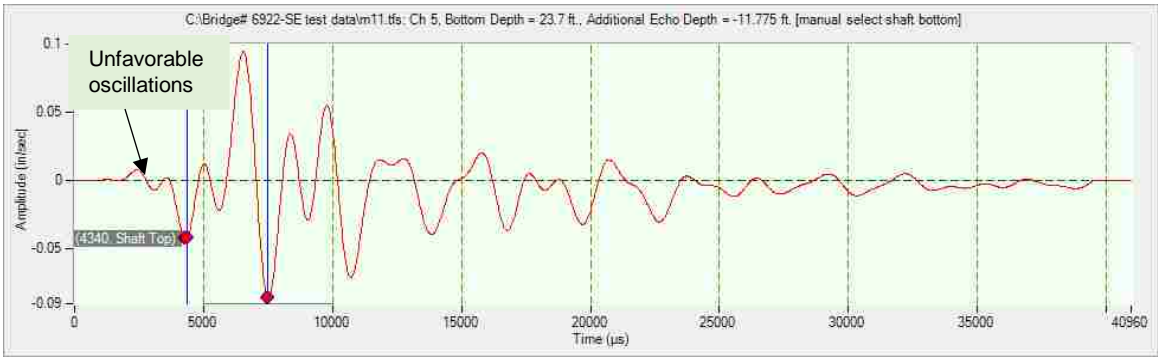


Figure 5-39: Velocity Trace of SE Test m11- Ch5- Using Medium Hard Tip-Downward on Aluminum Block

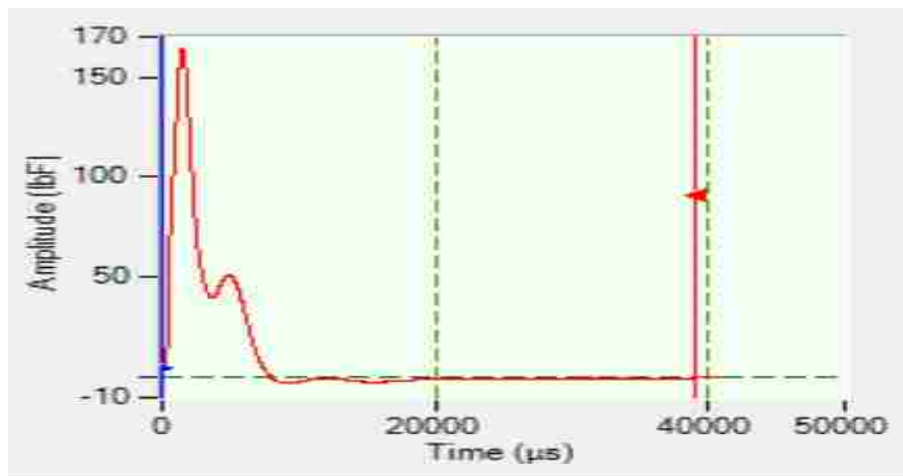


Figure 5-40: Impulse Graph of the Hammer for Test m11 Shows Two Peaks

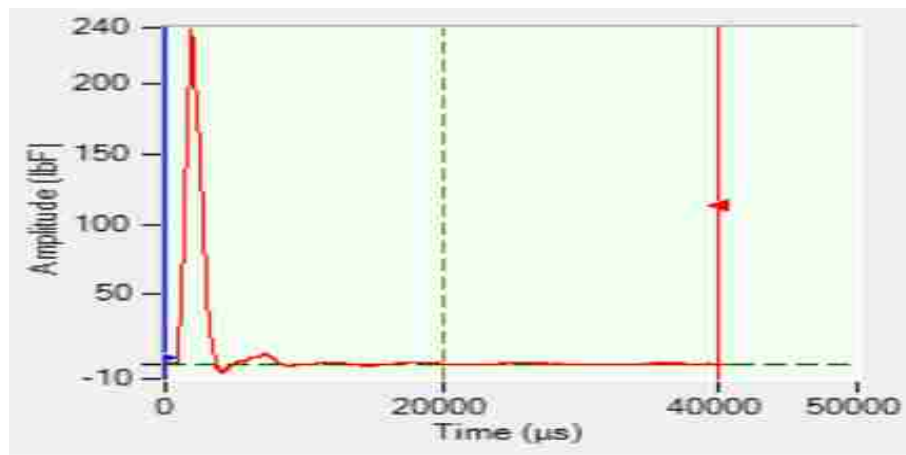


Figure 5-41: Typical Impulse Graph- Shows One Clear Peak

5.2.3.3 Pile 2

Pile 2 is located at the east side of the bridge beside Pile 1, as shown in Figure 3-19. Here, nine SE tests were conducted on Pile 2 and, similar to Pile 1, three types of hammer tips are used for providing the impact: hard, medium hard, and medium soft. The striking direction applied was downward on the pile cap at point A. Two accelerometers were used, accelerometer 1 was connected to channel 5 and accelerometer 2 to channel 6. The distance between the accelerometers was 1.5 feet, as shown in Figure 5-42. Table 5-12 shows the characteristics and results of the SE field tests for Pile 2.

The velocity traces that obtained from accelerometer 1 indicated reasonable data results when hard and medium hard hammer tips were used for striking the top of the pile cap directly at point A. The velocity trace has an unclear initial impulse and echo when the medium soft hammer tip was used, as shown in Figure 5-43. The cause of this unreliable data is due to the longer impact duration and lower amplitude of energy. Furthermore, the results from accelerometer 2 again shows a range of variation in the pile depth assessments for all types of hammer tips. Hence, the average total depth of Pile 2 that was assessed from the data obtained from accelerometer 1 is 22.4 feet, and the average buried depth is 13 feet.

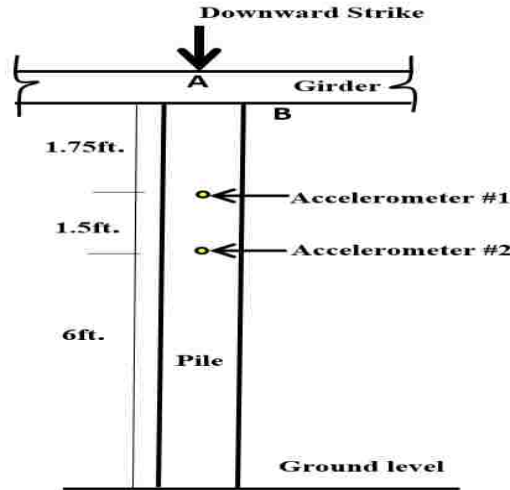


Figure 5-42: SE Test Setup for Pile 2 of Bridge #6922

Table 5-12: Characteristics and Results of SE Field Test for Pile 2

Test No	Hammer Tip's Type	Direction of Strike	Accelerometer 1			Accelerometer 2		
			Δt (μs)	L_t (ft.)	L_b (ft.)	Δt (μs)	L_t (ft.)	L_b (ft.)
m13	Hard	A -Downward	2780	22.6	13.35	1980	18.1	8.85
m14	Hard	A -Downward	2780	22.6	13.35	2020	18.4	9.15
m15	Hard	A -Downward	2320	19.15	9.9	2420	21.4	12.15
m16	Med-hard	A -Downward	2660	21.7	12.45	3000	25.75	16.5
m17	Med-hard	A -Downward	NS	NS	NS	NS	NS	NS
m18	Med-hard	A -Downward	3220	25.9	16.65	NS	NS	NS
m19	Med-soft	A -Downward	NS	NS	NS	NS	NS	NS
m20	Med-soft	A -Downward	NS	NS	NS	NS	NS	NS
m21	Med-soft	A -Downward	NS	NS	NS	NS	NS	NS

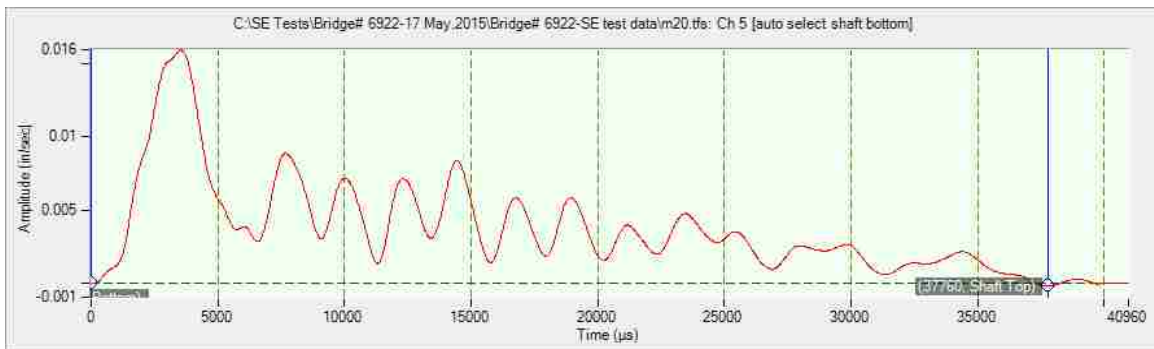


Figure 5-43: Velocity Trace of SE Test No. m20 Using Medium Sot Tip Shows Unclear Initial Impulse

5.2.3.4 Pile 3

Pile 3 is located at the east side of the bridge beside Pile 2, as shown in Figure 3-19. Here, twelve SE tests were conducted on Pile 3, and two types of hammer tips were used in striking the pile: hard and medium hard. There is no access to strike the top of Pile 3, so the impact was conducted downward using both wooden and aluminum wedges (block). Two accelerometers were used; accelerometer 1 was connected to channel 5 and accelerometer 2 to channel 6, and the distance between the accelerometers is 1.5 feet, as shown in Figure 5-44. Table 5-13 shows the characteristics and results of the SE field tests for Pile 3.

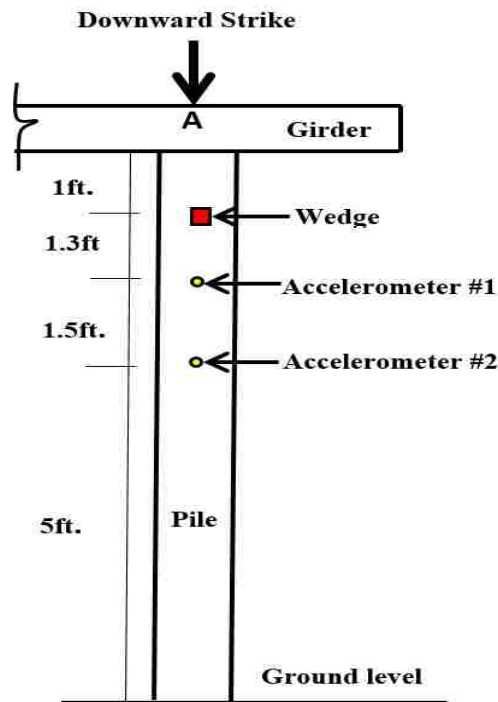


Figure 5-44: SE Test Setup for Pile 3 of Bridge #6922

Table 5-13: Characteristics and Results of SE Field Test for Pile 3

Test No	Hammer Tip's Type	Direction of Strike	Accelerometer 1			Accelerometer 2		
			Δt (μs)	L_t (ft.)	L_b (ft.)	Δt (μs)	L_t (ft.)	L_b (ft.)
m25	Hard	Wood Block-Downward	2820	23.5	14.5	2420	22.0	13.1
m26	Hard	Wood Block-Downward	2800	23.3	14.4	2500	22.6	13.7
m27	Hard	Wood Block-Downward	2800	23.3	14.4	2400	21.8	12.9
m28	Hard	Al- Block-Downward	1720	15.2	6.3	1960	18.5	9.6
m29	Hard	Al- Block-Downward	NS	NS	NS	NS	NS	NS
m30	Hard	Al- Block-Downward	1400	12.8	3.9	NS	NS	NS
m31	Med-hard	Wood Block-Downward	3300	27.1	18.1	NS	NS	NS
m32	Med-hard	Wood Block-Downward	3220	26.5	17.5	2900	25.6	16.7
m33	Med-hard	Wood Block-Downward	3220	26.5	17.5	2800	24.8	15.9
m34	Med-hard	Al- Block-Downward	NS	NS	NS	NS	NS	NS
m35	Med-hard	Al- Block-Downward	NS	NS	NS	NS	NS	NS
m36	Med-hard	Al- Block-Downward	NS	NS	NS </td <td>NS</td> <td>NS</td> <td>NS</td>	NS	NS	NS

Table 5-13 indicated reliable and consistent results for the data obtained from both accelerometers when hard and medium hard tips were used in providing the impact at the wood wedge (block). The results obtained from striking the aluminum wedge showed an unreliable assessment for pile depth for all types of tips. The velocity trace indicated an unclear initial impulse and echo when the aluminum block was used. Therefore, all results that were obtained from striking on the aluminum block are neglected for the same reasons as that indicated in section 5.2.3.2. The velocity traces for tests m25, m26, and m27 that obtained from accelerometer 1 are presented in Figures 5-45 to 5-47, respectively.

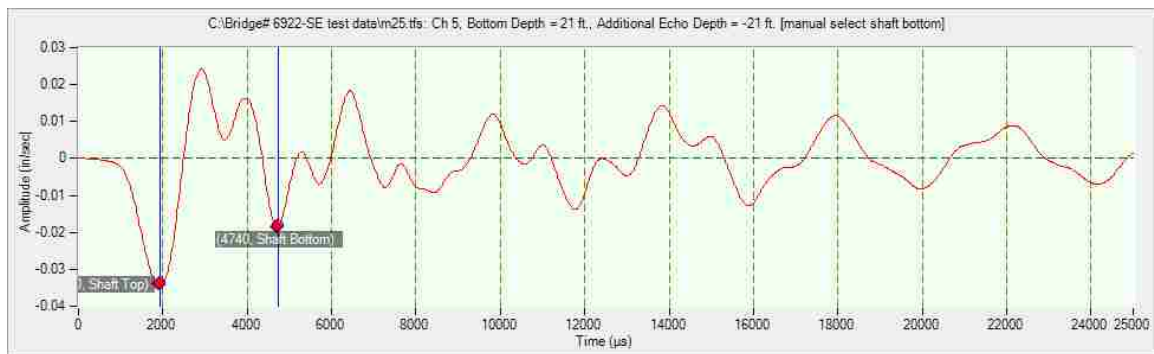


Figure 5-45: Velocity Trace of SE Test No. m25 Using Hard Tip- Wooden Block

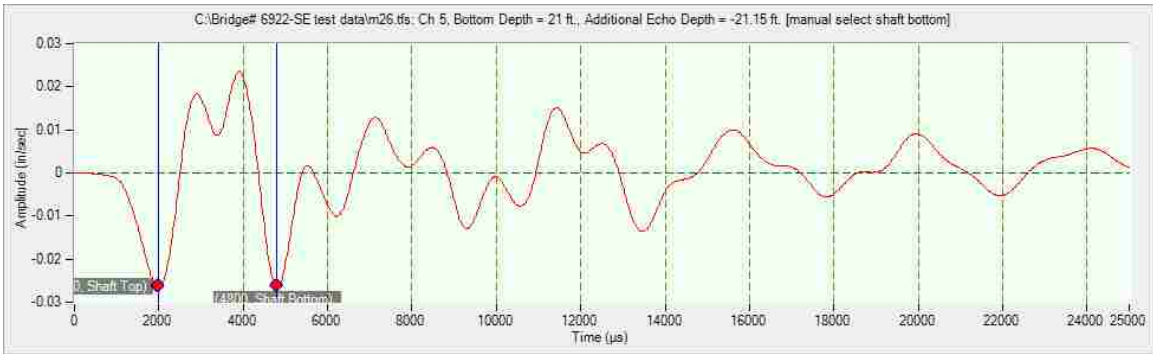


Figure 5-46: Velocity Trace of SE Test No. m26 Using Hard Tip- Wooden Block

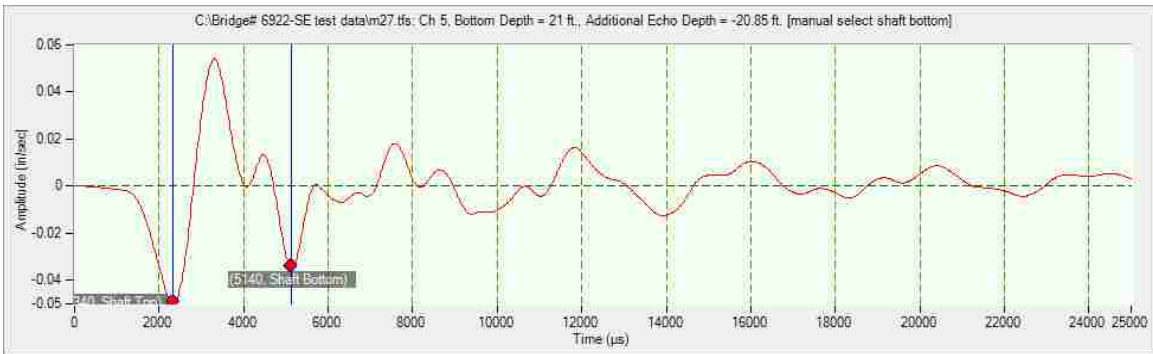


Figure 5-47: Velocity Trace of SE Test No. m27 Using Hard Tip- Wooden Block

Figures 5-45 to 5-47 indicate typical and clear initial results in the impulse and echo data obtained from accelerometer 1. However, Figure 5-48 shows two concavities in the initial impulse for unknown reasons. However, when an aluminum wedge was used, it was difficult to recognize the first echo clearly because multiple concavities appeared in the velocity trace; This may have occurred due to an inadequate connection between the aluminum wedge and pile surface which could cause a sliding. In conclusion, it is not recommended that the aluminum block be used in SE tests because of the resulting frequent unreliable data that make it impossible to identify the time lapse Δt . The average total depth of Pile 3 that was assessed using the data that were obtained from accelerometer 1 is 25 feet, and the average buried depth is 14 feet.

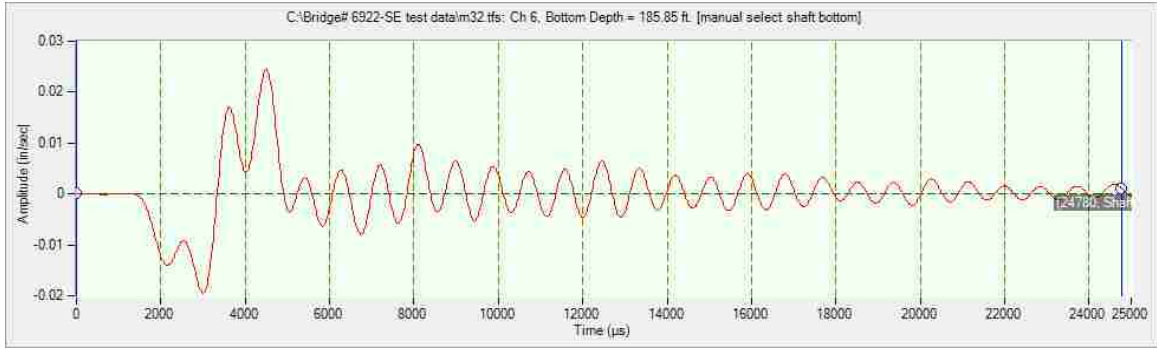


Figure 5-48: SE Test No. m32 Using Medium Hard Tip & Aluminum Block Shows Unclear Initial Impulse

5.2.3.5 Pile 14

Pile 14 is located at the west side of the bridge as shown in Figure 3-19. Six SE tests were conducted on Pile 14, using the hard hammer tip only. The strikes were conducted downward at point A and at the wooden wedge. Two accelerometers were used, accelerometer 1 was connected to channel 5 and accelerometer 2 to channel 6, and the distance between the accelerometers was 1.5 feet, as shown in Figure 5-49. Table 5-14 shows the characteristics and results of the SE field tests for Pile 14.

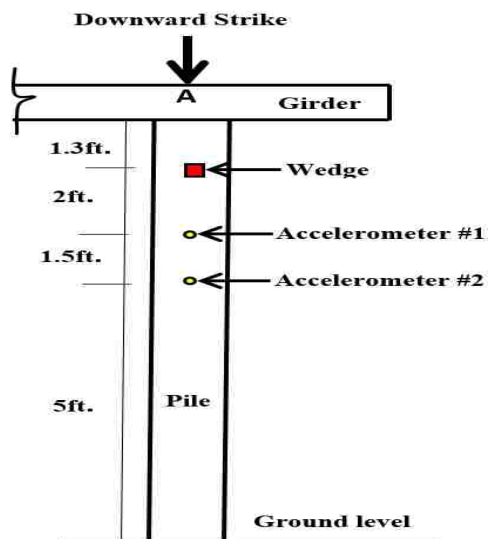


Figure 5-49: SE Test Setup for Pile 14 of Bridge #6922

Table 5-14: Characteristics and Results of SE Field Test for Pile 14

Test No	Hammer Tip's Type	Direction of Strike	Accelerometer 1			Accelerometer 2		
			Δt (μs)	L_t (ft.)	L_b (ft.)	Δt (μs)	L_t (ft.)	L_b (ft.)
m37	Hard	A -Downward	1800	16.83	7.58	1840	18.63	9.38
m38	Hard	A -Downward	1620	15.48	6.23	1760	18.03	8.78
m39	Hard	A -Downward	1620	15.48	6.23	1740	17.88	8.63
m40	Hard	Wood Block-Downward	NS	NS	NS	NS	NS	NS
m41	Hard	Wood Block-Downward	NS	NS	NS	NS	NS	NS
m42	Hard	Wood Block-Downward	1720	16.23	6.98	2020	19.98	10.73

Table 5-14 shows that the average assessed total depth of Pile 14 is 16 feet, which is an inconsistent length, as compared to the previous depths of piles 1, 2, and 3. The reason of this discrepancy is due to the presence of a large longitudinal crack located along Pile 14, as shown in Figure 5-50. This large crack may have disrupted the path of the wave causing an internal reflection. Table 5-15 summarized the average total and buried depths of tested piles for Bridge #6922.



Figure 5-50: Longitudinal Crack Along Pile 14

Table 5-15: Piles Depths Assessment for Bridge #6922

Pile No.	Assessed Total Pile Depth (ft.)	Assessed Buried Pile Depth (ft.)
Pile 1	25	16
Pile 2	22.4	13
Pile 3	25	14
Pile 14	16	7
Pile 15	16	7
Pile A	15	9.3

5.2.4 Bridge #1190 SE Field Test Results

SE tests were conducted on eight piles of Bridge #1190 in order to study the outcomes that obtained from acquisition platform equipment. Piles 1, 8,10,15,19,21, A and B were selected to be tested. However, only the data that obtained from conducting SE tests on Pile 8 and Pile 21 will be reviewed and discussed, for brevity and to avoid repeating discussion of the results of piles that have similar test characteristics to those mentioned previously. These two piles were selected because they have different characteristics from piles already discussed. Pile 8 has 4 inches of visible space at the pile top edge, which provided the capability to strike the pile top directly. In addition, the location of Pile 21 is such that the intermediate bent of the bridge cuts the stream path, which provided an opportunity to study the influences of water pressure and sound on SE test results.

5.2.4.1 Determination of Wave Velocity Within Timber Pile

The Bridge #1190 has the same characteristics as Bridge #6922, as well as the same pile dimensions, joined girder type, and also pile type. Therefore, the

same average wave velocity (15000 ft./sec) that was used to determine the piles depths of Bridge #6922 was also used to assess the piles depths of Bridge #1190.

5.2.4.2 Pile 8

Pile 8 is located at the west side of the bridge, as shown in Figure 3-21. Six SE tests were conducted on Pile 8 and three types of hammer tip were used for providing the impact: hard, medium hard, and medium soft. The top edge of the pile was accessible so that the direction of the striking applied was vertically downward at point A on the top of the pile's edge. One accelerometer was used and connected to channel 6. Figure 5-51 illustrates the details of SE test setup for Pile 8. Table 5-16 shows the characteristics and results of the SE field tests for Pile 8. The same procedure that was used to estimate the total depth L_t and buried L_b depth was followed to estimate Bridge #1190 piles. Examples of the results that were obtained from the accelerometer for tests t14, t17 and t18 are presented in Figures 5-52 to 5-54, respectively.

The initial impulses and initial echoes are obvious in all velocity traces when hard, medium hard, and medium soft hammer tips were used. Thus, these figures indicated reliable data for all types hammer tips when the strike is conducted at top of the pile's edge. Hence, the results indicate that the average total depth of Pile 8 is 24 feet and the average buried depth is 17 feet.

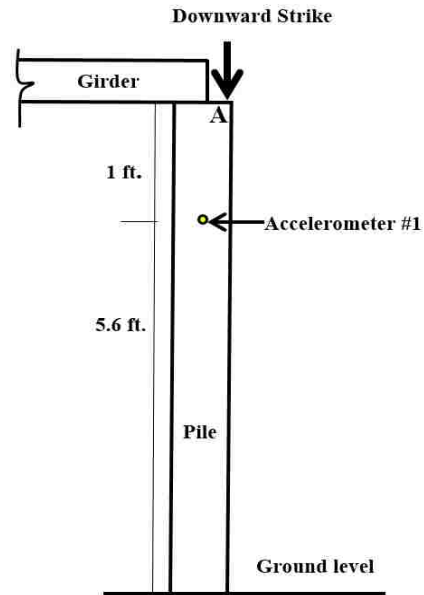


Figure 5-51: SE Test Setup for Pile 8 of Bridge #1190

Table 5-16: Characteristics and Results of SE Field Test for Pile 8

Test No	Hammer Tip's Type	Direction of Strike	Accelerometer		
			Δt (μs)	L_t (ft.)	L_b (ft.)
t14	Hard	A -Downward	2640	20.9	14.2
t15	Hard	A -Downward	2660	21.05	14.35
t16	Med-hard	A -Downward	2640	20.9	14.2
t17	Med-hard	A -Downward	2980	23.45	16.75
t18	Med-soft	A -Downward	3060	24.5	17.35
t19	Med-soft	A -Downward	3080	24.2	17.5

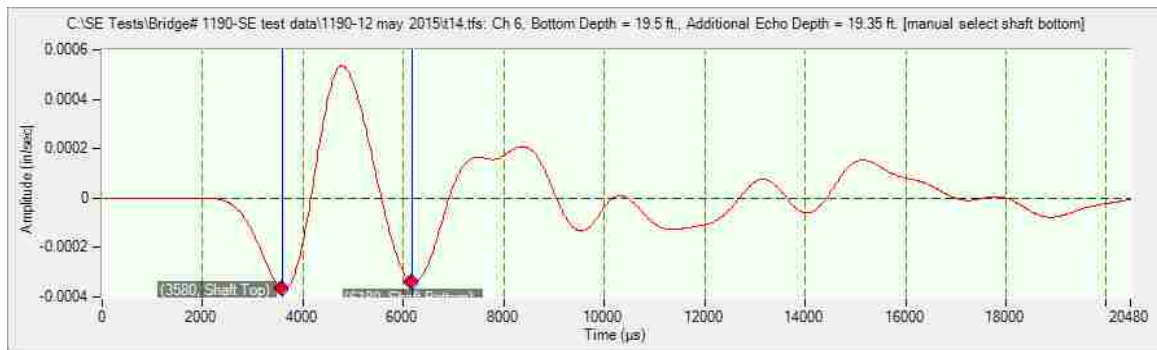


Figure 5-52: Velocity Trace of SE Test No. t14 Using Hard Tip- On Pile Top Edge

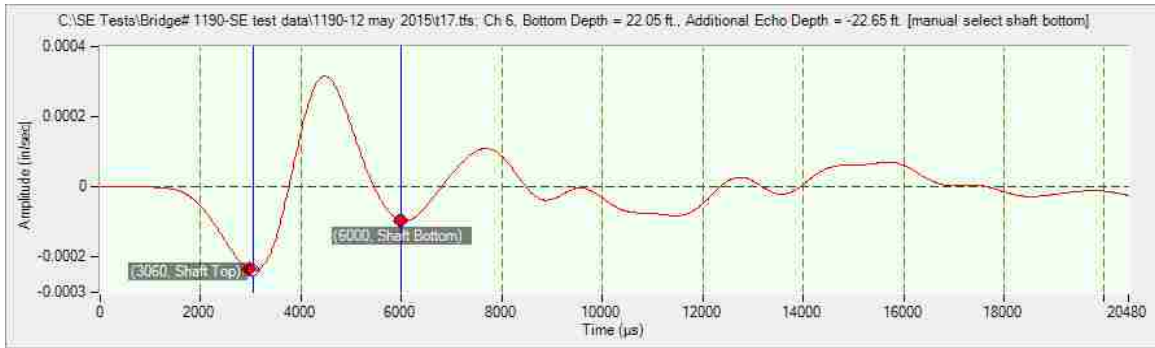


Figure 5-53: Velocity Trace of SE Test No. t17 Using Medium Hard Tip- On Pile Top Edge

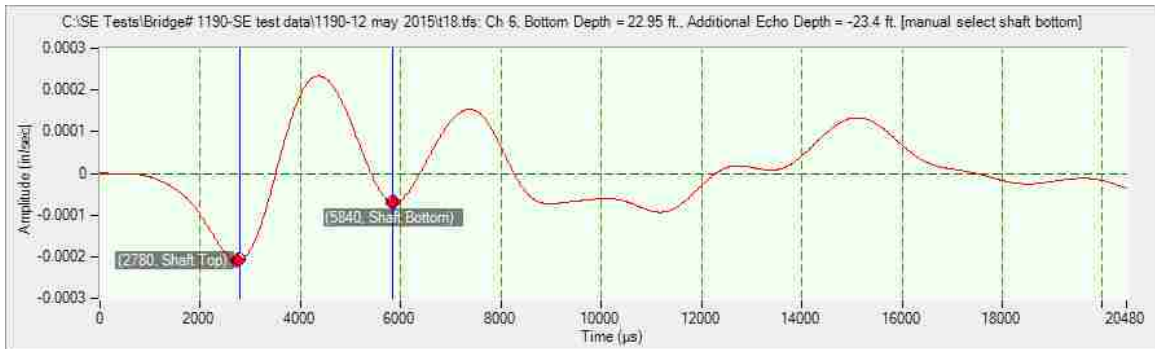


Figure 5-54: Velocity Trace of SE Test No. t18 Using Medium Soft Tip- On Pile Top Edge

5.2.4.3 Pile 21

Pile 21 is located at the intermediate bent of the bridge, as shown in Figure 3-21. Twenty-four SE tests were conducted on Pile 21 in order to study the influence of water pressure and sound on the SE test results. This pile is located in a natural soil moisture zone. Four types of hammer tips were used for striking the pile: hard, medium hard, medium soft, and soft. The top of the pile cap is accessible, so the strikes are conducted downward on the pile cap at point A. Also, vertically upward strikes are applied on the pile cap at point B. For these SE tests, two accelerometers were attached and used, accelerometer 1 was connected to channel 6 and accelerometer 2 to channel 7. The distance between the accelerometers was 3.5 feet. Figure 5-55 illustrates the details of the SE test setup

for Pile 21. Table 5-17 shows the characteristics and results of the SE field test for Pile 21. The results obtained from accelerometer 1 for tests c1, c5, c7 and c10 are presented in Figures 5-56 to 5-59, respectively.

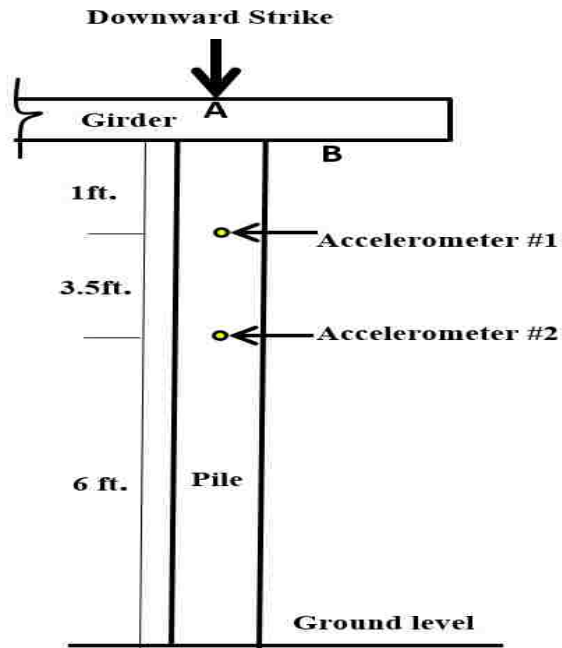


Figure 5-55: SE Test Setup for Pile 21 of Bridge #1190

Table 5-17: Characteristics and Results of SE Field Test for Pile 21

Test No	Hammer Tip's Type	Direction of Strike	Accelerometer 1			Accelerometer 2		
			Δt (μs)	L_t (ft.)	L_b (ft.)	Δt (μs)	L_t (ft.)	L_b (ft.)
c1	Hard	A -Downward	3280	25.6	15.1	3100	27.75	17.25
c2	Hard	A -Downward	3340	26.05	15.55	3480	30.6	20.1
c3	Hard	A -Downward	3520	27.4	16.9	3480	30.6	20.1
c4	Med-hard	A -Downward	3220	25.15	14.65	3280	29.1	18.6
c5	Med-hard	A -Downward	3300	25.75	15.25	3220	28.65	18.15
c6	Med-hard	A -Downward	3260	25.45	14.95	3260	28.95	18.45
c7	Med-soft	A -Downward	3280	25.6	15.1	3360	29.7	19.2
c8	Med-soft	A -Downward	3560	27.7	17.2	3660	31.95	21.45
c9	Med-soft	A -Downward	3500	27.25	16.75	3460	30.45	19.95
c10	Soft	A -Downward	3480	27.1	16.6	3520	30.9	20.4
c11	Soft	A -Downward	3540	27.55	17.05	3520	30.9	20.4
c12	Soft	A -Downward	3540	27.55	17.05	3460	30.45	19.95
c13	Hard	B -Upward	2960	23.2	12.7	3120	27.9	17.4
c14	Hard	B -Upward	3000	23.5	13	3100	27.75	17.25
c15	Hard	B -Upward	2980	23.35	12.85	3040	27.3	16.8
c16	Med-hard	B -Upward	3100	24.25	13.75	3040	27.3	16.8
c17	Med-hard	B -Upward	3040	23.8	13.3	2980	26.85	16.35
c18	Med-hard	B -Upward	3120	24.4	13.9	3000	27	16.5
c19	Med-soft	B -Upward	NS	NS	NS	3040	27.3	16.8
c20	Med-soft	B -Upward	3160	24.7	14.2	2980	26.85	16.35
c21	Med-soft	B -Upward	3100	24.25	13.75	2920	26.4	15.9
c22	Soft	B -Upward	NS	NS	NS	NS	NS	NS
c23	Soft	B -Upward	NS	NS	NS	NS	NS	NS
c24	Soft	B -Upward	NS	NS	NS	NS	NS	NS

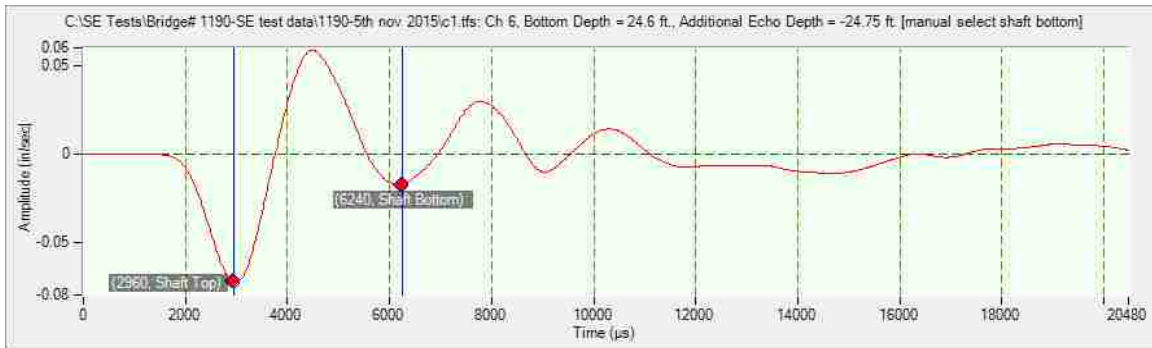


Figure 5-56: Velocity Trace of SE Test No. c1 - Using Hard Tip- A Downward- Ch6

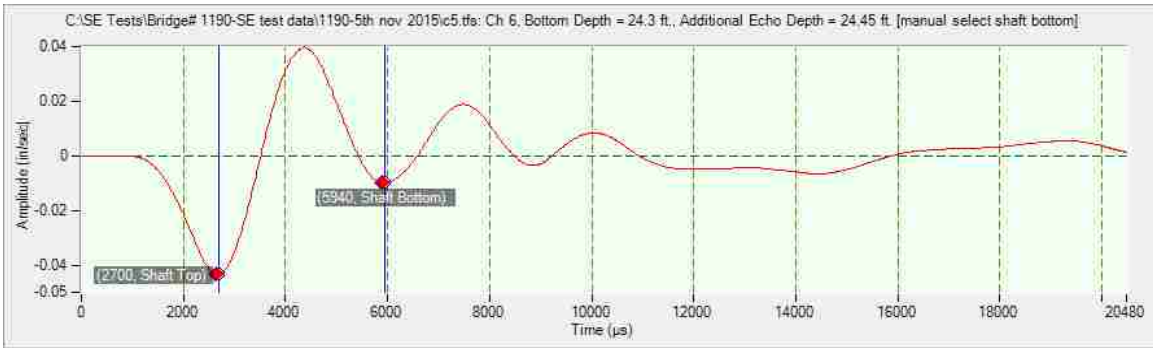


Figure 5-57: Velocity Trace of SE Test No. c5- Using Medium Hard Tip- A Downward- Ch6

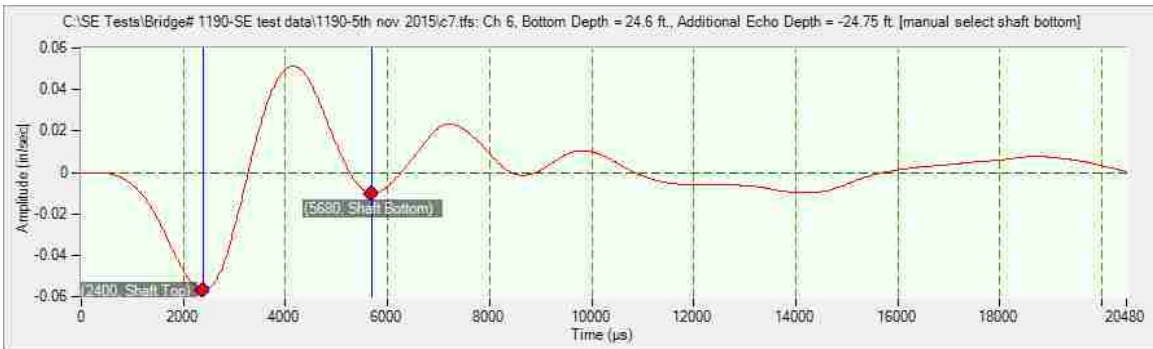


Figure 5-58: Velocity Trace of SE Test No. c7- Using Medium Soft Tip- A Downward- Ch6

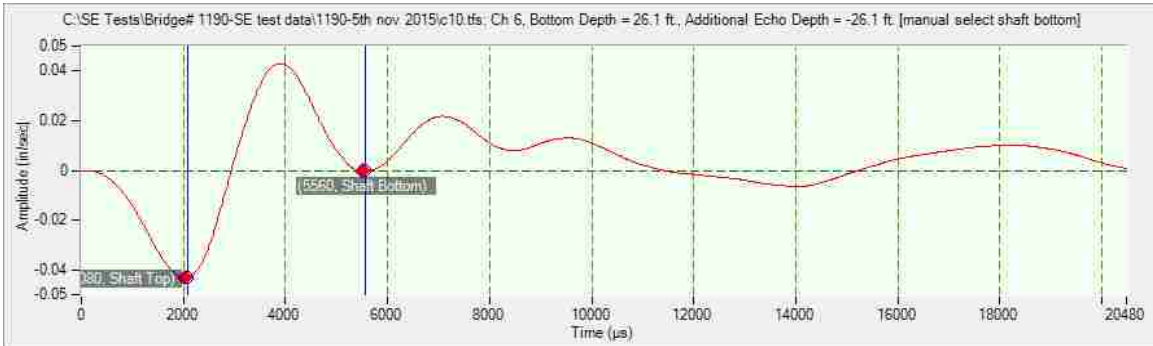


Figure 5-59: Velocity Trace of SE Test No. c10- Using Soft Tip- A Downward- Ch6

The velocity traces that obtained from accelerometer 1 present reliable and reasonable data set for all tests c1, c5, c7 and c10. Hence, hard, medium hard, medium soft, and soft hammer tips can achieve successful test results with good data when the pile is struck at point A. In conclusion, the data obtained from accelerometer 2, if mounted far from the source of energy, indicates longer time differences Δt which lead to assessing greater depths. The average total and

buried depths of Pile 21 as assessed from data obtained from accelerometer 1 are 26.5 feet and 16 feet, respectively. Whereas, the average total and buried depths of Pile 21 that were computed from data obtained from accelerometer 2 are 30 feet and 19.5 feet, respectively.

The results of the SE tests obtained from the accelerometers, when the strikes were conducted upward at point B, were consistent and reliable except when the soft tip was used. When the softer hammer tip was used, the data presented an unclear echo which complicates the interpretation of the velocity trace. The average total and buried depths of Pile 21 that were obtained from accelerometer 1 (when the upward strikes were conducted) are 26 feet and 16 feet, respectively. Furthermore, the average total and buried depths of Pile 21 that were determined from the data obtained from the accelerometer 2 are 27 feet and 17 feet, respectively.

Figures 5-60 to 5-63 illustrate examples of data obtained from accelerometer 1 when the strikes were conducted upward at point B using all types of hammer tips.

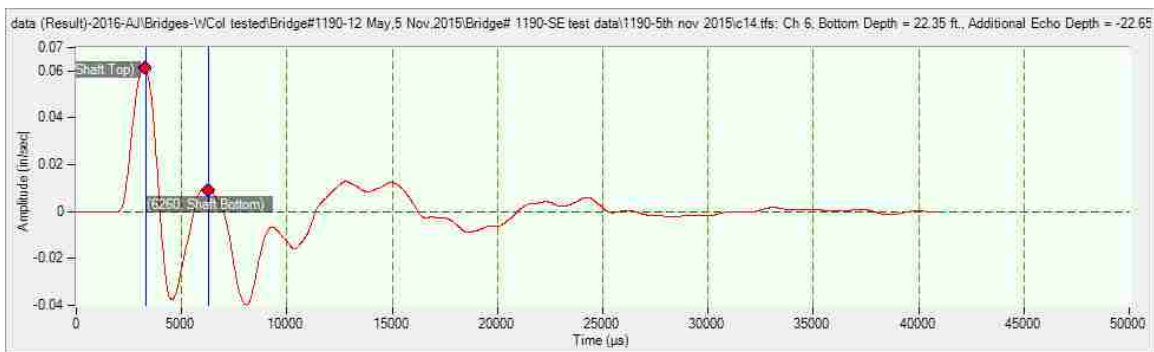


Figure 5-60: Velocity Trace of SE Test No. c14 - Using Hard Tip- B Upward- Ch6

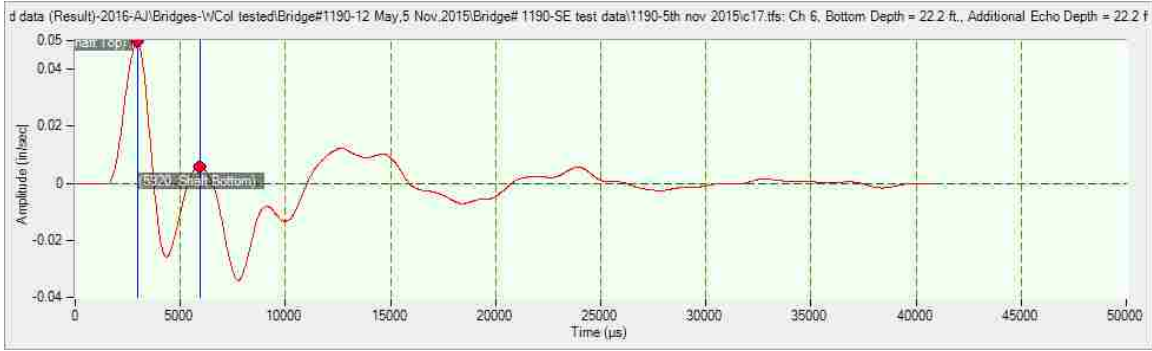


Figure 5-61: Velocity Trace of SE Test No. c17- Using Medium Hard Tip- B Upward- Ch6

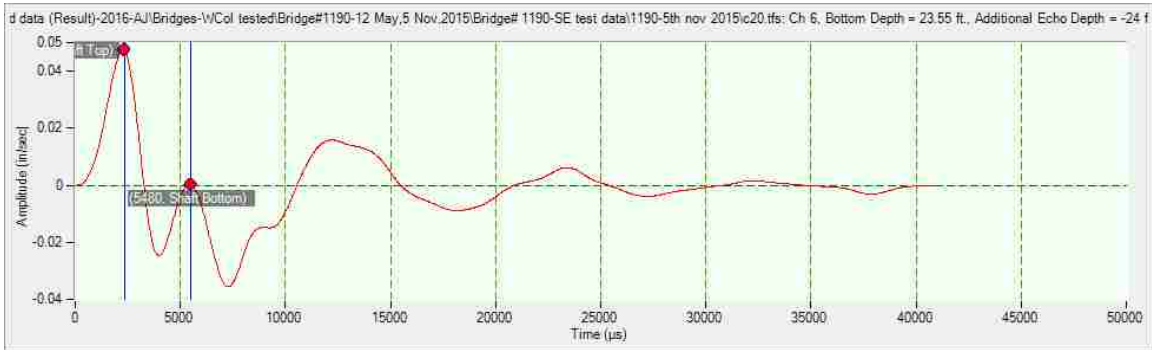


Figure 5-62: Velocity Trace of SE Test No. c20- Using Medium Soft Tip- B Upward- Ch6

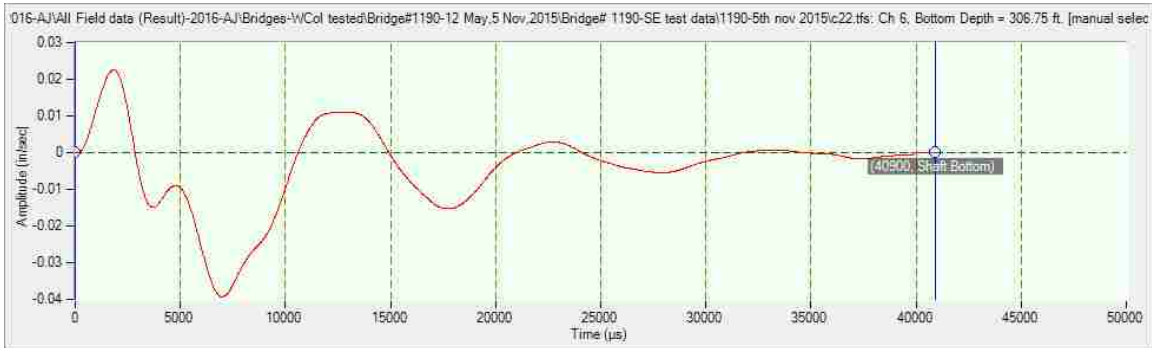


Figure 5-63: Velocity Trace of SE Test No. c22 - Using Soft Tip- B Upward- Shows Unclear Echo

Table 5-18 summarizes the average total and buried lengths of tested piles for Bridge #1190.

Table 5-18: Piles Depths Assessment for Bridge #1190

Pile No.	Assessed Total Pile Depth (ft.)	Assessed Buried Pile Depth (ft.)
Pile 1	25.4	18
Pile 8	24	17
Pile 10	25	18
Pile 15	NS	NS
Pile 19	34	24
Pile 21	26	16
Pile A	24	18
Pile B	19	14

5.3 Validation of SE Test Results

A total of 18 timber piles from different bridges were tested using Olson Freedom Data PC equipment. Here, the SE field test data, obtained from testing Pile 1 of Bridge #6922, were selected for equipment evaluation and validation testing of the results using resonant frequency analysis. Figures 5-64 to 5-66 indicate resonant frequency data obtained from accelerometer 1 which was connected to channel 5. The SE tests were conducted on the top of timber piles using different hammer tips. From these figures, the resonant frequency spacing (Δf) can be estimated to equal 317 Hz. Then the total and buried depths of Pile 1 were computed as shown in Table 5-19 using Eq. 3.6 and Eq. 3-7. The estimated depth of Pile 1 using the resonant frequency analysis approach is consistent and reliable, and the values were close to those estimated depths that obtained from using the time domain analysis. Thus, the results that were obtained from the SE filed tests could be evaluated and validated by using resonant frequency that obtained from Impulse Response Mobility plots.

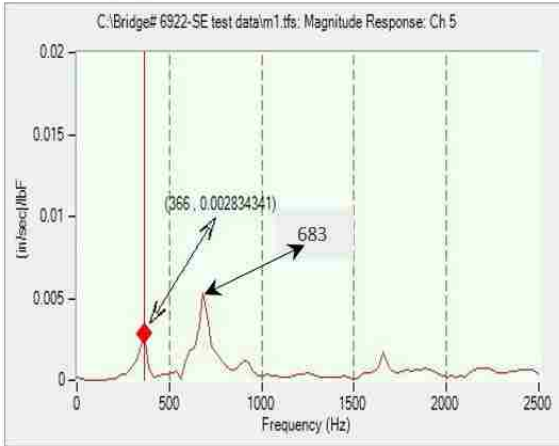


Figure 5-64: IR Mobility Plot for Test No. m1 Using Hard Tip- Pile 1- Bridge #6922

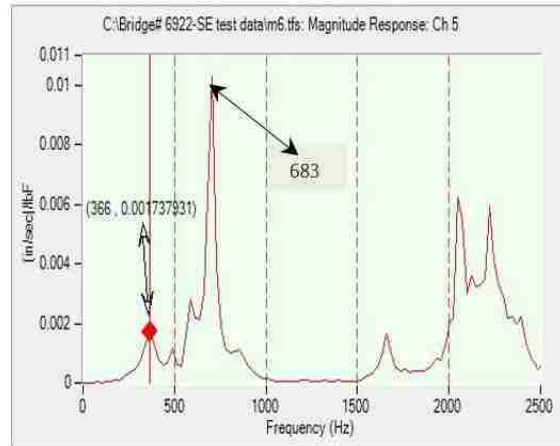
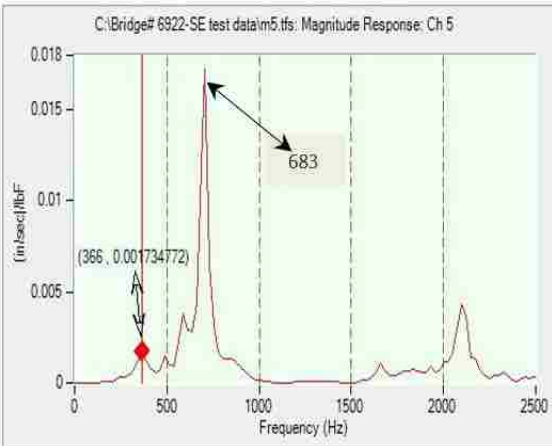
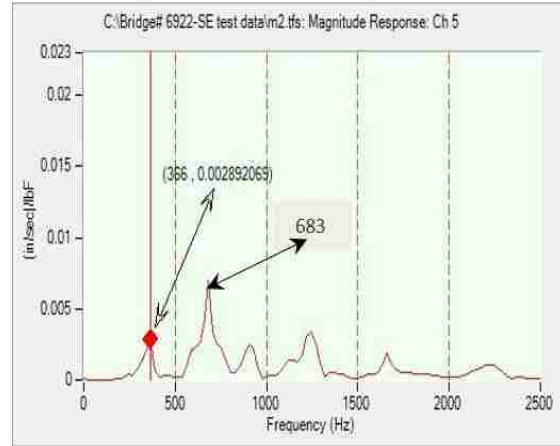


Figure 5-65: IR Mobility Plot for Test No. m5 Using Medium Hard Tip- Pile 1- Bridge #6922

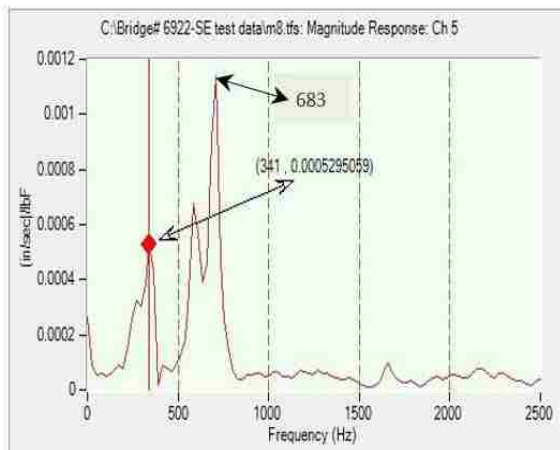
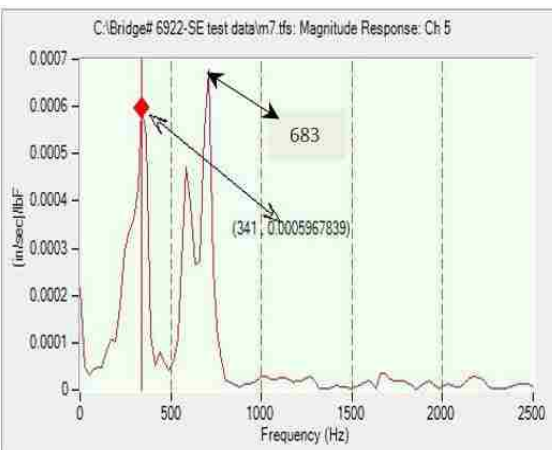


Figure 5-66: IR Mobility Plot for Test No. m7 Using Medium Soft Tip- Pile 1- Bridge #6922

Table 5-19: Validation of the Pile 1 Depths Using Resonant Frequency Approach

Test No.	Using Resonant Frequency Analysis			Using Time Domain Analysis		
	Δf (Hz)	L_t (ft.)	L_b (ft.)	Δt (μ s)	L_t (ft.)	L_b (ft.)
m1	317	25.7	16.4	3000	24.5	15.25
m2	317	25.7	16.4	3000	24.5	15.25
m5	317	25.7	16.4	2840	23.3	14.05
m6	317	25.7	16.4	2960	24.2	14.95
m7	317	25.7	16.4	3100	25.25	16
m8	317	25.7	16.4	3000	24.5	15.25

The percentage of successful SE tests can be calculated using the following formula:

$$\text{Percentage of Successful} = \frac{\text{Number of Successful Attempts}}{\text{Total Attempts}} \times 100 \quad 5.1$$

$$\text{Percentage of Successful} = \frac{17}{18} \times 100 = 94\%$$

Chapter 6

Conclusion and Recommendations

6.1 Summary

The objective of this study was to investigate the effectiveness of determining the unknown bridge foundation depth by using the Sonic Echo method. The SE test method was observed to be suitable for the determination of unknown pile depth for bridges that are supported by timber pile abutments or timber pile bents. The SE test method provides reliable and reasonable results for determination of the depth of all tested piles except Pile 15 which belongs to Bridge #1190. The reason for this unreliable data result for Pile 15 was that the pile was submerged in the Rayado Creek stream. Pile 15 encounters high pressure from water which provides a possibility of noise amplification that can lead to misleading results, and made the interpretation of the data impossible. However, when Pile 21 is at the downstream of Rayado Creek, it encounters low pressure from water which leads to a successful SE test performance. Therefore, it is recommended that SE tests are conducted on the pile that is located in a low pressure water zone.

The SE test method provides reliable and reasonable results for determination the unknown depth for all tested piles with an accuracy rate of $\pm 15\%$. SE tests were conducted on 18 timber piles in different location at New Mexico. The success rate of using the Sonic Echo method to determine the depth of unknown bridge piles is 94%. The range of the depth of tested timber piles was between 16 feet and 38 feet.

Using the hard and medium hard hammer tips provided the best results, especially when the strike was implemented at top of the pile (at point A). In cases of absence of accessibility, a wooden wedge (block) can be attached to the pile side using two anchor bolts (to prevent sliding) as an alternative method to provide the strike. Upward strikes on the pile cap provide less accurate results but could still be used as an alternative method. The assessed depth obtained when the upward strike was conducted could be adjusted using the following empirical equation:

$$\text{Total Depth} = 1.1 \times \text{Total Depth Obtained From Upward Strike Results} \quad 6.1$$

Strikes using medium soft and soft hammer tips are not recommended for use in providing the impact in timber piles. When the aluminum wedge was used to perform the SE test, the results were unreliable and the interpretation was difficult in most situations. Therefore, use of an aluminum wedge is not recommended with timber piles.

The data obtained from accelerometers that are attached close to the source of energy provided the best results. Therefore, it is recommended that the accelerometer is attached one feet from the top end of the pile. It is also recommended that the SE test is repeated at least three times to avoid erroneous results and readings.

6.2 Recommendation for Future Studies

For the current study to be even more effective, it is recommended that this investigation is continued as follows:

1. Verify the SE method by applying the test in different types of known timber bridge foundations.
2. Investigate the geology specifications of site location, especially the soil in the surrounding area and underneath the pile to study its possible influences on the reflection time and velocity trace shape.
3. Create a timber pile sample collection at the Structural Lab at the University of New Mexico for future indoor study and investigation by students to practice using the SE equipment before they use it in the field.
4. Improve SE equipment to obtain a clear signal when the test is applied on timber piles that are located in areas where water flow noise may influence results.
5. Used Fuzzy Logic method to determine the material properties of material.

References

- Ambrosini, D., Ezeberry, J., & Danesi, R. (2005). Long piles integrity through Impact Echo technique. In *VIII Congreso Argentino de Mecánica Computacional* (pp. 651-669).
- Anthony, R. W., & Pandey, A. K. (1996, October). Determining the length of timber piles in transportation structures. In *National conference on wood transportation structures* (No. FPL-GTR-94).
- Chakraborty, S., & Brown, D. A. (1997). EVALUATION OF UNKNOWN PILE LENGTH UNDER EXISTING BRIDGES IN ALABAMA.
- Council, T. P. (2002). Timber pile design and construction manual. *Vancouver (WA): American Wood Preservers Institute.*
- Finno, R. J., & Gassman, S. L. (1998). Impulse response evaluation of drilled shafts. *Journal of geotechnical and geoenvironmental engineering*, 124(10), 965-975.
- Gassman, S. L., & Finno, R. J. (2000). Cutoff frequencies for impulse response tests of existing foundations. *Journal of performance of constructed facilities*, 14(1), 11-21.
- Gassman, S. L., & Finno, R. J. (1999). Impulse response evaluation of foundations using multiple geophones. *Journal of performance of constructed facilities*, 13(2), 82-89.
- Green, D. W., Winandy, J. E., & Kretschmann, D. E. (1999). Mechanical properties of wood. *Wood handbook: wood as an engineering material*. Madison, WI: USDA

Forest Service, Forest Products Laboratory, 1999. *General technical report FPL*, 4-1.

Hertlein, B., & Davis, A. (2007). *Nondestructive testing of deep foundations*. John Wiley & Sons.

Hibbeler, R.C. (2005). *Mechanics of Materials*. New Jersey, NJ: Pearson Prentice Hall.

Hoyle Jr, R. J., & Rutherford, P. S. (1987). *STRESS WAVE INSPECTION OF BRIDGE TIMBERS AND DECKING. FINAL REPORT* (No. WA-RD 146.1).

Hoyle, R. J., & Rutherford, P. S. (1995). Stress wave inspection of bridge timbers and decking. *NDT and E International*, 6(28), 394.

Huang, Y. H., Ni, S. H., Lo, K. F., & Charng, J. J. (2010). Assessment of identifiable defect size in a drilled shaft using sonic echo method: Numerical simulation. *Computers and Geotechnics*, 37(6), 757-768.

Kolsky, H. (1963). *Stress Waves in Solids*, Dover Publications, Inc.

Li, J., Subhani, M., & Samali, B. (2012). Determination of embedment depth of timber poles and piles using wavelet transform. *Advances in Structural Engineering*, 15(5), 759-770.

Lin, Y., Sansalone, M., & Carino, N. J. (1991). Impact-echo response of concrete shafts.

Lo, K. F., Ni, S. H., & Huang, Y. H. (2010). Non-destructive test for pile beneath bridge in the time, frequency, and time-frequency domains using transient loading. *Nonlinear Dynamics*, 62(1), 349-360.

- Massoudi, N., & Teferra, W. (2004). Non-destructive testing of piles using the low strain integrity method.
- Miranda, L., Cantini, L., Guedes, J., Binda, L., & Costa, A. (2012). Applications of sonic tests to masonry elements: influence of joints on the propagation velocity of elastic waves. *Journal of Materials in Civil Engineering*, 25(6), 667-682.
- Ni, S. H., Huang, Y. H., Lo, K. F., & Charng, J. J. (2011). Estimating the flaw size in drilled shafts using an impulse response method. *KSCE Journal of Civil Engineering*, 15(7), 1197-1207.
- No, T. C. S. (2002). Guidebook on non-destructive testing of concrete structures.
- Olson, L., Aouad, M., & Sack, D. (1998). Nondestructive diagnosis of drilled shaft foundations. *Transportation Research Record: Journal of the Transportation Research Board*, (1633), 120-127.
- Rausche, F., Likins, G., & Shen, R. K. (1992, September). Pile integrity testing and analysis. In *Memories Proceedings of the Fourth International Conference on the Application of Stress-Wave Theory to Piles*. The Netherlands (pp. 613-617).
- Richart, F. E., Hall, J. R., & Woods, R. D. (1970). *Vibrations of soils and foundations*. New Jersey, NJ: Prentice-Hall, Inc. (pp. 60-72).
- Ritter, M. A. (1990). *Timber bridges: Design, construction, inspection, and maintenance*.
- Romanescu, C., & Ionescu, C. (2010). The use of non-destructive methods for testing indirect foundations of bridges on A3 motorway. *INTERSECTII/INTERSECTIONS*, 7(1).

Ross, J. T. (2010). *Fuzzy Logic with Engineering Application* (3rd ed.): John Wiley & Sons, Ltd.

Soo, K. D., & Woo, K. H. (2004). Evaluation of the base condition of drilled shafts by the impact-echo method.